Università degli Studi di Padova

DIPARTIMENTO DI FISICA E ASTRONOMIA "GALILEO GALILEI"
Corso di Laurea Magistrale in Astronomia

Non-parametric reconstruction of cosmological functions

Supervisor: Prof. Nicola Bartolo

Assistant Supervisors: Dr. Alessandra Silvestri, Dr. Matteo Martinelli

Student: Francesca Gerardi

A.Y. 2017-2018

Einstein: *What I most admire about your art, is your universality. You don't say a word, yet the world understands you!*

Chaplin: *True. But your glory is even greater! The whole world admires you, even though they don't understand a word of what you say.*

Abstract

This Master Thesis work is about testing gravity on cosmological scales and studying the physics of Dark Energy.
The main purpose is to reconstruct cosmological functions through a non-parametric approach, in order to not be model dependent, and, later, to implement correlation priors encoding theoretical requirements of broad classes of models. In particular, the functions are reconstructed via smoothed step function and a Machine Learning technique, called Gaussian Process, using modified versions of CosmoMC and MGCosmoMC.
In the context of Dark Energy and Modified Gravity models, the non-parametric approach is applied to the reconstruction over redshift of the Dark Energy Equation of State $w_{DE}(z)$, for the Quintessence case, along with that of the two phenomenological functions $\mu(z)$ and $\Sigma(z)$, in the Horndeski case.
These reconstructed functions are then compared with currently available data, in order to obtain their best fit trend, using Bayesian statistics techniques.

Sommario

Questo lavoro di tesi Magistrale concerne l'analisi della gravità su scale cosmologiche e lo studio della fisica dell'Energia Oscura.
Il principale obiettivo è quello di ricostruire funzioni cosmologiche mediante un approccio non parametrico, di modo che siano indipendenti dall'assunzione di un modello specifico, e in seguito di implementare delle *priors* di correlazione che includano le condizioni teoriche per ampie classi di modelli. In particolare, le funzioni sono state ricostruite mediante una funzione a scalino regolarizzata ed una tecnica di Machine Learning, chiamata Processo Gaussiano, facendo uso di versioni modificate di CosmoMC e MGCosmoMC.
Nel contesto di Energia Oscura e modelli di Gravità Modificata, l'approccio non parametrico è stato applicato per la ricostruzione in redshift dell'Equazione di Stato dell'Energia Oscura $w_{DE}(z)$, nel caso di Quintessenza, insieme alle funzioni fenomenologiche $\mu(z)$ and $\Sigma(z)$, nel caso di Horndeski.
Le funzioni ricostruite sono poi state confrontate con dati attualmente disponibili, di modo da ricostruire nella maniera più adatta il loro andamento, mediante tecniche di statistica Bayesiana.

Contents

Introduction

One of the most puzzling phenomena studied by modern Cosmology is the late time acceleration of the Universe. Before 1998, when the two groups High-Z Supernova Search Team [1] and Supernova Cosmology Project [2] observed this phenomenon, it was already known that the Universe is expanding, with a rate encoded in the Hubble parameter $H(t)$, which depends on the constituents of the Universe and on their energy content. Before these Supernovae observations, cosmologists were trying to measure a deceleration parameter, since a Universe filled with matter and radiation is expected to slow down its expansion due to gravitational effects.
Once the late time acceleration was observed, there was the necessity to introduce new constituents of the Universe or new physical mechanisms, since matter and radiation are not able to produce the observed accelerated phase within the General Relativity framework: the simplest candidate is a Cosmological Constant Λ, that, together with the assumption of the existence of Cold Dark Matter, provides the successful ΛCDM model, which had a striking success in explaining cosmological observations.
Recently, the final release of the European Space Agency satellite Planck, observing the Cosmic Microwave Background (CMB) [3], strongly reaffirmed the success of this model in describing the evolution and content of the Universe from its first moments to present time.
However, some theoretical issues related to Λ prompted the exploration of alternative ways of sourcing the cosmic acceleration, which led to the introduction of Dark Energy (DE) and Modified Gravity (MG) models.
Other than theoretical reasons, some recent observations might also hint for deviations from the ΛCDM paradigm; the measurement of the current expansion rate of the Universe H_0 from local observations [4] is in fact in tension with the value inferred from high-z measurements [3] which obtain H_0 under the assumption of ΛCDM

$$H_0^{SH_0ES} = 73.48 \pm 1.66 \ kms^{-1}Mpc^{-1} \qquad H_0^{Planck} = 67.36 \pm 0.54 \ kms^{-1}Mpc^{-1}$$

While unforeseen systematic effects might also drive this tension, a fascinating possibility is that this discrepancy might be explained by models departing the standard ΛCDM assumption.
At the background level, departures from Λ have been largely investigated parameterizing the Equation of State of a dynamic exotic component [3][5][6][7].
Observations of the growth of structures add information to this and provide a powerful way to constrain models beyond ΛCDM. These can potentially distinguish between new components of the Universe (DE) and modifications to the laws of Gravity (MG), since they can possibly measure departures from the ΛCDM evolution of perturbations, which are usually encoded in general functions of time and scale $\mu(t,k)$ and $\gamma(t,k)$.
Due to their relevance, these two functions have been deeply investigated and many ways to parameterize their time and scale dependence have been proposed [8][9][10][11], in order to detect or rule out possible deviations from General Relativity.

The purpose of this Master project is to develop a model-independent reconstruction method in order to understand the behaviour over time of these functions, that could potentially shed light on the nature of the mechanism driving the late cosmic acceleration.

First, for the most simple DE model, named Quintessence, I will reconstruct the EoS alone, while for the most generic class of scalar tensor theory, i.e. Horndeski model, I will reconstruct, together with the EoS, the two phenomenological functions $\mu(a)$ and $\Sigma(a)$. The choice of the latter function instead of the already mentioned $\gamma(a)$ will be later justified by their different link to observables, though the two choices are equivalent.

The work is organized as follows.
Chapter I I will first focus on the bases of the standard model of Cosmology [12] [13] [14], through the construction of the theory itself and its application. Secondly, in light of a highly structured Universe at smaller scales, I will furnish a brief summary of the cosmological perturbation theory, via both Newtonian and Relativistic treatment, and the key observables. Finally, I will analyze the late cosmic acceleration observations and the properties of the Cosmological Constant.
Chapter II I will briefly introduce some alternative Dark Energy and Modified Gravity models, where a deeper treatment can be found in the following reviews [15] [16] [17] [18] [19] [20], and the past literature attempts of solving the H_0 tension, via parameterizations of the EoS and of the two phenomenological functions cited above.
Chapter III I will develop the non-parametric approach to reconstruct these functions, going through the details of the reconstruction methods and the Bayesian statistics tools used for the analysis, addressing with a particular focus the use of a correlation prior within the Monte Carlo parameter estimation.
Chapter IV I will present the results and reconstructions obtained for Quintessence (DE) and Horndeski (MG) models.
Chapter V I will provide a further discussion of the obtained results and a look to the future surveys, aimed at improving our knowledge about the late cosmic acceleration nature.

The modified versions of the softwares used to reconstruct and analyze the functions related respectively to DE and MG models are publicly available at:

- https://github.com/FrancescaGerardi/CosmoMC_binneda
- https://github.com/FrancescaGerardi/MGCosmoMC_binMG_w

1 The standard cosmological model

The Cosmological model describes how the fluid components of the Universe behave and how they influence its structure; for this reason, we need a theory that relates the dynamics and distribution of these fluids to the geometry and dynamics of the Universe itself. This theory is General Relativity, where the metric tensor is built up under the hypothesis of homogeneity and isotropy of space, namely the Cosmological Principle.

1.1 Theory of gravity

Of the four fundamental interactions, gravity is the one playing the crucial role in the history of the Universe; since the nuclear, both weak and strong ones, are short-range interactions ($10^{-15} - 10^{-18}$m) and the observed Universe is electromagnetically neutral on average, gravity is the main interaction of cosmological interest.
Thus, to determine the evolution of the Universe, we need a theory of gravity to be the pillar of any cosmological model: for modern standard cosmology this theory is Einstein's General Relativity. Einstein's theory is based on the equivalence principle, that states that there is no experiment that can distinguish a uniform acceleration from a uniform gravitational field [21]. In order to understand the meaning of this principle, let us consider, for instance, a light ray travelling in a straight line with respect to an inertial frame. This principle means that as we expect this ray to be deflected once we move to an uniformly accelerated frame, the same will happen as soon as the ray enters a gravitational field, being deflected towards the gravitational source.
This result was though interpreted geometrically as a curvature of spacetime and free falling particles move within this geometry along the trajectory that minimizes their proper time τ, which is defined by the geodesics equation:

$$\frac{d^2x^\mu}{d\tau^2} + \Gamma^\mu_{\alpha\beta}\frac{dx^\alpha}{d\tau}\frac{dx^\beta}{d\tau} = 0 \tag{1.1}$$

with $dx^\mu = (dt\ dx\ dy\ dz)$, $(\mu = 0, 1, 2, 3)$ and $\Gamma^\mu_{\alpha\beta}$ the affine connection. The latter naturally arises when redefining the notion of derivative in a curved spacetime. The differentiation process is defined via the incremental ratio, thus, given a vector A^μ, the computation of its partial derivative with respect to a space(time) direction $\vec{x}$ necessarily requires the difference between the vector evaluated at two different points ($A^\mu(P)$, $A^\mu(Q)$), separated by an infinitesimal space(time) interval δx. However, in a curved spacetime the tangent space, with respect to which a certain vector is defined, changes point by point, hence we are no more allowed to compare $A^\mu(P)$ and $A^\mu(Q)$. This brought to the definition of covariant derivative; still referring to the incremental ratio definition, what we can do, before comparing the two vectors, is to move one of them to the point where the other is defined by parallel transport. The covariant derivative of a generic vector A^μ is defined as

$$\nabla_\nu A^\mu = \frac{\delta A^\mu}{\delta x^\nu} + \Gamma^\mu_{\alpha\nu}A^\alpha \tag{1.2}$$

where new terms linked to the affine connection come up. $\Gamma^\mu_{\alpha\beta}$ measures how much the vector, moved by parallel transport, is altered from a point to another, due to the curvature.

Moreover, this tensor is defined only in terms of the metric; once the latter is defined, this is uniquely determined as

$$\Gamma^{\sigma}_{\alpha\beta} = \frac{1}{2} g^{\rho\sigma}(\partial_\alpha g_{\beta\rho} + \partial_\beta g_{\rho\alpha} - \partial_\rho g_{\alpha\beta}) \tag{1.3}$$

where $g_{\mu\nu}$ is the metric tensor, which is the tensor that enters the invariant line element

$$ds^2 = g_{\mu\nu} dx^\mu dx^\nu \quad . \tag{1.4}$$

By construction, the affine connection can be further used to define the Riemann curvature tensor

$$R^{\rho}_{\mu\sigma\nu} = \partial_\sigma \Gamma^{\rho}_{\nu\mu} - \partial_\nu \Gamma^{\rho}_{\sigma\mu} + \Gamma^{\rho}_{\sigma\lambda}\Gamma^{\lambda}_{\nu\mu} - \Gamma^{\rho}_{\nu\lambda}\Gamma^{\lambda}_{\sigma\mu} \tag{1.5}$$

The revolutionary idea of Einstein's theory is that gravity is not a force, in a Newtonian sense, but a geometric property of spacetime, and the geometry is intrinsically connected to any energy source distribution via field equations (I assume here and for the rest of the Thesis that the value of the speed of light c is equal to 1, unless in rare cases, where useful):

$$R_{\mu\nu} - \frac{1}{2} R g_{\mu\nu} = 8\pi G T_{\mu\nu} \tag{1.6}$$

The l.h.s. of Eq.(1.6) is the geometric member, in particular it includes only functions of the metric tensor $g_{\mu\nu}$. The symmetric Ricci tensor $R_{\mu\nu}$ and the Ricci scalar R, which is its trace, are respectively

$$\begin{cases} R_{\mu\nu} = R^{\sigma}_{\mu\sigma\nu} \\ R = R^{\mu}_{\mu} = g^{\mu\nu} R_{\mu\nu} \end{cases} \tag{1.7}$$

obtained by the Riemann curvature tensor $R^{\rho}_{\mu\sigma\nu}$ and the affine connection, defined by $g_{\mu\nu}$ as seen above.

On the r.h.s. there is the symmetric energy-momentum tensor, in which the physical properties of any energy density source are encoded. Under the assumption of a perfect homogeneous and isotropic fluid component, with energy density ρ, pressure p and four-velocity u_μ, the energy-momentum tensor assumes the following form

$$T_{\mu\nu} = (\rho + P) u_\mu u_\nu + P g_{\mu\nu} \tag{1.8}$$

In particular, from the T^{μ}_{ν} conservation law

$$\begin{aligned} \nabla_\mu T^{\mu}_{\nu} &= 0 \\ \partial_\mu T^{\mu}_{\nu} + \Gamma^{\mu}_{\mu\alpha} T^{\alpha}_{\nu} + \Gamma^{\alpha}_{\mu\nu} T^{\mu}_{\alpha} &= 0 \end{aligned} \tag{1.9}$$

it is possible to derive the time evolution of that fluid component, once the metric is given.

Einstein's field equations are derived from the action S; for a generic physical system, S is the quantity that characterizes its dynamics and from which its equations of motion can be derived through the principle of least action. If we consider only gravity and matter field minimally coupled to it, then the action is of the form $S = S_{EH} + S_M$, where the two addenda refer respectively to gravitational and matter sectors

$$S = S_{EH} + S_M = \frac{1}{16\pi G} \int d^4x \sqrt{-g}\, (R + 16\pi G \mathcal{L}_M) \tag{1.10}$$

with g the determinant of the metric, $G = 6.67408 \cdot 10^{-11}$ m^{3}kg^{-1}s^{-2} the gravitational constant, R the Ricci scalar and $\mathcal{L}_M$ the matter Lagrangian density.
So, applying the variational principle $\frac{\delta S}{\delta g^{\mu\nu}} = 0$ and keeping in mind that $R = g^{\mu\nu} R_{\mu\nu}$:

$$\begin{aligned}\frac{\delta S}{\delta g^{\mu\nu}} &= \frac{1}{16\pi G}\int d^4x \left(\frac{\delta(\sqrt{-g}R)}{\delta g^{\mu\nu}} + 16\pi G\frac{\delta(\sqrt{-g}\mathcal{L}_M)}{\delta g^{\mu\nu}}\right)\delta g^{\mu\nu} \\ &= \frac{1}{16\pi G}\int d^4x \left(\frac{\delta(\sqrt{-g})}{\delta g^{\mu\nu}}R + \sqrt{-g}\frac{\delta(g^{\mu\nu}R_{\mu\nu})}{\delta g^{\mu\nu}} + 16\pi G\frac{\delta(\sqrt{-g}\mathcal{L}_M)}{\delta g^{\mu\nu}}\right)\delta g^{\mu\nu} \\ &= \frac{1}{16\pi G}\int d^4x\sqrt{-g}\left(\frac{\delta\sqrt{-g}}{\delta g^{\mu\nu}}\frac{R}{(\sqrt{-g})} + \frac{\delta g^{\mu\nu}}{\delta g^{\mu\nu}}R_{\mu\nu} + g^{\mu\nu}\frac{\delta R_{\mu\nu}}{\delta g^{\mu\nu}} + 16\pi G\frac{1}{\sqrt{-g}}\frac{\delta(\sqrt{-g}\mathcal{L}_M)}{\delta g^{\mu\nu}}\right)\delta g^{\mu\nu} \\ &= 0\end{aligned} \tag{1.11}$$

where [15]

$$\frac{\delta\sqrt{-g}}{\delta g^{\mu\nu}}\frac{R}{(\sqrt{-g})} = -\frac{1}{2}g_{\mu\nu}R\ ; \quad \frac{1}{\sqrt{-g}}\frac{\delta(\sqrt{-g}\mathcal{L}_M)}{\delta g^{\mu\nu}} = -\frac{1}{2}T_{\mu\nu} \tag{1.12}$$

and

$$g^{\mu\nu}\delta R_{\mu\nu} = \nabla_\rho(g^{\mu\nu}\delta\Gamma^\sigma_{\mu\nu} + g^{\mu\sigma}\delta\Gamma^\rho_{\rho\mu}) \tag{1.13}$$

which is zero, since it is a total derivative that will be integrated over null bounds [15].

Combining Eqs.(1.11)(1.12)(1.13) we obtain the final expression of Eq.(1.6).

As a supporter of a static Universe, Einstein introduced the Cosmological Constant Λ, in order to furnish the negative pressure required to prevent the gravitational contraction, caused by matter in a finite Universe. This will be formally demonstrated later in Sect.1.4.2, once the FLRW metric is introduced. Hence, Einstein added Λ to the Einstein-Hilbert action

$$S_{HE} = \frac{1}{16\pi G}\int d^4x\sqrt{-g}(R - 2\Lambda) \tag{1.14}$$

such that, following the same procedure used above

$$\begin{aligned}\frac{\delta S_{extra}}{\delta g^{\mu\nu}} &= \frac{1}{16\pi G}\int d^4x \left(-2\frac{\delta\sqrt{-g}\Lambda}{\delta g^{\mu\nu}}\right) \\ &= \frac{1}{16\pi G}\int d^4x \left[-2\Lambda\left(-\frac{1}{2}g_{\mu\nu}\sqrt{-g}\right)\right] \\ &= \frac{1}{16\pi G}\int d^4x \left(\sqrt{-g}\right)\left[\Lambda g_{\mu\nu}\right]\end{aligned} \tag{1.15}$$

So, the modified Einstein's field equations are:

$$R_{\mu\nu} - \frac{1}{2}Rg_{\mu\nu} + \Lambda g_{\mu\nu} = 8\pi G T_{\mu\nu} \tag{1.16}$$

On one hand, after Lemaître demonstrated that a static solution would have been unstable once considered density perturbations, Λ has been passed over. On the other hand, in 1929, the first evidence of the Universe expansion came from Edwin Hubble observations: he found out there was a linear relation between the distance d of extra-galactic nebulae and their recession velocities

$$v = const \cdot d$$

where the constant is the Hubble parameter $H(t)$ evaluated at present time $H_{today} = H_0$.

He measured the recession velocity via the spectral lines shift, defined as

$$z = \frac{\lambda_o - \lambda_e}{\lambda_e} = \sqrt{\frac{1 + v/c}{1 - v/c}} - 1 \sim \frac{v}{c} \tag{1.17}$$

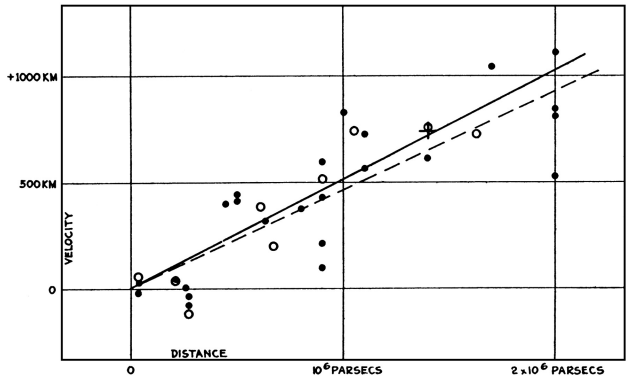

Figure 1.1: Original velocity-distance relation diagram, taken from [22].

where λ_o and λ_e are respectively the observed and the emission wavelengths of the incoming radiation; moreover, the last equality is valid only in the limit $v \ll c$.
In particular, the recession velocity due to the Universe expansion is what characterizes the so called Hubble flow. Given a source in the sky, this will take part to the Hubble flow and will have also a peculiar velocity, linked to the environment in which it is placed.

The rate at which the Universe expands depends on the energy content, as it is going to be demonstrated in the next Section, once we restrict ourselves to the choice of a particular metric tensor.
All the different epochs the Universe had been through, during its expansion, are characterized by a different distribution of the energy density content among the different constituents, which means that, for instance, a component which is subdominant at present, could have been the dominant source of energy density in the past, and viceversa.
Writing the field equations, we have basically considered the gravitational and matter sectors, encoded respectively in S_{EH} and S_M, where actually the matter content to be considered is not trivially what we define as ordinary matter. This sector broadly refers to both non-relativistic ($T \ll m$[1]) and relativistic ($T \gg m$) particles and scalar fields.
At present, the majority of the energy budget E_B is unknown and it goes under the name of Dark Sector, that includes both Dark Energy and Dark Matter. According to Planck results [3][23] [2], the present energy content is predicted to consist of:

Dark Energy, which is the energy source for the late cosmic acceleration and it acts as a repulsive force, i.e. as a fluid component with negative pressure. According to the standard cosmological model this source is the Cosmological Constant Λ; however, there are still other viable candidates, as dynamical Dark Energy (DE), or modifications to the theory of General Relativity at large scales, where the theory has not been tested with the same precision as in the Solar System. As both these mechanisms add dynamics to the system, both of them consist of the addition of extra degrees of freedom to the standard GR action (Eq.(1.10)), as it is going to be discussed in Sect.2.1. This component makes up $\sim$69% of E_B.

Matter, which is split into Dark Matter and ordinary matter. On one hand, Dark Matter consists of particles that interact only gravitationally and, according to the standard model, it is the fluid component that provided the potential wells where baryons fell to form large scale structure, right after the decoupling between photons and baryons ($t_{dec} \sim 378000 yrs$). As it is going to be cleared later in Sect.1.5, the Dark Matter component in agreement with large scale observations must have been cold, i.e. $T \ll m$, when it decoupled from the thermal bath; thus, the standard cosmological model is also called ΛCDM, since at present the Universe energy budget is mainly made up of Dark Energy (Λ) and Cold Dark Matter (CDM). The DM sector

[1] A particle is defined non-relativistic/cold (relativistic/hot) if its temperature T is largely smaller (larger) than its mass m
[2] together with other cosmological observations, in order to break degeneracies between parameters

makes up ∼26% of E_B.
On the other hand, by ordinary (baryonic) matter I mean the light products of the Big Bang Nucleosynthesis (BBN), such as free hydrogen and helium ∼4% E_B, the stars ∼0.5% E_B they formed and heavy elements ∼0.03% E_B produced by stellar evolution.

Radiation, that constitutes nowadays an infinitesimal component of E_B. By radiation we refer to relativistic particles, mainly to photons of the Cosmic Microwave Background (CMB) radiation, discovered in 1964 by Penzias and Wilson. CMB radiation is, up to now, the best example of a black-body spectrum, whose specific intensity I_ν is given by the Planck law

$$I_\nu = \frac{2h}{c^2} \frac{\nu^3}{e^{h\nu/kT} - 1} \tag{1.18}$$

where ν and T are the frequency and temperature of photons and h is the Planck constant $h = 6.626 \times 10^{-34}$ J · s. Hence, given that the Universe was far more dense in the past, this radiation must have generated under thermal equilibrium at a certain temperature T_i; this condition was fulfilled until the recombination epoch (at $T \sim 3000K$), before which photons and matter were strongly coupled. CMB constitutes a strong evidence for the Hot Big Bang model, according to which the Primordial Universe was a mixture of hot plasma and photons in thermal equilibrium, which then cooled down because of the expansion, allowing the formation of atoms and molecules. The adiabatic expansion of the Universe affects the mean temperature of the Cosmic Microwave Background, that, since we are dealing with a black-body radiation, evolves as $T(t) = T_i \frac{a(t_i)}{a(t)}$ [3], reaching then the current average temperature $T_0 = 2.72548 \pm 0.00057K$.

Neutrinos, that are very light leptons with no charge, involved, for instance, in β-decay and in the electron capture

$$n \longrightarrow p^+ + e^- + \bar{\nu}_e \qquad\qquad p^+ + e^- \longrightarrow n + \nu_e$$

Depending on their mass they could be included within the relativistic or non-relativistic sectors. While at the beginning neutrinos were believed to be massless, in which case

$$\rho_\nu \propto \left(\frac{4}{11}\right)^{4/3} \rho_\gamma, \tag{1.19}$$

the neutrino oscillation phenomenon [24] have determined that they are massive and the three species (ν_e, ν_μ, ν_τ) have different masses. It has been envisaged that they have behaved as relativistic particles in the early Universe, and as matter particles later [25]. This component makes up ∼0.3% of E_B.

[3] As later in Sec.1.2.1 we are going to see, defined the scale factor $a(t)$, the energy density of photons will evolve as $\rho_\gamma \propto a^{-4}(t)$ and since for relativistic non-degenerate bosons [13] $\rho \propto T^4$ (Eq.(1.93)), then the temperature will evolve over time as $T \propto a^{-1}(t)$

1.2 The homogeneous expanding Universe

Einstein's equations are powerful tools to understand the dynamics of the Universe, but to reach that goal two main ingredients are required: the metric tensor and the energy sources properties. However, as already said, there is an intimate connection between geometry and matter distribution; this means that an assumption on one of them will reflect as a property of the other. In particular, the existence of some symmetries in the matter distribution implies a simpler metric, since there are less degrees of freedom.
This is the role played by the Cosmological Principle, which is the second cornerstone for modern cosmology; it states that at a given time, over a sufficiently large scale ($\sim 300Mpc$), the Universe observed by a comoving observer [4] is nearly homogeneous and isotropic (in space)[5]. This means, respectively, that, given a certain physical property, its average is invariant by translation and rotation.
The striking observational evidence of isotropy comes from CMB radiation, which has the same mean temperature ($T_0 = 2.72548 \pm 0.00057K$ at present) independently of the line of sight direction, besides anisotropies of the order of $10^{-5}K$, whose nature will be discussed in Sect.1.3. On the other hand, there is no way to experimentally probe homogeneity. The Universe would be automatically homogeneous, if, along with the observed isotropy, the Copernican Principle is assumed to be valid, as it states that the observer is not in a special position in the Universe.

The metric describing a homogeneous and isotropic expanding universe is the Friedmann-Lemaître-Robertson-Walker (FLRW), where the line element in spherical-polar coordinates is

$$ds^2 = -c^2dt^2 + a^2(t)\left[\frac{dr^2}{1-kr^2} + r^2(d\theta^2 + sin^2\theta d\phi^2)\right] \quad . \tag{1.20}$$

In Eq.(1.20) r, θ and ϕ are comoving spatial coordinates, t is the cosmic time, $a(t)$ is the scale factor and k is the curvature parameter.
The scale factor is defined as a dimensionless function of time that encodes the expansion, it relates the comoving coordinates to the physical ones. As a simple example, let us consider the 2-dimensional spacetime; in this case the FLRW line element can be written as $ds^2 = -c^2dt^2 + a^2(t)dx^2$: dx is defined as the comoving distance, that does not change in time due to the expansion of spacetime, while $dl = a(t)dx$ is defined as the physical distance, that takes into account the expansion of the Universe at time t. In particular $a(t_0) = a_0 = 1$.

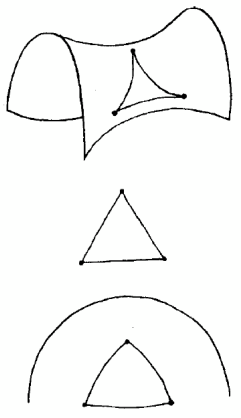

There exist different cosmological models depending on the value of the curvature parameter, in particular it can be positive, negative or equal to zero; once normalized it assumes one of the following values

$$\begin{cases} -1 & \text{open Universe} \\ 0 & \text{flat Euclid spacetime} \\ +1 & \text{closed Universe} \end{cases} \tag{1.21}$$

We will see that k is dependent on the quantity of matter, which is still intuitive from a Newtonian point of view: the more matter I have the more the Universe is going to be "closed" under the effect of its potential well. Observationally, the Universe is highly close to flat [27].

[4] i.e. comoving with the Hubble flow

[5] Before the discovery of the CMB properties, there had been the development of the steady-state cosmology, based on the Perfect Cosmological Principle, according to which the Universe was the same not only in all places and in all directions, but also at all times. [26]

1.2.1 The background dynamics

Once the FLRW is assumed, the Einstein's equations provide the equations that rule the dynamics of the background, where by background I mean the perfect homogeneous and isotropic Universe described exactly by the FLRW metric. These are the Friedmann equations.
Considering the i-th perfect fluid [6] component, at rest in comoving coordinates, its energy-momentum tensor is equal to

$$\begin{aligned} T^{\mu}_{\nu} &= (\rho + P)u_{\nu}u^{\mu} + pg^{\mu}_{\nu} \\ &= \begin{pmatrix} -\rho & 0 & 0 & 0 \\ 0 & p & 0 & 0 \\ 0 & 0 & p & 0 \\ 0 & 0 & 0 & p \end{pmatrix} \end{aligned} \tag{1.22}$$

since $u^{\mu} = (1, 0, 0, 0)$ and the metric tensor is diagonal. Moreover, it should also be noted that the form of the energy-momentum tensor of Eq.(1.22) is required for compatibility with the Cosmological Principle, anisotropic pressure is not permitted [26].
Hence, from Eq.(1.6) using Eqs.(1.20)(1.22), this yields the Friedmann equations

$$\left(\frac{\dot{a}(t)}{a(t)}\right)^2 = \frac{8\pi G}{3}\sum_i \rho_i(t) - \frac{k}{a^2(t)} \tag{1.23a}$$

$$\frac{\ddot{a}(t)}{a(t)} = -\frac{4\pi G}{3}\sum_i (\rho_i(t) + 3p_i(t)) \tag{1.23b}$$

where $\dot{a}(t)$ and $\ddot{a}(t)$ are respectively the first and the second derivative of the scale factor $a(t)$ with respect to the cosmic time.

Usually the properties of these fluid components are expressed in terms of their Equation of State (EoS) $w(t) = p(t)/\rho(t)$; hence, the time evolution of the density can be written in terms of $w(t)$.
Assuming that an i-th component does not exchange energy with the others, for the first law of thermodynamics, considering a comoving volume:

$$\begin{gathered} d(\rho_i a^3) = -p_i d(a^3) \\ \mapsto \dot{\rho}_i a^3 + 3\rho_i a^2 \dot{a} = -3p_i a^2 \dot{a} \Leftrightarrow \dot{\rho}_i a + 3(\rho_i + p_i)\dot{a} = 0 \Leftrightarrow \\ \Leftrightarrow \dot{\rho}_i a + 3\rho_i(1 + w_i)\dot{a} = 0 \Leftrightarrow \frac{\dot{\rho}_i}{\rho_i} = -3(1 + w_i)\frac{\dot{a}}{a} \\ \mapsto \frac{d\rho_i}{\rho_i} = -3(1 + w_i)\frac{da}{a} \end{gathered} \tag{1.24}$$

where the density and the scale factor are functions of time and the derivatives are computed with respect to it.
Eq.(1.24) is a differential equation with solution

$$\rho \propto e^{3\int_{a(t)}^{1} \frac{1+w(a)}{a} da} \tag{1.25}$$

that reduces to

$$\rho \propto a^{-3(1+w)} \tag{1.26}$$

if $w = const$. The same result is obtained working with Eqs.(1.23), deriving the first one and using both

$$\begin{aligned} 2\frac{\dot{a}}{a}\left[\frac{\ddot{a}}{a} - \left(\frac{\dot{a}}{a}\right)^2\right] &= \frac{8\pi G}{3}\frac{d\rho}{dt} \\ 2\frac{\dot{a}}{a}\left[-\frac{4\pi G}{3}\rho(1 + 3w) - \frac{8\pi G}{3}\rho\right] &= \frac{8\pi G}{3}\frac{d\rho}{dt} \\ \frac{\dot{a}}{a}\left[-\frac{8\pi G}{3}3\rho(1 + w)\right] &= \frac{8\pi G}{3}\frac{d\rho}{dt} \end{aligned} \tag{1.27}$$

[6] A fluid is perfect if, for instance, the mean free path between particle collisions is much less than the scales of physical interest [26]

that yields the same last equation in Eq.(1.24).

For a flat single-component Universe, using Eqs.(1.23)(1.26), in the hypothesis of constant Equation of State, it is simple to obtain the evolution over time of the scale factor:

$$\left(\frac{\dot{a}(t)}{a(t)}\right)^2 \propto \rho_0 a^{-3(1+w)} \Leftrightarrow \frac{\dot{a}(t)}{a^{-(1+3w)/2}} \propto const \Rightarrow a^{\frac{(1+3w)}{2}} da \propto dt \tag{1.28}$$

where $\rho_0 = \rho(t_0)$, so that by integration

$$a \propto t^{2/[3(1+w)]} \tag{1.29}$$

In Tab.1.1 the time dependence for the matter, radiation and Cosmological Constant densities are given, once specified their Equations of state w_i, and plotted in Fig.1.2.

Component	w	a	ρ
radiation	1/3	$t^{1/2}$	a^{-4}
matter	0	$t^{2/3}$	a^{-3}
Cosmological Constant	-1	e^{Ht}	a^0

Table 1.1: Main ΛCDM Universe components with their EoS and the evolution of the scale factor and density over time, under the hypothesis of a single component Universe. In particular, the EoS of matter is $w = 0$ because a fluid of non-relativistic particles exerts a pressure which is negligible compared to their energy density.

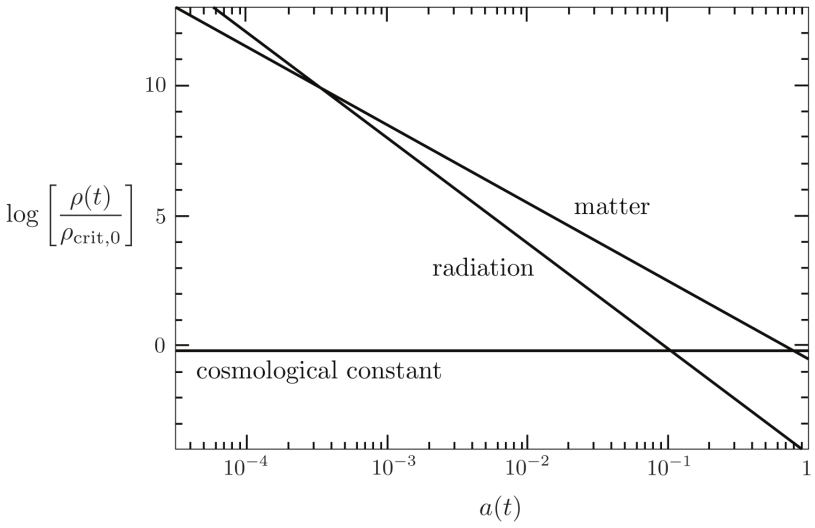

Figure 1.2: Behaviour over time of the matter, radiation and Cosmological Constant densities. The intersection between the matter and radiation curves is defined as the time of equivalence. Figure from [25].

Neglecting for the moment the Cosmological Constant contribution, which is relevant at late times, from Fig.1.2 it can be seen that there exists a value of the scale factor, defined as $a_{eq} = a(t_{eq})$, at which the matter and radiation densities are equivalent. Thus, the standard cosmological model distinguishes two main eras, that dominated by radiation, for $a < a_{eq}$, and the latter by matter, for $a > a_{eq}$, as long as we neglect the Dark Energy dominance at present. Currently, the equivalence epoch is estimated to be $a_{eq} \sim 3 \cdot 10^{-4}$, far before than the baryons-radiation decoupling ($a_{dec} \sim 10^{-3}$).

The standard cosmological model provides a mathematical description of the Universe dynamics as a consequence of its fluid components, accounting for the observed expansion. Since the Universe is expanding, we expect that it must have generated as a highly dense and hot environment; for this reason the standard cosmological model is also called the Hot Big Bang model.
The Big Bang is defined as the initial singularity at which the scale factor is null and the thermodynamic parameters, as density, diverge. Starting from this highly chaotic phase, the rate of interactions between particles was much higher than the rate of expansion, hence these particles were in thermodynamic equilibrium and constituted a thermal bath. But, as the Universe adiabatically expanded, it cooled down. Hence, since different species have different interaction rates, the time at which a certain particle species decouples from the thermal bath depends on the interaction rate of that species and how the latter is affected by the cooling. For instance, the standard cosmological model successfully explains the black-body CMB radiation as a relic of this hot phase, where in particular CMB photons decoupled from baryons at $t_{dec} \sim 378000 yrs$, allowing the formation of atoms and molecules.
Moreover, the model successfully predicts [26] the light element abundance, i.e. hydrogen, helium and lithium, via the Big Bang Nucleosynthesis theory (BBN), that is dated around 3 minutes after the Big Bang ($E \sim 100 keV$).

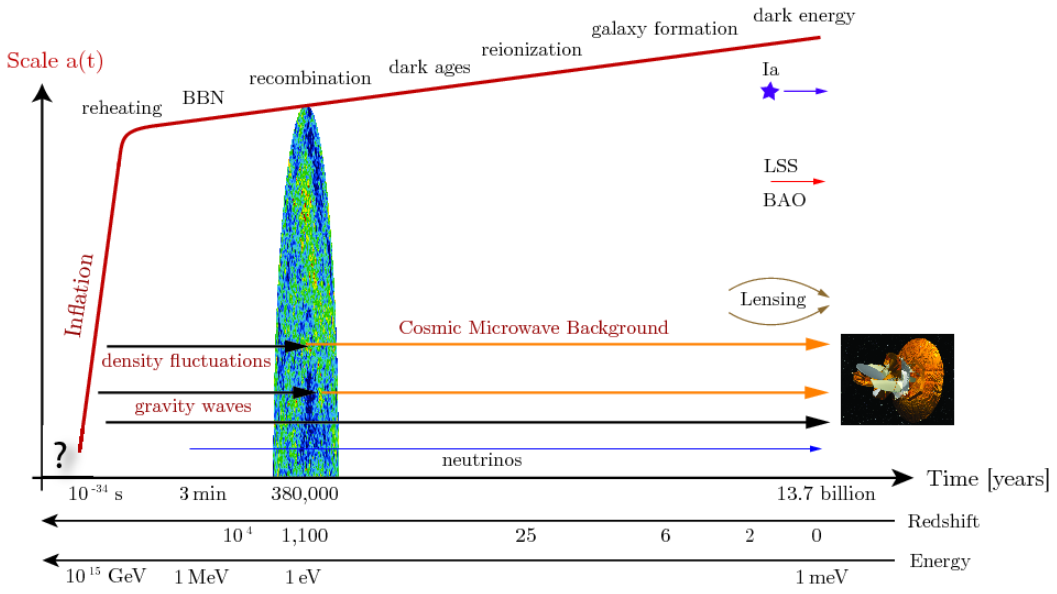

Figure 1.3: Evolutionary stages of the Universe. Figure adapted from [28].

1.2.2 Cosmological parameters

Given the above cosmological model, some cosmological parameters can be defined. There exist two parameters linked to the dynamical properties of the Universe: the Hubble and the deceleration parameters

$$H(t) = \frac{\dot{a}(t)}{a(t)} \qquad\qquad q(t) = -\frac{a(t)\ddot{a}(t)}{\dot{a}(t)^2} \quad . \tag{1.30}$$

The Hubble parameter is defined as the expansion rate. Before the observation of the late cosmic acceleration [1][2], cosmologists were trying to measure the deceleration of the Universe expansion, since matter alone is supposed to slow it down. However, in light of the late cosmic acceleration, i.e. $\ddot{a}(t) > 0$, the deceleration parameter at present is negative.

Then, there exist parameters linked to the density of the fluid constituents. Once defined the critical density $\rho_c(t) = \frac{3H^2(t)}{8\pi G}$, as the energy density in the case of a flat Universe (Eq.(1.23a) with $k = 0$), the fraction of the total energy density linked to the i-th component will be given by the dimensionless density parameter

$$\Omega_i(t) = \frac{\rho_i(t)}{\rho_c(t)} \quad . \tag{1.31}$$

The critical density is named after its link with the curvature k. Indeed, if we write Eq.(1.23a) in terms of the density parameters of all the fluid components, then

$$\begin{aligned} 1 &= \frac{8\pi G}{3H^2}\sum_i \rho_i - \frac{k}{H^2a^2} \\ 1 &= \frac{\sum_i \rho_i}{\rho_c} - \frac{k}{H^2a^2} \end{aligned} \Rightarrow \Omega - 1 = \frac{k}{H^2a^2} \tag{1.32}$$

with $\Omega = \sum_i \Omega_i$.

Consequently, from Eq.(1.32) it can be immediately seen that

$$\begin{cases} \sum_i \rho_i < \rho_c \Rightarrow k < 0 \\ \sum_i \rho_i = \rho_c \Rightarrow k = 0 \\ \sum_i \rho_i > \rho_c \Rightarrow k > 0 \end{cases} \tag{1.33}$$

By the definition of these parameters it can be finally cleared why the rate at which the Universe expands depends on the energy content. The expansion history, starting from the first Friedmann equation (Eq.(1.23a)), is defined as a function of the density parameters

$$H(a) = H_0\left[\Omega_m a^{-3} + \Omega_\gamma a^{-4} + \Omega_{DE} a^{-3(1+w_{DE})}\right]^{1/2} \tag{1.34}$$

where I have taken into account matter, radiation and a general Dark Energy component, with constant EoS. From the latter equation, it can be immediately seen that depending on the density parameters, i.e. on the dominant energy sources, the Universe will expand at different rates.
In the specific case in which the Dark Energy is the Cosmological Constant, namely according to ΛCDM model, the expansion rate of Eq.(1.34) becomes

$$H(a) = H_0\left[\Omega_m a^{-3} + \Omega_\gamma a^{-4} + \Omega_\Lambda\right]^{1/2} \tag{1.35}$$

1.2.3 Cosmological redshift and distances

Now that we know how the scale factor evolves as a function of the Universe energy content, via Eq.(1.34), we can predict how the physical distances will evolve over time. However in order to compare the theoretical predictions to observations, two important quantities must be adequately defined: cosmological redshift and distances.

Cosmological Redshift

As already seen in Eq.(1.17), generically considering a distant light source, we can define the redshift(blueshift) as the change in wavelength of the emitted photons to a redder(bluer) one. In particular, the cosmological redshift refers to a change in wavelength of photons due to the cosmic expansion. Thus, considering a photon on his path to the observer, as the Universe expands, wavelengths get stretched, since photons loose energy against the expansion, i.e. decrease their frequency, while reaching the observer.
There exists a relation between redshift and the scale factor. Let us consider the path of a photon, characterized by $ds^2 = g_{\mu\nu}dx^\mu dx^\nu = 0$ and $d\theta = d\phi = 0$; assuming it is emitted at t_e from the source and it reaches the observer at t_0 then

$$\begin{aligned} cdt &= a\frac{dr}{\sqrt{1-kr^2}} \\ \int_{t_e}^{t_0} \frac{cdt}{a(t)} &= \int_0^r \frac{dr}{\sqrt{1-kr^2}} \end{aligned} \tag{1.36}$$

where the r.h.s. is constant because r is the comoving coordinate and is constant by definition. Then, let us consider a second light emission at $t_e + \delta t_e$ received at $t_0 + \delta t_0$:

$$\int_{t_e+\delta t_e}^{t_0+\delta t_0} \frac{cdt}{a(t)} = \int_0^r \frac{dr}{\sqrt{1-kr^2}} \tag{1.37}$$

if δt_i is sufficiently small

$$\frac{\delta t_0}{a_0} = \frac{\delta t_e}{a_e} \Leftrightarrow \nu_0 a_0 = \nu_e a_e \Leftrightarrow \frac{1}{\lambda_0} = \frac{a_e}{\lambda_e} \tag{1.38}$$

and then by the definition in Eq.(1.17)

$$1 + z = \frac{1}{a} \tag{1.39}$$

Luminosity distance

Luminosity distance is an important tool to constrain the expansion history via objects of which we know the intrinsic luminosity, to which we refer as *standard candles*; let us derive it. There exists a relation between the flux and the luminosity, that is

$$F = \frac{L}{4\pi r_0^2} \tag{1.40}$$

where r_0 is the comoving distance between the source and the observer, equal to the physical distance at present time, since $a_0 = 1$. This would be the relation if there would not be any expansion, but since the observed Universe is expanding we must take into account the photons loss of energy and the difference between the frequency of emission and that of observation, so that

$$F = \frac{L}{4\pi r_0^2(1+z)^2} = \frac{L}{4\pi d_L^2} \quad . \tag{1.41}$$

Thus, the distance in the flux-luminosity relation is no more the comoving one, but it becomes the so called luminosity distance d_L, such that $d_L = r_0(1+z)$.
As the comoving distance between the source and the observer is defined as

$$\begin{aligned} r_0 &= \int_{t_e}^{t_0} \frac{cdt}{a(t)} \\ &= c\int_0^z \frac{dz}{H(z)} \end{aligned} \tag{1.42}$$

at the end this yields

$$d_L(z) = (1+z)c\int_0^z \frac{dz}{H(z)} \tag{1.43}$$

It's worth mentioning here that the Hubble expansion law can be obtained from Eq.(1.43) Taylor expanding the scale factor around its value today:

$$\begin{aligned} a(t) &= a_0 + (t-t_0)\left(\frac{da}{dt}\right)_{t_0} + \frac{1}{2}(t-t_0)^2\left(\frac{d^2a}{dt^2}\right)_{t_0} + .. \\ &= 1 + (t-t_0)H_0 + \frac{1}{2}(t-t_0)^2 q_0 H_0^2 + .. \\ &\Rightarrow d_L = \frac{c}{H_0}\left(z + \frac{1}{2}(1-q_0)z^2 + ..\right) \end{aligned} \tag{1.44}$$

where q_0 is the deceleration parameter at present time.

Angular diameter distance

Moreover, it is possible to constrain the expansion history via geometrical probes, known as *standard rulers*. In particular, assuming that the angular dimension $d\theta$ and the linear dimension l of an object are known, in the limit of small angles, the following approximation is valid

$$d_A = \frac{l}{d\theta} \tag{1.45}$$

where d_A is defined as the angular diameter distance. There exists a relation between d_A and d_L, this can be derived working with the FLRW metric, under the assumption that the two ends of the object are at the same comoving distance r_0, so that $dr = 0$ and $dt = 0$, laying on the same plane, such that $d\phi = 0$, then $l = \sqrt{ds^2} = a(t)r_0 d\theta$ so that

$$\begin{aligned} d_A = \frac{a(t)r_0 d\theta}{d\theta} \Leftrightarrow d_A = a(t)r_0 \Leftrightarrow d_A = \frac{r_0}{(1+z)} \\ \Rightarrow d_A = \frac{d_L}{(1+z)^2} \end{aligned} \tag{1.46}$$

1.3 The inhomogeneous Universe

The background theory evolution described in the previous Section is based on the assumption that at sufficiently large scales the Universe is homogeneous and isotropic, however this no longer holds on smaller scales, where the Universe tends to be highly structured (Fig.1.4). Thus, that is the clear evidence that there exist deviations from these conditions.

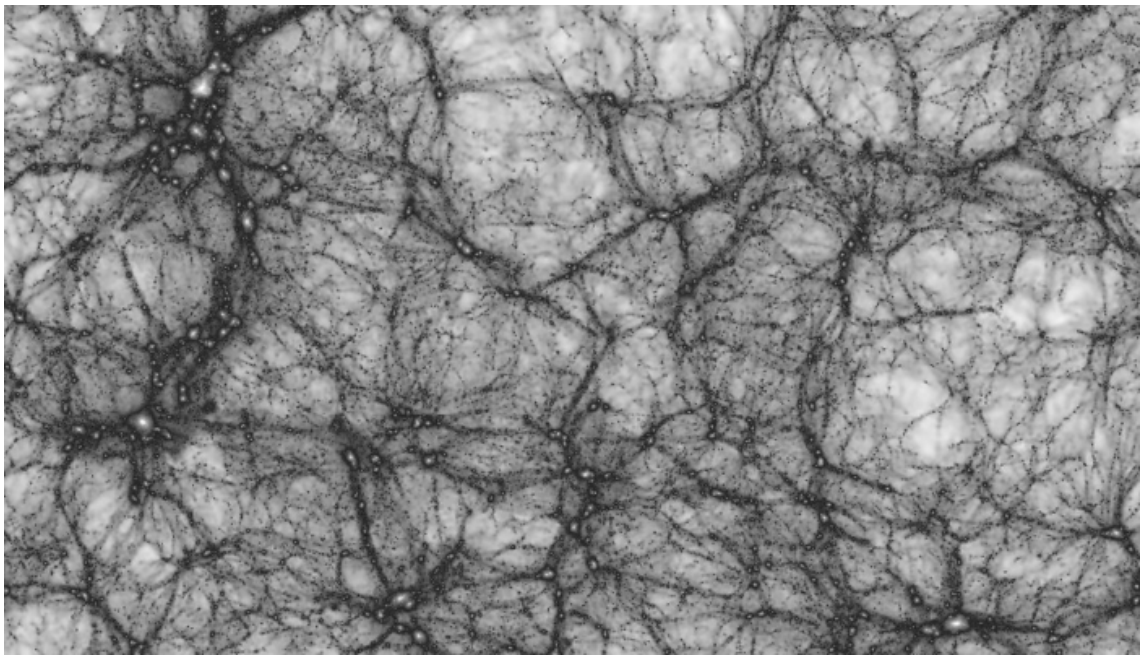

Figure 1.4: Image of the large scale structure as created by The Millennium Simulation (https://wwwmpa.mpa-garching.mpg.de/galform/virgo/millennium/).

The underlying idea behind large scale structure formation is that the whole homogeneous Universe background [7] presented locally matter overdensities $\delta\rho(\mathbf{x},t)$, defined as $\delta\rho(\mathbf{x},t) = \rho(\mathbf{x},t) - \rho_{BCK}(t)$ [8], that subsequently evolved, affected by the opposite effects of pressure and gravitational forces, schematically [13]

$$\ddot{\delta} + (Pressure \ - \ Gravity)\delta = 0 \ . \tag{1.47}$$

That is the gravitational instability theory, first formulated by Jeans in 1902, in order to determine the mechanism of stars and planets formation and later adopted as the standard model theory for the formation of galaxies and large scale structure (LSS) in linear regime.

Since these fluctuations are originally random Gaussian distributed, we can statistically characterize and study their amplitude as a function of the cosmological scale, defining the two-point correlation function, or as a function of the wavenumber k, in Fourier space, via the power spectrum.
Thus, having a stochastic fluctuations field $\delta(\mathbf{x},t)$, in real space the mean value of the statistic ensemble is

$$\langle \delta(\mathbf{x},t) \rangle = 0 \tag{1.48}$$

by construction, hence it does not give us any information. On the contrary, the two-point correlation function is statistically meaningful, since it is defined as

$$\xi(\delta\mathbf{x}) \equiv \langle \delta(\mathbf{x}), \delta(\mathbf{x}+\delta\mathbf{x}) \rangle \tag{1.49}$$

[7] Studying the evolution of the perturbations, we will refer to the background as the manifold described exactly by the flat FLRW metric.

[8] By the properties of homogeneity and isotropy, the mean value of the background will be only a function of time.

where the two fluctuations $\delta(\mathbf{x})$ and $\delta(\mathbf{x}+\delta\mathbf{x})$ are specified at the same time t, but at two positions that differ by $\delta\mathbf{x}$.
As close regions of the Universe can influence each other, perturbations localized in such regions can not evolve independently one with respect to the other, it is more useful to think of the perturbation as a superposition of plane waves, that evolve independently while the fluctuations are still linear [26]. In Fourier space, the fluctuation is defined as

$$\delta(\mathbf{x},t) = \frac{1}{(2\pi)^3}\int \delta_{\mathbf{k}}(t)e^{i\mathbf{k}\cdot\mathbf{x}}d^3k \tag{1.50}$$

and its Fourier transform $\delta_{\mathbf{k}}(t)$ fulfills the condition

$$\langle\delta_{\mathbf{k}}(t),\delta_{\mathbf{k}'}(t)\rangle = (2\pi)^3P(k,t)\delta^{(3)}(\mathbf{k}+\mathbf{k}') \tag{1.51}$$

demanded by the fact that the two point correlation function, also in Fourier space, must meet the Cosmological Principle. Indeed, defined the function of scale k and time t $P(k,t)$ as the power spectrum, the latter expresses the isotropy property, while the term $\delta^{(3)}(\mathbf{k}+\mathbf{k}')$ encodes homogeneity, i.e. translation invariance.
Hence, in Fourier space the two-point correlation function will be

$$\xi(\delta\mathbf{x}) = \langle\ \frac{1}{(2\pi)^6}\int d^3k\delta_{\mathbf{k}}(t)e^{i\mathbf{k}\cdot\mathbf{x}}\int d^3k'\delta_{\mathbf{k}'}(t)e^{i\mathbf{k}'\cdot(\mathbf{x}+\delta\mathbf{x})}\ \rangle \tag{1.52}$$

where using now Eq.(1.51) yields

$$\xi(\delta\mathbf{x}) = \frac{1}{(2\pi)^3}\int P(k,t)e^{-i\mathbf{k}\cdot\delta\mathbf{x}}d^3k\ \ . \tag{1.53}$$

Thus, the measure of the amplitude of fluctuations as a function of the wavenumber k will be given by the power spectrum, which is defined by the Wiener-Khintchine theorem (Eq.(1.53)) to be the Fourier transform of the two-point correlation function, for a statistically homogeneous random field.
If $\delta\mathbf{x}=0$, then Eq.(1.49) yields the variance

$$\langle\delta(\mathbf{x},t)^2\rangle = \int\frac{dk}{k}\Delta(k,t) \tag{1.54}$$

where $\Delta(k,t)$ is defined as the adimensional power spectrum

$$\Delta(k,t) = \frac{1}{(2\pi)^3}k^3P(k,t) \tag{1.55}$$

The standard cosmological model can not predict the magnitude of the fluctuations $\delta(\mathbf{x},t)$, but only the statistical properties of these perturbations, encoded in the power spectrum $P(k,t)$.

Let us then proceed to the theory that provides an explanation for the evolution of these fluctuations, working under the assumption that $\delta\rho(\mathbf{x},t) \ll \rho_{BCK}(t)$ (small perturbations), in which case, it is possible to study their evolution via a perturbative approach: the perturbed quantities will be described as $y(t,\mathbf{x}) = y_0(t)+\delta y(t,\mathbf{x})$, where $y_0(t)$ is the mean background value and by the assumed homogeneity and isotropy it does not depend on the spatial coordinate $\mathbf{x}$.

1.3.1 Newtonian approach

The gravitational Jeans instability theory dates back to 1902, even before the development of the General Relativity theory, thus it is fully based on a Newtonian treatment. The underlying idea of Jeans theory is to determine the role of the two opposite pressure and gravity forces on the evolution of δ, depending on the scale of the fluctuations. Especially, the theory naturally defines a critical scale, the Jeans scale λ_J, that divides the two regimes in which one of the two forces is dominant with respect to the other.
Let us formally derive the expression of the Eq.(1.47).

As the theory was formulated under non-relativistic assumptions (back then Relativity did not exist) and these perturbations refer to the fluid constituents of the Universe, the starting point is then to consider fluid dynamics laws for a non-relativistic fluid component, with density ρ, pressure p and velocity $\mathbf{u}$. Its equation of motion is given by a combination of:

- the continuity equation, implied by the mass conservation

$$\delta_t \rho = -\nabla_{\mathbf{r}}(\rho \mathbf{u}) \tag{1.56}$$

- the Euler equation

$$(\delta_t + \mathbf{u}\nabla_{\mathbf{r}})\mathbf{u} = -\frac{\nabla_{\mathbf{r}} p}{\rho} - \nabla_{\mathbf{r}}\Phi \tag{1.57}$$

  that is inferred from momentum conservation.

Moreover, the gravitational potential Φ induced by the massive fluid is linked to the fluid density via the Poisson equation

$$\nabla_r^2 \Phi = 4\pi G \rho \tag{1.58}$$

Since we want to combine these three equations to determine the evolution over time of small perturbations, we first decompose the density, pressure and velocity into their background and perturbed quantities, i.e. $\rho(t, \mathbf{x}) = \rho_0(t) + \delta\rho(t, \mathbf{x})$, where $\delta\rho(t, \mathbf{x})$ must satisfy the condition $\delta\rho(t, \mathbf{x}) \ll \rho_0(t)$ to enable us to apply perturbative theory.

The expansion of the Universe was not known at that time, however, for our aims we are going to take it into account. Hence, it is more convenient to pass to the frame comoving to the fluid, i.e. to Lagrangian coordinates:

$$\mathbf{r} = a(t)\mathbf{x} \tag{1.59}$$

Thus, both the space and time derivatives will transform as

$$\begin{aligned} &\nabla_{\mathbf{r}} = a^{-1}\nabla_{\mathbf{x}} \\ &\frac{\delta}{\delta t} = \frac{\delta \mathbf{x}}{\delta t}\frac{\delta}{\delta \mathbf{x}} + \frac{\delta t}{\delta t}\frac{\delta}{\delta t} = \frac{\delta}{\delta t}\left(\frac{\mathbf{r}}{a(t)}\right)\frac{\delta}{\delta \mathbf{x}} + \frac{\delta}{\delta t} = \frac{\delta}{\delta t} - H\mathbf{x}\nabla_{\mathbf{x}} \end{aligned} \tag{1.60}$$

and due to this change of frame the velocity field will be then

$$\mathbf{u}(t) = \frac{d\mathbf{r}}{dt} = \frac{da(t)\mathbf{x}}{dt} = \dot{a}(t)\mathbf{x} + a(t)\dot{\mathbf{x}} = H\mathbf{r} + \mathbf{v} \quad , \tag{1.61}$$

where $H\mathbf{r}$ is the Hubble flow and $\mathbf{v} = a(t)\dot{\mathbf{x}}$ the peculiar velocity.

The evolution of adiabatic density perturbations obtained combining Eqs.(1.56)(1.57)(1.58) transformed in the new reference frame is

$$\ddot{\delta} + 2H\dot{\delta} - \frac{c_s^2}{a^2}\nabla^2\delta = 4\pi G\rho_0\delta \tag{1.62}$$

where $c_s = \left(\frac{\partial P}{\partial \rho}\right)^{1/2}$ is the sound speed and δ is the density contrast, defined as

$$\delta = \frac{\delta\rho}{\rho_0} \tag{1.63}$$

Before proceeding, let us first derive the Jeans scale, as the main parameter of the theory. Assuming $a(t) = const$ ($\Rightarrow H = 0$), i.e. a static Universe, Eq.(1.62) yields

$$\ddot{\delta} - \frac{c_s^2}{a^2}\nabla^2\delta = 4\pi G\rho_0\delta \tag{1.64}$$

and admits the oscillating solution of amplitude A

$$\delta\rho(t, \mathbf{r}) = Aexp\left[i\left(\omega t - \mathbf{k}\cdot\mathbf{r}\right)\right] \tag{1.65}$$

where

$$\omega^2 = c_s^2k^2 - 4\pi G\rho_0 \tag{1.66}$$

with $k = |\mathbf{k}|$.
There exists a critical wavenumber associated to ω^2 and that is the Jeans wavenumber

$$k_J = \frac{\sqrt{4\pi G\rho_0}}{c_s} \tag{1.67}$$

or equivalently the Jeans length

$$\lambda_J = \frac{2\pi}{k_J} = c_s\sqrt{\frac{\pi}{G\rho_0}} \tag{1.68}$$

which are found imposing the condition $\omega = 0$, namely that the two opposite pressure and gravitational forces balance each other.
Below that length ($k > k_J$) the pressure is dominant, then the fluctuations oscillate with constant amplitude; on the contrary if $k < k_J$ ω is imaginary and the argument of the exponential solution is real, i.e. the perturbations grow exponentially.

Adding the friction term $2H\dot{\delta}$ due to the expansion (as in Eq.1.62), the fluctuations below the Jeans length oscillate with decreasing amplitude (rather than keeping it constant), while above they grow as a power law (rather than exponential).

Since we are interested in structure formation, let us focus on the matter component, i.e. on a pressure-less fluid ($p \ll \rho$), such that Eq.(1.62) becomes

$$\ddot{\delta}_m + 2H\dot{\delta}_m = 4\pi G\rho_0\delta_m \tag{1.69}$$

where δ_m denotes the density contrast related to the matter fluid.
The evolution of matter density perturbations over time will be then determined once the epoch of interest is specified; indeed this will make clear the time dependence encoded into the Hubble parameter as well as the background densities that must be considered (radiation, matter and/or Dark Energy), in order to solve the equation.
The full treatment can be found in [25][26].

As already pointed out more than once, this theory restricts us to the treatment of density perturbations for non-relativistic fluids, besides we could be interested in determining an equation for the evolution of density perturbation even for the radiation component.
Moreover, these approach is a good approximation as long as we are dealing with perturbations whose size is far smaller than the Hubble radius

$$R_C(t) = \frac{c}{H(t)} \sim c\tau_H$$

defined as the radius of the sphere, centered on the observer, that contains all the points that had been in causal connection with the observer within one Hubble time $H(t)^{-1}$.
By definition, the comoving Hubble radius will be then equal to

$$\begin{gathered} r_H(t) = \frac{1}{a(t)}\frac{c}{H(t)} = \frac{c}{\dot{a}(t)} \\ \Downarrow \\ r_H(t) \propto \begin{cases} t^{1/2} & \text{radiation dominated era} \\ t^{1/3} & \text{matter dominated era} \end{cases} \end{gathered} \tag{1.70}$$

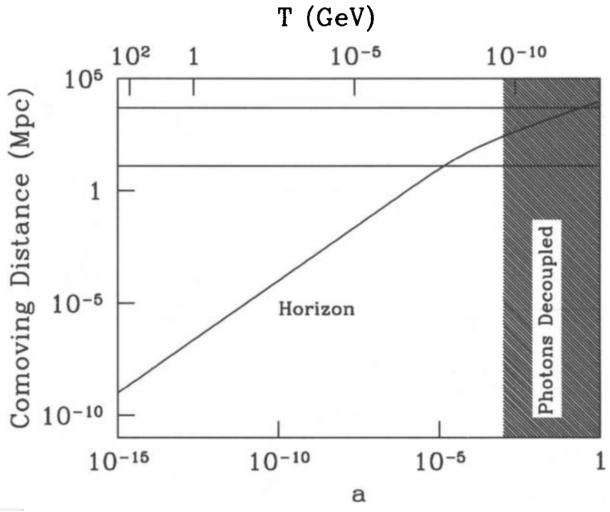

Figure 1.5: Two regimes can be distinguished with respect to the Hubble radius: the sub-horizon and the super-horizon regimes. Given the relation between the comoving scale λ of the perturbation and the wavenumber k, the perturbation crosses the horizon when the condition $k = aH$ is satisfied. Figure adapted from [13]

The necessity of a full relativistic treatment can be dimensionally understood as follows. Considering Eq.(1.58) and combining it to the first Friedmann equation (Eq.(1.23a)), the Poisson equation leads to

$$\nabla_r^2 \Phi = \frac{3}{2} a^2 H^2 \delta \tag{1.71}$$

that by a dimensional analysis, including the light velocity c explicitly, means

$$\frac{\Phi}{c^2} \sim \left(\frac{\lambda}{r_H} \right)^2 \delta \tag{1.72}$$

Hence, on sub-horizon regime $\lambda \ll r_H$ the Newtonian approach is a good approximation as $\Phi \ll c^2$, but this is no longer true at higher scales (i.e. $\lambda \geq r_H$) where a full General Relativity treatment is required.

1.3.2 Relativistic approach

As it can be already seen by the Newtonian treatment, gravity plays a fundamental role in the evolution of density perturbations. As in GR gravity is a geometric property of spacetime and geometry is linked to any energy source via field equations, the Relativistic approach to study the evolution of density perturbations consists of perturbing Einstein's equations. A perturbation of the energy source causes a perturbation of the metric, with respect to the background (unperturbed) FLRW $g_{\mu\nu}$.
Thus, perturbing Eq.(1.6) and collecting the whole l.h.s. member into the Einstein tensor

$$G_{\mu\nu} = R_{\mu\nu} - \frac{1}{2}Rg_{\mu\nu} \tag{1.73}$$

the perturbed field equations will assume the form of

$$G^0_{\mu\nu} + \delta G_{\mu\nu} = T^0_{\mu\nu} + \delta T_{\mu\nu} \tag{1.74}$$

where the apex 0 denotes unperturbed quantities.
Hence, both the geometric and the energy source members must be properly modified. On one hand, perturbations of the metric tensor will automatically imply perturbations of the Einstein tensor, since the Ricci tensor and scalar are functions of the $g_{\mu\nu}$ by definition. On the other hand, perturbations to the energy-momentum tensor will be sourced by perturbations in every quantity that constitutes it, as density, pressure and the four-velocity.
Let us though start from perturbations of the metric tensor.

Metric tensor perturbations

The perturbed metric tensor will be of the form of

$$g_{\mu\nu} = g^0_{\mu\nu} + \delta g_{\mu\nu} \tag{1.75}$$

such that FLRW line element in conformal time $\tau = t/a(t)$ will be perturbed in

$$\begin{gathered} ds^2 = a^2(\tau)\left[-d\tau^2 + \delta_{ij}dx^i dx^j\right] \\ \Downarrow \\ ds^2 = a^2(\tau)\left[-(1+2A)d\tau^2 + 2B_i dx^i d\tau + (\delta_{ij} + h_{ij})dx^i dx^j\right] \end{gathered} \tag{1.76}$$

where A, B_i and h_{ij} are functions of space and time, respectively scalar, vector and tensor perturbations.
Since we are only interested in scalar perturbations, it is now useful to operate the scalar-vector-tensor (SVT) decomposition, in order to isolate all the scalar contributions to the perturbed metric. Indeed, since the three kind of perturbations evolve independently one with respect to the others at linear order, we can treat the evolution of scalar, vector and tensor perturbations separately.
Hence, applying the SVT decomposition to vector and tensor perturbations, they are decomposed in their scalar, vector (divergenceless) and tensor (traceless) part for Helmholtz theorem, as [25]

$$B_i = \partial_i B + \hat{B}_i \tag{1.77}$$

$$h_{ij} = 2C\delta_{ij} + \left(\partial_i\partial_j - \frac{1}{3}\nabla^2\delta_{ij}\right)\partial_i E + \frac{1}{2}\left(\partial_i\hat{E}_j + \partial_j\hat{E}_i\right) + \hat{E}_{ij} \tag{1.78}$$

Finally, the metric perturbative degrees of freedom are encoded in

- four scalars A, B, C, E
- two vectors $\hat{B}_i, \hat{E}_i$
- one tensor $\hat{E}_{ij}$

The Gauge problem In perturbation theory any perturbed tensor T can be expressed as the sum of the unperturbed one, to which I am going to refer as the background T_0, and the perturbation δT, such that $\delta T = T - T_0$. Here comes the Gauge problem: perturbations are not uniquely defined. Let us consider two manifolds: the background flat FLRW M_0 and the perturbed M; on M_0 lays the tensor T_0, while T on M. The problem is how to define their difference, since two tensors must belong to the same manifold to be comparable. The solution is then up to the choice of a gauge (a map), that can establish a 1:1 correspondence between the manifolds.

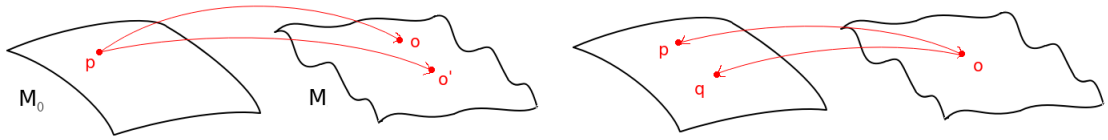

Consider the points $p \in M_0$ and $q \in M_0$ both corresponding to the same point $o \in M$ via two different gauges: $p = \Psi(o)$ and $q = \Phi(o)$, in general the perturbations δT = T - T_0 for the first gauge and $\delta\tilde{\mathrm{T}} = \tilde{\mathrm{T}}$ - $\tilde{\mathrm{T}}_0$ for the second gauge will differ from each other. We might then wonder what is the transformation law for these perturbations.
Formally gauge and coordinate transformations are two different things, however since we know how scalars, vectors and tensors transform under a ordinary change of coordinates, we would like to interpret the gauge transformation in terms of the latter [29]. Hence, starting from p, we can interpret the gauge transformation within an active approach, namely moving from p to q, defining a map in the background manifold as

$$\Theta : p \to q = \Theta(p) = \Phi(\Psi^{-1}(p)) \quad . \tag{1.79}$$

From this point of view the gauge transformation is defined as an active coordinates transformation; thus, let us outline schematically the practical approach: first we need to fix the M_0 coordinates x^μ. Secondly, we define the vector $\xi^\mu(x) = \frac{dx^\mu}{d\lambda}$, where λ is the x^μ curves parameter, that must be small since we are interested in linear perturbations; hence, moving from p to q yields

$$x^\mu(q) \to x^\mu(p) + \lambda\xi^\mu(x(p)) \quad . \tag{1.80}$$

Without getting any deeper, scalars, vectors and tensors consequently transform as $\delta\tilde{\mathrm{T}} = \delta\mathrm{T} + \mathcal{L}_\xi \mathrm{T}$, where $\mathcal{L}_\xi$ is the Lie derivative along the vector $\xi^\mu(x)$ [30]:

$$\mathcal{L}_\xi S = \xi^\nu \frac{\partial S}{\partial x^\nu}$$

$$\mathcal{L}_\xi V^\mu = \xi^\nu \frac{\partial V^\mu}{\partial x^\nu} + \frac{\partial \xi^\mu}{\partial x^\nu} V^\nu$$

$$\mathcal{L}_\xi T_{\mu\nu} = \xi^\lambda \frac{\partial T_{\mu\nu}}{\partial x^\lambda} + \frac{\partial \xi^\lambda}{\partial x^\mu} T_{\lambda\nu} + \frac{\partial \xi^\lambda}{\partial x^\nu} T_{\mu\lambda}$$

If we define [30]

$$\begin{cases} \xi^0 = \alpha \\ \xi^i = \partial^i \beta + d^i \end{cases} \tag{1.81}$$

then choosing a gauge means, via the transformation law above, giving conditions on α, β and d^i.

One way to proceed is working with the Bardeen [31] variables, defined by the gauge-invariant combination of the perturbative terms of the metric tensor; these are: the two scalar variables [25]

$$\Psi \equiv A + \mathcal{H}(B - E') + (B - E')' \tag{1.82}$$

$$\Phi \equiv -C - \mathcal{H}(B - E') + \frac{1}{3}\nabla^2 E \tag{1.83}$$

the vector and tensor perturbations

$$\hat{\Phi}_i \equiv \hat{E}_i' - \hat{B}_i \qquad\qquad \hat{E}_{ij} \tag{1.84}$$

where $\mathcal{H} = aH$ is the Hubble parameter in conformal time τ and $'$ denotes derivatives with respect to τ.

Anyway, a gauge must be fixed, before proceeding with all the calculations.
The gauge I will use is the Newtonian gauge, that is defined by the choice

$$B = E = 0 \tag{1.85}$$

so that in terms of the Bardeen variables: $A = \Psi$ and $C = \Phi$. Hence, the flat FLRW perturbed line element at linear order in Newtonian gauge is

$$ds^2 = -(1 + 2\Psi(x,t))dt^2 + a^2(t)(1 - 2\Phi(x,t))d\vec{x}^2 \tag{1.86}$$

$$\Downarrow$$

$$g_{\mu\nu} = g^{(0)}_{\mu\nu} + \delta g_{\mu\nu} = a^2 \begin{pmatrix} -(1 + 2\Psi(x,t)) & 0 \\ 0 & (1 - 2\Phi(x,t))\delta_{ij} \end{pmatrix} \tag{1.87}$$

Source tensor perturbations

The perturbed energy-momentum tensor will be of the form of

$$T_{\mu\nu} = T^0_{\mu\nu} + \delta T_{\mu\nu} \tag{1.88}$$

with the perturbation with respect to the background equal to

$$\delta T^\mu_\nu = (\delta\rho + \delta P)u^\mu_{(0)}u^{(0)}_\nu + (\rho_0 + P_0)(\delta u^\mu u^{(0)}_\nu + u^\mu_{(0)}\delta u_\nu) - \delta P\delta^\mu_\nu - \Pi^\mu_\nu \tag{1.89}$$

where a priori there could be added also a traceless anisotropic stress tensor Π^μ_ν.
In particular, the source properties, as density, pressure and four-velocities, will be expressed as the addition to the background quantities of the sum over the (r) perturbative orders (r=1:linear order) as in [30]:

$$\rho = \rho_0 + \sum_{r=1}^{\infty} \frac{\delta\rho^{(r)}}{r!} \qquad p = p_0 + \sum_{r=1}^{\infty} \frac{\delta p^{(r)}}{r!}^9 \qquad u^\mu = \frac{1}{a}\left[\delta^\mu_0 + \sum_{r=1}^{\infty} \frac{v^\mu_{(r)}}{r!}\right] \tag{1.90}$$

where $\delta\rho$ and δp are scalar perturbations, while v^μ is a vector one.
From the normalization condition of the four-velocity $u^\mu u_\mu = -1$, or better from its perturbation at linear order, it is possible to explicitly derive a link between the linear perturbative order of the peculiar velocity $v^0_{(1)}$ and the scalar perturbations of the metric, where only $A = \Psi$ and $C = \Phi$ differ from zero, as we put ourselves in the Newtonian gauge. If we would have perturbed the normalization condition at the r-th order, we would have found the link between $v^0_{(r)}$ and the metric perturbations. Especially, at linear order [25]

$$u^\mu = a^{-1}[1 - A, v^i] \qquad\qquad u_\mu = a[1 + A, -(v^i + B_i)] \tag{1.91}$$

Finally, the perturbed energy-momentum tensor (1.89) will have non-zero off-diagonal terms, due to peculiar velocities v^i [32]:

$$T^0_0 = -\rho(1 + \delta)$$
$$T^0_i = -(\rho + P)v_i$$
$$T^i_j = (P + \delta P)\delta^i_j + \Pi^i_j$$

with $\delta = \delta\rho/\rho$ density contrast.

[9] $\delta\mathrm{p} = \mathrm{c}_s^2\delta\rho + \delta p_{non\ adiabatic}$

1.3.3 Probes of inhomogeneities

Cosmic Microwave Background anisotropies

As we already said at the very beginning of this Section, the first evidence of matter density inhomogeneities comes from large scale structure (LSS), indeed the standard cosmological model provides, in both Newtonian and General Relativity frameworks, powerful tools to calculate the evolution over time of these perturbations.
However, up to now, we have restricted our observations to the matter sector, whereas at earlier times radiation was a relevant component, as already argued while dealing with the homogeneous FLRW Universe, and it was also strongly coupled to baryons before t_{dec}. Hence, we should find imprints of these baryon density perturbations in the form of radiation density perturbations as well. Since the CMB is the relic of the earliest hot and dense phase of the Universe, it constitutes the most promising way to obtain information on the evolution of the Universe, namely of perturbations as well.

The signature of perturbations related to the radiation sector, specifically to the CMB, is the presence of temperature anisotropies, defined as

$$\frac{\Delta T}{T_0}(\theta,\phi) = \frac{T(\theta,\phi) - T_0}{T_0} \tag{1.92}$$

where (θ,ϕ) are angular sky coordinates, while T_0 is the current mean temperature of the Cosmic Microwave Background radiation.

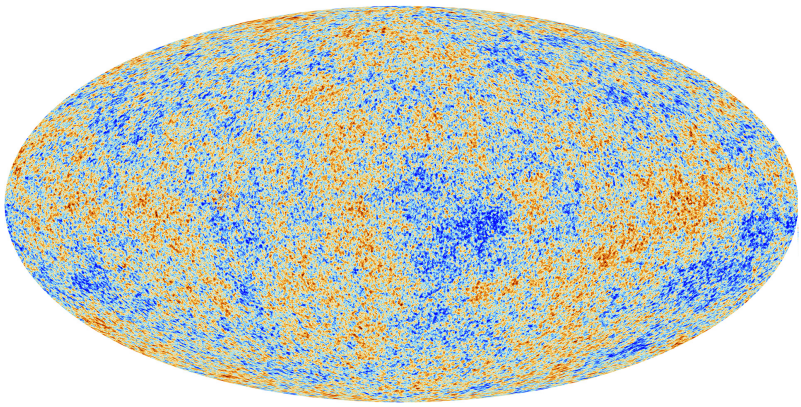

Figure 1.6: This is a map of the CMB temperature from Planck. Figure from `https://www.esa.int/spaceinimages/Images/2013/03/Planck_CMB`

The first detection of fluctuations in the sky temperature of the CMB dates back to 1992 by the COBE team, while, more recently, WMAP and Planck satellites revealed a pattern of anisotropies, that are nowadays estimated to be of the order of $10^{-5}K$.

The main reason why we find these features in the temperature distribution is that for relativistic non-degenerate bosons [13]

$$\rho_\gamma = \frac{\pi^2}{30} g_* T^4 \quad , \tag{1.93}$$

where photons have two spin states ($g_* = 2$). Hence, density perturbations led to perturbations in temperature, as

$$\frac{\Delta T}{T_0} = \frac{1}{4}\frac{\delta\rho_\gamma}{\rho_\gamma} \quad . \tag{1.94}$$

In order to provide a statistical characterization of fluctuations in the CMB temperature on the sky, the usual procedure is to expand Eq.(1.92) in spherical harmonics, such that

$$\frac{\Delta T}{T}(\theta,\phi) = \sum_{l=0}^{\infty}\sum_{m=-l}^{l} a_{lm}Y_{lm}(\theta,\phi) \tag{1.95}$$

where l is defined as the multipole order. Commonly the sum over the multipole orders is taken over $l \geq 2$, since we are interested in analyzing the intrinsic nature of these anisotropies, as consequences of density fluctuations. Indeed, on one hand, the monopole ($l = 0$) basically alters the mean temperature on a particular observers sky, while, on the other hand, the dipole term ($l = 1$) is caused by the motion of the observer (i.e. the Earth) through space. The remaining $l \geq 2$ modes are attributable to both primary and secondary effects, where the former are related to phenomena that affect photons energy (i.e. temperature, frequency) at the last scattering surface ($z_{rec} \sim 1080$), while the latter are related to those that act from the last scattering surface to the observer.

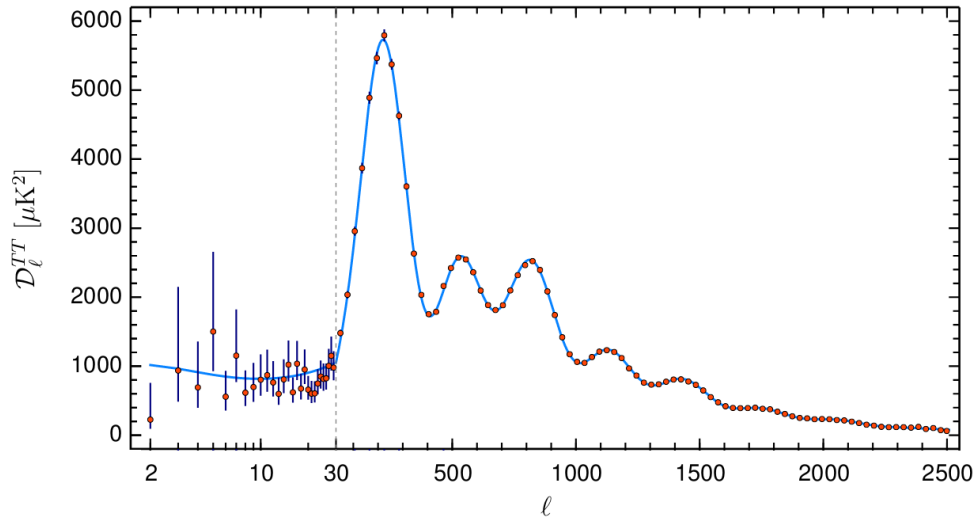

Figure 1.7: Cosmic Microwave Background (CMB) angular power spectrum of temperature anisotropies, where $D_l^{TT} = l(l+1)C_l^{TT}/2\pi$. The solid line is ΛCDM, the best fit. Figure adapted from [3]

$Y_{lm}(\theta,\phi)$ functions constitute a complete orthonormal set of functions on the sphere surface and their coefficients a_{lm} are generally complex and satisfy the condition

$$\langle a^*_{l'm'}a_{lm}\rangle = C_l\delta_{ll'}\delta_{mm'} \tag{1.96}$$

where $C_l = \langle|a_{lm}|^2\rangle$ is defined as the angular power spectrum.

From the entire temperature anisotropies angular power spectrum of Fig.1.7 we can distinguish three main regimes: large ($2 \lesssim l \lesssim 30$), intermediate ($30 \lesssim l \lesssim 1000$) and small scales ($1000 \lesssim l \lesssim 2500$). The standard model of Cosmology provides a full explanation of the evolutionary mechanisms of these anisotropies; in particular, depending on the scale there will be different contributions, as for instance, we expect gravitational effects alone at the largest scales, while decreasing the scale also pressure starts acting very efficiently, resulting in the oscillating pattern of Fig.1.7. The nature of these effects will be explained throughout the following sections.

Integrated Sachs Wolfe effect On larger scales the only interaction is the gravitational one, hence all the effects on CMB at these scales, in terms of cosmological perturbations, will be linked to the Newtonian potentials Ψ and Φ. The Integrated Sachs Wolfe (ISW) effect is the source of secondary anisotropies on large scales and it is linked to the evolution of the potentials over time. Considering for example a photon that enters a potential well and suffers blueshift, this can be then redshifted, while exiting the well, of a different quantity, resulting in an overall change in frequency.
In particular, [33]

$$\frac{\Delta T_{ISW}}{T_0} = -\int \frac{d(\Psi+\Phi)}{dt} a(t) d\chi \tag{1.97}$$

with χ defined as the comoving distance and the integration is along the line of sight. Hence, by definition, the ISW give information on the evolution over time of the sum of the two potentials along the line of sight.

Sunyaev-Zel'dovich effect The SZ effect is a source of CMB secondary anisotropies at small scales. While CMB photons are passing through a cluster, they get scattered; however, since the electrons of the hot-plasma are far hotter than photons, the latter suffer inverse Compton scattering. Thus, this effect induces a shift and moderately changes to the black-body spectrum shape, as shown in Fig.1.8.

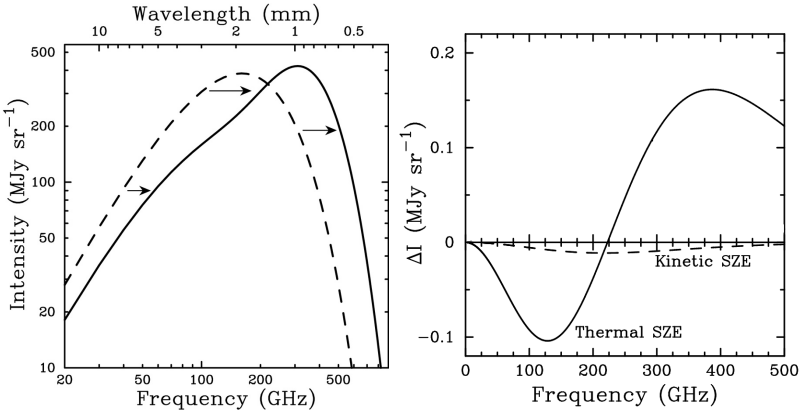

Figure 1.8: The left panel shows the Cosmic Microwave Background (CMB) spectrum, undistorted (dashed line) and distorted by the Sunyaev-Zeldovich effect (SZE) (solid line). The right panel shows the intensity distortions, due to kinetic and thermal SZ effects. [34]

There is an overall decrease of photons in the lower frequency region, as they move to the higher one.
Depending on the motion of the electrons, it is possible to distinguish between thermal and kinetic SZ effects, where in the first case the high energy of electrons is linked to their temperature T_e and the produced anisotropy [34]

$$\frac{\Delta T_{SZE}}{T_0} = f(x) \int n_e \frac{k_B T_e}{m_e c^2} \sigma_T dl \tag{1.98}$$

depends on the Thomson cross section σ_T, on the electron number density n_e and rest mass energy $m_e c^2$, on the Boltzmann constant k_B, and the integration is along the line of sight. Moreover, x is defined as a dimensionless frequency $x = \frac{h\nu}{k_B T_{CMB}}$ and $f(x)$ is a specific function of it [34]. In the second case electrons are highly energetic due to their bulk motions and generate a thermal distortion of magnitude

$$\frac{\Delta T_{SZE}}{T_0} = -\tau_e \frac{v_e}{c} \tag{1.99}$$

that depends on their relative velocity v_e and on the optical depth τ_e.

Matter distribution and peculiar velocities

The relevant variables for observables describing LSS are the two Newtonian potentials Φ and Ψ, the matter density contrast δ_m and the matter velocity perturbation v. Then, the evolution of these variables will be provided by four equations, calculated using cosmological perturbation theory in Fourier space, restricting ourselves to linear order. The equation for the evolution of matter density perturbations is given by a combination of fluidodynamics laws: the continuity and the Euler equations. Since we are interested in perturbations well within the horizon, we are enabled to restrict to the Newtonian treatment, in which case the evolution of matter density perturbations is determined by Eq.(1.69).
The r.h.s. of Eq.(1.69) can be expressed as a function of the Newtonian potential Ψ, via the Poisson equation (Eq.(1.58)), that can be even obtained from the (00)-component of the Einstein's equations, in the Newtonian limit. Hence, passing to Fourier space, the evolution equation becomes

$$\ddot{\delta}_m + 2H\dot{\delta}_m + \frac{k^2}{a^2}\Psi = 0 \tag{1.100}$$

The evolution of matter density perturbations is linked to the expansion history and Ψ: to solve Eq.(1.100) the Dark Energy equation of state is needed, as well as the potential Ψ. The latter is constrained by the anisotropic stress Eq.(1.101) and the Poisson Eq.(1.102) equations, respectively found solving the trace-free part of the linearly perturbed Einstein's equations and combining the (00) and $(0i)$ components

$$k^2(\Phi - \Psi) = 12\pi G a^2(\rho + P)\sigma \tag{1.101}$$

$$k^2\Phi = -4\pi G a^2 \rho\Delta \tag{1.102}$$

with $\rho\Delta = \rho\delta + 3\frac{aH}{k}(\rho + P)v$ the comoving density perturbation and the anisotropic stress σ such that $(\rho + P)\sigma = -(k^i k_j - \frac{1}{3}\delta^i_j)\Pi^i_j$ [25], where δ^i_j is the Kronecker δ. During the epoch relevant for structure formation, in ΛCDM the two potentials are equal, due to a null anisotropic stress, and very simply related to the density contrast via the Poisson equation.
Finally, the equation that determines the velocity field can be derived by the covariant conservation of the perturbed energy-momentum tensor and yields [13]

$$\dot{\delta}_m + ikv = 0 \tag{1.103}$$

in Fourier space.

As the evolution of the matter density contrast (Eq.(1.100)) is linked only to Ψ, matter distribution and peculiar velocities can give information on the Newtonian potential.
First, the evolution over redshift of matter distribution can be obtained by Galaxy Counts (GC) at different redshifts, that consists of determining the observed number of galaxies with flux higher than a fixed lower limiting magnitude. Many projects were involved in order to do GC, as 2MASS (Two Micron All-Sky Survey) and SDSS (Sloan Digital Sky Survey).
Second, the main observations of peculiar velocities come from redshift-space distortions (RDS) and from the Sunyaev-Zel'dovich (SZ) effect.
As the name suggests, redshift-space distortions consist of shapes distorted in the redshift space. For example, let us consider a distant galaxy cluster that is undergoing a spherical collapse, as soon as we move from real space to redshift space its shape get distorted, as the moving boundary points of the cloud will contribute with different peculiar velocities along the line of sight, i.e. with different redshifts (Eq.(1.17) in the local Universe) in addition to that caused by the cosmological expansion. Indeed, the galaxies closest to us moving toward the center of the overdense region and hence away from us, will appear farther from us than they actually are. Similarly, galaxies on the opposite side of the perturbation are moving toward us, so they appear closer to us than they actually are [13]. The magnitude of the distortion rises, as the region becomes more overdense.
RSD is one of the main scientific targets in ongoing and forthcoming galaxy redshift surveys such as BOSS (The Baryon Oscillation[10] Spectroscopic Survey) in SDSS-III, eBOSS in SDSS-IV, SKA

[10] discussed in Sect.1.4.1

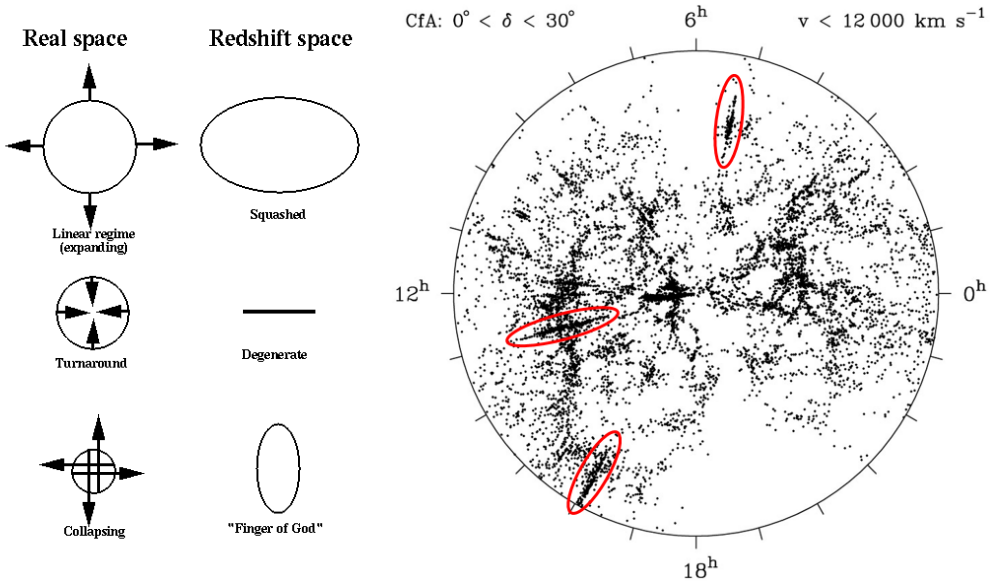

Figure 1.9: The left panel shows the shape distortions due to peculiar velocities, passing from the real space to the redshift space; the Figure is taken from http://www.astr.ua.edu/keel/galaxies/hamcollapse.gif. The right panel is the map of the distribution of galaxies in the nearby Universe, between declination $\delta = 0°$ and $30°$, where the maximum recession velocity is 12000 km $\cdot$ s^{-1}. The highlighted regions are the so called 'fingers of god', that point radially towards the center of the diagram, where our Galaxy is located.

(Square Kilometre Array), DESI (Dark Energy Spectroscopic Instrument, starting in 2019)[11] and EUCLID (launch in 2021)[12].

Weak Lensing of galaxies

Photon's geodesics are linked to a linear combination of Ψ and Φ, indeed the photon trajectory $x^\mu(\lambda)$, following from the geodesics equation, will satisfy [33]

$$\frac{d^2x^\mu}{d\lambda^2} \propto \vec{\nabla}_\perp(\Psi + \Phi) \tag{1.104}$$

so that any information strictly related to photon path will give information on the potentials combination, thus their evolution.
Gravitational Lensing, in a general manner, consists of the deflection of light rays when they propagate through an inhomogeneous gravitational field, in particular we define the sources of this field as lenses. In this context, we are interested in the Weak gravitational Lensing (WL) of galaxies photons, which is sourced by the structure they go through. Hence, it can track the matter distribution and the i-th component of deflection angle (two component vector in the sky) given by [33] is

$$\alpha_i = \int -\partial_i(\Psi + \Phi)ds \tag{1.105}$$

where ds is the path infinitesimal element.
Hence, measurements of the Weak Lensing shear distribution over multiple redshift bins can provide an estimate of the space and time variation of the Lensing potential, defined as $\frac{\Psi+\Phi}{2}$ [16]. WL measurements comes from LSST (Large Synoptic Survey Telescope), HST (Hubble Space Telescope), SKA and EUCLID.

[11] https://www.desi.lbl.gov/
[12] http://sci.esa.int/euclid/

1.4 The late cosmic acceleration

1.4.1 Observational evidence

There exist numerous observational evidences for the late cosmic acceleration, in particular related to the background evolution directly (geometrical probes for example) and to the growth of structures. I will first start with Type Ia SNe, since they provided the first evidence of the late phenomenon, then I will move on to the simplest evidence coming from the direct estimate of the Universe age today and finally I will focus on the CMB probes.

Type Ia Supernovae

The first evidence of the cosmic acceleration came from Type Ia Supernovae observations in 1998, measuring their luminosity distances $d_L(z)$ [2] [1], as they are sources of which the intrinsic luminosity can be known.

Type Ia supernovae are thermonuclear explosions of Carbon-Oxygen white-dwarves (WDs), that exceed the Chandrasekhar mass limit M_{Ch}. In particular, the WD of a binary system accretes mass from the companion star within the Roche lobe: the WD is, roughly speaking, a core whose pressure is sustained by electron degeneracy, once the WD has reached M_{Ch} while accreting, this pressure can not balance self-gravity anymore. The star reaches the temperature and density for Carbon burning, but since the core is degenerate, then the burning is unstable and the star undergoes the incineration of all material in the WD core up to Fe-peak elements. An explosive burning flame starts to propagate outwards, behind which material undergoes explosive nuclear burning.

Two main properties of this kind of SNe led to the discovery: they are very bright explosion events and they are standardizable candles with a nearly constant absolute magnitude $M_V \sim -19.5mag$. From the absolute magnitude M and the observed apparent magnitude m, the luminosity distance can be inferred using the distance modulus

$$M - m = 5 - 5logd_L \tag{1.106}$$

So, on one hand, Type Ia SNe observations give us the observed dependence of the luminosity distance over redshift z, which is independently known from the spectral lines shifts (Eq.(1.17)). On the other hand, this dependence can be then fitted via the theoretical relation between the luminosity distance and the Hubble parameter $H(z)$, which is that of Eq.(1.43) for a flat Universe. In this way Type Ia SNe can constrain the density parameters.

Theoretically, if we consider the second Friedmann equation (Eq.(1.23b)), under the assumption of a single fluid component, the condition of cosmic acceleration is satisfied whenever

$$\ddot{a}(t) > 0 \Leftrightarrow -\frac{4\pi G}{3}(\rho(t) + 3p(t)) > 0 \Leftrightarrow p < -\frac{1}{3}\rho \Leftrightarrow w < -\frac{1}{3} \quad , \tag{1.107}$$

hence, if there exists a fluid component with EoS $w < -1/3$. Then, the Cosmological Constant is a good candidate to explain this acceleration, since $w_\Lambda = -1$ (Tab.1.1). Furthermore, if we generally define Dark Energy as the fluid with constant EoS $w < -\frac{1}{3}$, DE affects the expansion history as

$$H(z) = H_0[\Omega_M(1+z)^3 + \Omega_{rad}(1+z)^4 + \Omega_{DE}(1+z)^{3(1+w_{DE})}]^{1/2} \tag{1.108}$$

Different models can fit the data (Fig.1.10), in particular, referring to the ΛCDM model, there is a degeneracy between the two density parameters Ω_m and Ω_Λ [13]. To break this degeneracy it is necessary to obtain other constraints on this two cosmological parameters, from other datasets, for instance BAO (Baryon acoustic oscillations) and CMB (right panel Fig.1.12).

[13] Ω_{DE} in the Λ scenario.

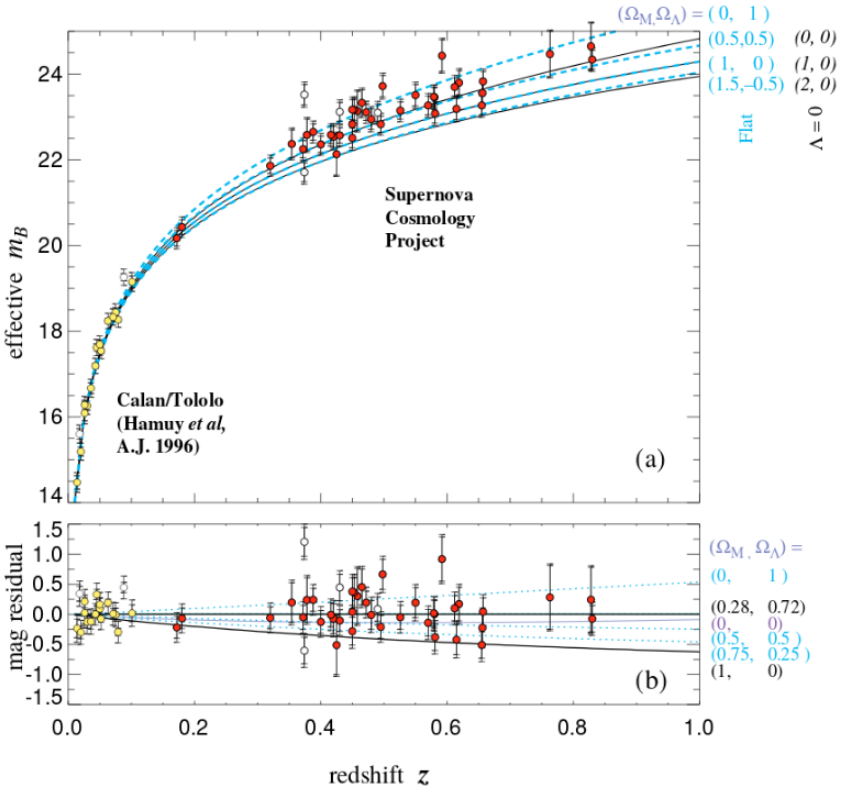

Figure 1.10: Hubble diagram for Type Ia Supernovae, [2]. In this plot is shown the effect of the density parameters choice on the luminosity distance evolution.

Age of the Universe

Cosmic acceleration can be supported considering the theoretically inferred age of a near-flat Universe and its consistency with the oldest globular clusters age.
From the expansion history (1.108), it is possible to estimate the age of the Universe today t_0 via the density parameters:

$$\begin{aligned} t_0 &= \int_0^{t_0} dt = \int_0^1 \frac{dt}{da}\frac{a}{a} da = \int_1^\infty \frac{1}{H(z)(1+z)} dz \\ &= \frac{1}{H_0}\int_1^\infty \frac{dz}{\left[\Omega_M(1+z)^3 + \Omega_{DE}(1+z)^{3(1+w_{DE})}\right]^{1/2}(1+z)} \end{aligned} \tag{1.109}$$

having considered a flat Universe and neglecting the radiation contribution, since it is dominant only at high redshift, that are suppressed in the integration.
If there would not be any Dark Energy component, $\Omega_M \sim 1$ and $\Omega_{DE} = 0$, the integral would lead to [35]

$$t_0 = \frac{2}{3H_0} \tag{1.110}$$

which is, for the H_0 measured value, less than the globular clusters age.
The way to fix the problem is then to assume the presence of a Dark Energy component, since t_0 increases at decreasing Ω_M.

Cosmic Microwave Background

As we have just seen in Sec.1.3, the induced small deviations in the isotropic distribution of the Cosmic Microwave Background, namely its temperature anisotropies, is the most promising way to obtain information on the evolution of the Universe, hence on the late cosmic acceleration as well.

On one hand, we have already seen that the Integrated Sachs-Wolfe (ISW) effect, as defined in Eq.(1.97), provides a measure of the time variation of the two Newtonian potentials Φ and Ψ of the perturbed metric (Eq.(1.87)) along the line of sight. Indeed, while travelling towards the observers, CMB photons suffer a net change in frequency, as they go in and out gravitational potential wells that varies because of the Universe expansion. Moreover the rate of change of the potentials will be directly related to the rate at which the Universe is expanding, providing an evidence for the late cosmic acceleration.

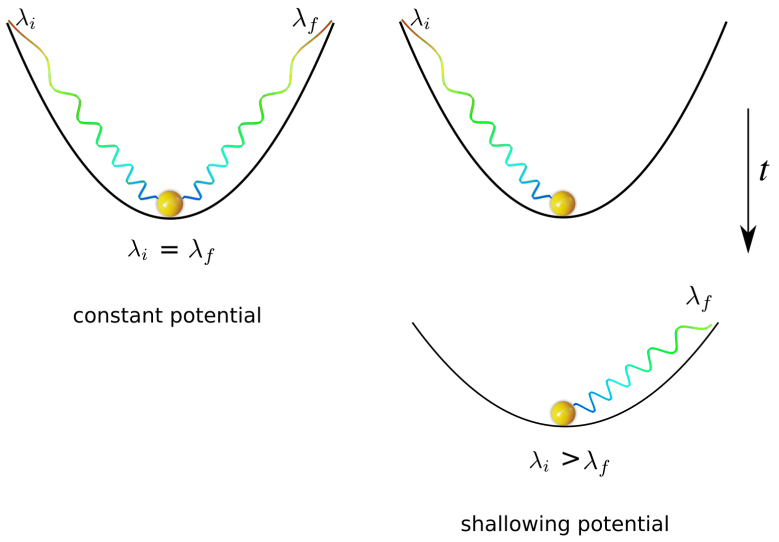

Figure 1.11: Schematic representation of the ISW effect, taken from [32]

ISW effect acts on large scales, where gravity alone plays the key role; however, as we move to smaller scales pressure starts to become important. Hence, on intermediate scales the CMB anisotropies power spectrum (Fig.1.7) clearly shows an oscillating pattern that, according to ΛCDM, is the result of forced oscillations, that took place before the decoupling between photons and baryons. Indeed, the strong coupling provided the pressure necessary to baryons to prevent the collapse inside the DM halos; this interplay between gravity and pressure gave rise to acoustic oscillations.
The first acoustic peak constrains the sum of all the density parameters to be approximately equal to 1 (i.e. curvature $k = 0$), a priori it does not constraint a non-zero Ω_Λ; but, it represents a very powerful tool to constrain its value together with Type Ia SNe and large scale data, that can constrain the contributes separately. Furthermore, the multipole order at which the first peak is located gives information on the size of the sound horizon at the decoupling, that is defined as the maximum distance that a sound wave could have traveled between the Big Bang and recombination. Therefore, since any l is defined as a function of the angular dimension θ, the observed l_{peak} yields the angular dimension of the sound horizon, which is then linked to the linear size via the angular diameter distance d_A (Eq.(1.45)).

CMB spectrum is well fitted by models that undergo late accelerated expansion. Currently, by the recent *Planck 2018* data release [3], CMB constrains the already mentioned standard cosmological parameters as in Tab.1.2.

Parameter	Planck TT,TE,EE+lowE+lensing
$H_0[km\ s^{-1}\ Mpc^{-1}]$	67.36 ± 0.54
Ω_Λ	0.6847 ± 0.0073
Ω_m	0.3153 ± 0.0073

Table 1.2: Some of the standard cosmological parameters from [3].

Baryon acoustic oscillations

The same acoustic oscillation visible in the CMB power spectrum left an imprint on the spatial distribution of baryons on large scales (left panel of Fig.1.12). Indeed, after decoupling, photons started to travel unimpeded, leaving behind a shell of baryonic matter at a radius fixed by the size of the sound horizon at t_{dec}; without the photons pressure, baryons and DM (left behind at the center of the perturbation) formed a configuration which included overdensities of matter at both the center of the perturbation and at the position where baryons decoupled from photons [14].
Baryon acoustic oscillations (BAO) constitutes a geometrical probe: measurement of this configuration over a wide range of redshifts give us the observed relation between distance and redshift $d_A(z)$, comparable with the theoretical one Eq. (1.45), as done above for Type Ia Supernovae.
Let us define the acoustic length scale r_s as the comoving distance traveled by a sound wave from $t = 0$ to the time of the photons-baryons decoupling t_{dec}, so [15]

$$r_s = \int_0^{t_{rec}} \frac{c_s(t)}{a(t)} dt = \int_{z_{rec}}^{\infty} \frac{c_s(z)}{H(z)} dz \quad . \tag{1.111}$$

A measure of BAO along the line of sight will give a measure of $H(z)r_s$, thus to derive the expansion history a measure of r_s will be needed from CMB, in particular from the position of the first acoustic peak.

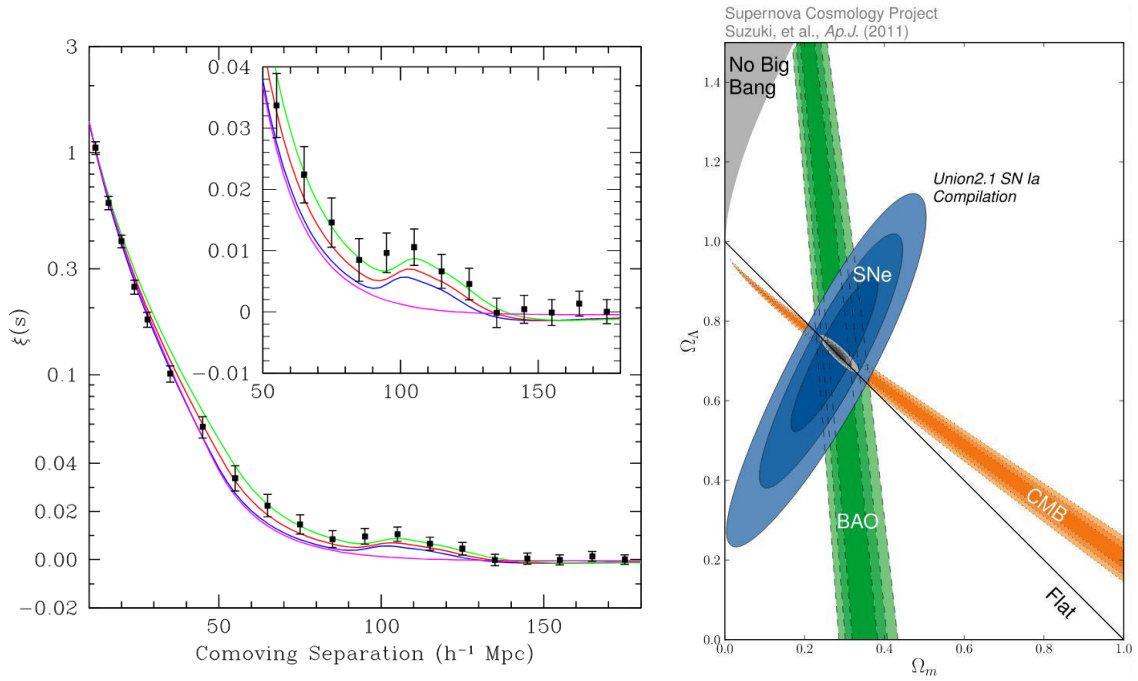

Figure 1.12: The left panel is the large scale redshift-space correlation function of the SDSS sample, from [36]. The right panel shows the observational constraints on the matter and Dark Energy density parameters, obtained by using Type Ia Supernovae, BAO and CMB. Figure taken from [37]

[14] Very useful animations can be found at https://www.cfa.harvard.edu/ deisenst/acousticpeak/acoustic_physics.html

1.4.2 Cosmological constant

As we have already seen, Einstein wrongly added a scalar degree of freedom to Eq.(1.10) in order to reproduce a static-Universe: that is the Cosmological Constant Λ, introduced as an extra term to the Einstein-Hilbert action as in Eq.(1.14). As demonstrated in Eq.(1.15), Λ contributes to the field equations

$$R_{\mu\nu} - \frac{1}{2}Rg_{\mu\nu} + \Lambda g_{\mu\nu} = 8\pi G T_{\mu\nu} \tag{1.112}$$

via the new covariant term $\Lambda g_{\mu\nu}$.

Due to this extra degree of freedom that influences the dynamics of the system, the derived Friedmann equations slightly change into

$$\left(\frac{\dot{a}(t)}{a(t)}\right)^2 = \frac{8\pi G}{3}\sum_i \rho_i(t) - \frac{k}{a^2(t)} + \frac{\Lambda}{3} \tag{1.113a}$$

$$\frac{\ddot{a}(t)}{a(t)} = -\frac{4\pi G}{3}\sum_i (\rho_i(t) + 3p_i(t)) + \frac{\Lambda}{3} \tag{1.113b}$$

where, now that they are computed, we can completely understand the mathematical reason why Λ would have led to a static Universe. A static Universe is characterized by the set of conditions

$$\begin{cases} \dot{a} = 0 \\ \ddot{a} = 0 \end{cases} \tag{1.114}$$

hence, from the Friedmann equations of Eq.(1.113) in the hypothesis of matter domination (i.e. $p = 0$), we find that the static Universe corresponds to

$$\begin{cases} \frac{8\pi G}{3}\rho_m(t) - \frac{k}{a^2(t)} = -\frac{\Lambda}{3} \\ \frac{4\pi G}{3}\rho_m(t) = \frac{\Lambda}{3} \end{cases} \Rightarrow \begin{cases} \frac{k}{a^2(t)} = \Lambda \\ \frac{\Lambda}{4\pi G} = \rho_m(t) \end{cases} \tag{1.115}$$

Despite the fact that the Einstein's Cosmological Constant was abandoned right after the Universe expansion discovery, Λ had been reintroduced to explain the late cosmic acceleration, as an energy density source with $w_\Lambda = -1$ (the Λ term then shifts to the r.h.s. of Eq.(1.112)).

In particular, one way to look at the Cosmological Constant is to represent it as vacuum energy, such that its energy is the one related to quantum fluctuation of the vacuum. Its pressure and density can be described by the extra term in Eq.(1.112):

$$\begin{aligned} 8\pi G T^{\Lambda}_{\mu\nu} &= -\Lambda g_{\mu\nu} \\ &= 8\pi G\left[(\rho_\Lambda + p_\Lambda)u_\mu u_\nu + p_\Lambda g_{\mu\nu}\right] \quad \Leftrightarrow p_\Lambda = -\frac{\Lambda}{8\pi G} = -\rho_\Lambda \\ &= 8\pi G p_\Lambda g_{\mu\nu} \quad [w_\Lambda = -1] \end{aligned} \tag{1.116}$$

Up to now the Cosmological Constant constitutes the best fit to data. Referring to the right panel of Fig.1.12, Type Ia SNe, BAO and CMB data, under the Λ assumption, constrain the matter and Dark Energy density parameters to be respectively $\Omega_m \sim 0.3$ and $\Omega_\Lambda \sim 0.7$; hence, the standard model of cosmology is named ΛCDM after the late dominance of the Cosmological Constant, as source of the late cosmic acceleration, and Cold Dark Matter, that prevails over baryons abundance.

1.5 Problems of ΛCDM model

Besides the successful predictions of ΛCDM model, the latter comes along with many problems, mainly linked to the initial conditions:

- This model is based on the assumption that General Relativity still holds at large scales and early times (up to Planck time $t_P \sim 10^{-43}s$), but it does not give any explanation to what happened at $t < t_P$, as we enter the *quantum gravity* regime.
- The nature of Dark Matter (DM) is still unknown and largely studied, since it is one of the main constituents of the Universe energy content. Using DM, the standard model provides an explanation of cosmic structure formation and acoustic oscillations that left an imprint on both CMB anisotropies and matter distribution (BAO). Moreover, the standard model requires the DM component to be cold when it decoupled from the thermal bath; that is demanded in order to reproduce hierarchical clustering, which is the scenario in agreement with observations. Hot Dark Matter (HDM) would have suppressed small scales perturbations, leading first to the formation of the largest structures and, secondly, to those at lower scales by fragmentation.
- Increasing the temperature, going backward in time, the degree of symmetry rises, hence, even matter and anti-matter should have been in a symmetric configuration. The origin of the asymmetry between matter and antimatter, namely the *Baryogenesis problem*, is still not clear.
- It does not provide a mechanism for the origin of density perturbations
- **Horizon Problem** An important question that the model has to tackle, in order to justify its basic assumptions, is to understand the origin of the inferred homogeneity. Considering the region of characteristic comoving dimension λ entering the comoving Hubble radius r_H at time t_H (Fig.1.5), if $t_H > t_{rec}$ how could homogenization have happened at that scale if at that time photons were already decoupled?
- **Flatness Problem** Taking the last equality of Eq.(1.32) and defining $\Omega_k = -\dfrac{k}{a^2H^2}$ then

$$\Omega_{k,0} = 1 - \Omega_0 \quad . \tag{1.117}$$

  If $\Omega_{k,0} < 0.0005$ at 95% c.l. then $|1 - \Omega_0| < 10^{-2}$, which yields a fine tuning problem, why should the Universe have started with such a strict condition?

- **Cosmological constant problems** Since Λ is the dominant Universe component, from Eq.(1.113a) it is clear that at present we require Λ to be of the order of $H_0^2 \sim (2.1332h \times 10^{-42}Gev)^2$ [35]. Hence, since $\rho_\Lambda = \frac{\Lambda}{8\pi G}$,

$$\rho_\Lambda \sim H_0^2 M_{Pl}^2 \sim 10^{-47} GeV^4 \quad . \tag{1.118}$$

  Since the Cosmological Constant energy density ρ_Λ is constant over time by definition, its contribution to the Universe energy budget can be thought to be that of the vacuum energy, which is the state of minimum energy, characterized by a constant ρ_V. The calculation of the latter is computed within particle physics: considering a quantum field as a set of harmonic oscillators, since the theory is thought to be reliable up to Planck scale, the energy density of the vacuum can be written as

$$\rho_V \sim \frac{k_{max}^4}{16\pi^2} \sim \frac{M_{Pl}^4}{16\pi^2} \quad . \tag{1.119}$$

  From this calculation it results that $\rho_V \sim 10^{74} GeV^4$, a mismatch of ~ 120 order of magnitude with respect to ρ_Λ! That is the Cosmological Constant Problem: why such a tiny amount of ρ_Λ ?
  Another significant question would be: why now? That constitutes the so-called coincidence problem. Apart from its tiny value, $\rho_{\Lambda,0}$ has the same magnitude as the present matter density $\rho_{M,0}$, despite their ratio changes with time as $(1+z)^3$ and thus very rapidly.

- **H_0 tension** between the value obtained from local measurements [4] and that inferred by high redshift observations [3] under the Λ assumption

  $$H_0^{SH_0ES} = 73.48 \pm 1.66\ kms^{-1}Mpc^{-1} \qquad H_0^{Planck} = 67.36 \pm 0.54\ kms^{-1}Mpc^{-1}$$

  Is this tension due to systematic effects on the observations or is it a hint that we have to drop the assumption of a ΛCDM expansion?

As it goes beyond the scope of the Thesis, I will only mention that a solution to the Horizon and Flatness problems is assuming the existence of an early accelerated expansion phase, named Inflation (already spoiled in Fig.1.3). Since this phase is supposed to have been driven by a dynamical scalar field, its quantum fluctuation would have then caused the density fluctuations needed for LSS formation and imprinted in the CMB anisotropies. For a detailed description I suggest the further readings [13][14][28][38].

The two last problems are basically the main motivation to my Thesis work, as I will discuss in the following Chapter.

2 | Beyond ΛCDM model

As just pointed out in the previous Chapter, the standard cosmological model has still unclear aspects and some of the problems related to it are the motivations underlying my Thesis work. On one hand, the theoretical issues related to Λ have prompted the exploration for alternative dynamical ways of sourcing cosmic acceleration, as Dark Energy (DE) and Modified Gravity (MG) models. On the other hand, in absence of evident systematic effects, the discrepancy between local and high redshift measurements of the Hubble parameter have encouraged cosmologists to investigate beyond ΛCDM models.
First, I will introduce some of these alternative models, focusing on how they might be used as viable models for cosmic acceleration. Then, in the second part of the Chapter, I will overview some of the parametric approaches adopted in literature in order to ease the H_0 tension. In this context, referring for instance to the reconstruction of the DE Equation of State $w_{DE}(z)$, by parametric approach I mean that the redshift dependence is an assumed function of some parameters.
Thus, the aim of this Chapter is to set the ground to the non-parametric approach I will develop in the next one and apply to DE and MG models.

2.1 Alternative models to the Cosmological Constant

A good starting point is the action, since from it we can derive all we need to study the dynamics of the Universe, once the metric tensor $g_{\mu\nu}$ and the properties of the energy sources are specified. While Dark Energy models introduce a new dynamical component in the cosmic energy budget, typically modeled by a scalar field, Modified Gravity theories modify the laws of gravity in the low curvature regime, to admit self-accelerating solutions in the presence of negligible matter. For the regime of interest to us, they both result in the freeing of additional degrees of freedom to the standard action of Eq.(1.10)

$$S = S_{EH} + S_M = \frac{1}{16\pi G}\int d^4x\sqrt{-g}\,(R + 16\pi G\mathcal{L}_M) \quad . \tag{2.1}$$

2.1.1 Dark Energy

This class of models is based on the existence of a fluid (i.e. field), generally named as Dark Energy (DE), characterized by a negative w, since we require the second time derivative of the scale factor to be positive (Eq.(1.107)), in order to reach the acceleration regime.
There exist multiple DE models, from the simplest canonical scalar field, named Quintessence, to K-essence [39] [35] and coupled DE [40][35], i.e. models based on the interaction among the Dark sector components or between these and ordinary matter.
The new component will contribute to the energy-momentum tensor $T_{\mu\nu}$ of the standard fluids with $T^{DE}_{\mu\nu}$, where its pressure p_{DE} and density ρ_{DE} must satisfy the condition found in Eq.(1.107). Since we are simply modifying the Universe energy content, the extra energy-momentum tensor $T^{DE}_{\mu\nu}$ term will appear on the r.h.s. of Eq.(1.6), yielding

$$R_{\mu\nu} - \frac{1}{2}Rg_{\mu\nu} = 8\pi G T_{\mu\nu} + 8\pi G T^{DE}_{\mu\nu} \ . \tag{2.2}$$

Quintessence

Quintessence is a scalar field ϕ with slowly varying potential and it interacts with the others only gravitationally, so that the resulting total action is

$$\begin{aligned} S &= S_{EH} + S_\phi + S_M \\ &= \int d^4x\sqrt{-g}\left(\frac{M_P^2}{16\pi}R + \mathcal{L}_\phi + \mathcal{L}_M\right) \end{aligned} \tag{2.3}$$

where $\mathcal{L}_\phi$ is the Lagrangian density of the field. $\mathcal{L}_\phi$ is made up of the standard kinetic term and a potential that depends only on the scalar field itself

$$\mathcal{L}_\phi = \frac{1}{2}g^{\mu\nu}\partial_\mu\phi\partial_\nu\phi - V(\phi) \tag{2.4}$$

For any energy source that contributes to the dynamics of the system, i.e. to the action, with $S_i = \int d^4x\sqrt{-g}\mathcal{L}_i$, the energy-momentum tensor $T^{(i)}_{\mu\nu}$ is equal to

$$T^{(i)}_{\mu\nu} = -\frac{2}{\sqrt{-g}}\frac{\delta S_i}{\delta g^{\mu\nu}} \quad . \tag{2.5}$$

Quintessence will act as an energy density source with

$$\begin{aligned} T^\phi_{\mu\nu} &= \partial_\mu\phi\partial_\nu\phi - g_{\mu\nu}\mathcal{L}_\phi \\ &= \begin{pmatrix} \rho_\phi & 0 \\ 0 & p_\phi\delta_{ij} \end{pmatrix} = \begin{pmatrix} \frac{1}{2}\dot\phi^2 + V(\phi) & 0 \\ 0 & \left(\frac{1}{2}\dot\phi^2 - V(\phi)\right)\delta_{ij} \end{pmatrix} \end{aligned} \tag{2.6}$$

where we have assumed a perfect isotropic and homogeneous fluid (i.e. field), in the flat FLRW background.
Consequently, the Quintessence EoS is then

$$w_\phi = \frac{p_\phi}{\rho_\phi} = \frac{\frac{1}{2}\dot\phi^2 - V(\phi)}{\frac{1}{2}\dot\phi^2 + V(\phi)} \tag{2.7}$$

that takes value in $-1 \leq w_\phi \leq 1$, but, since the pressure must be negative, $-1 \leq w_\phi < 0$.
Assuming a flat Universe and Quintessence as the dominant energy source at present, the Friedmann equations take the form

$$\left(\frac{\dot a(t)}{a(t)}\right)^2 = \frac{8\pi G}{3}\left[\frac{1}{2}\dot\phi^2 + V(\phi)\right] \tag{2.8a}$$

$$\frac{\ddot a(t)}{a(t)} = -\frac{8\pi G}{3}(\dot\phi^2 - V(\phi)) \tag{2.8b}$$

From Eq.(2.8b) it is clear that, in order to reach an accelerated expansion, i.e. $\ddot a > 0$, $\dot\phi^2$ must be smaller than the potential $V(\phi)$. Thus, the potential must be flat enough. Since $V(\phi) > \dot\phi^2$, the EoS is lower than zero, while, in the case in which the kinetic term is completely negligible with respect to the potential, we retrieve the lower limit $w = -1$. The $V(\phi) > \dot\phi^2$ condition is very similar to that required in the Inflationary scenario, namely Inflation would have occurred if the slow-roll parameters

$$\epsilon = \frac{M_{Pl}^2}{16\pi}\left(\frac{V_{,\phi}}{V}\right)^2 \qquad\qquad \eta = \frac{M_{Pl}^2}{16\pi}\frac{V_{,\phi\phi}}{V} \tag{2.9}$$

with $V_{,\phi} = \frac{dV}{d\phi}$ and $V_{,\phi\phi} = \frac{d^2V}{d\phi^2}$, satisfied the conditions $\epsilon, |\eta| \ll 1$, i.e. if the scalar field driving inflation had a sufficiently flat potential. However, as stressed by [41], these conditions are designed assuming the dominance of the inflationary field; though, since at late times, during the

DE dominance epoch, there is a non negligible energy from Dark Matter, these slow-roll conditions are not completely trustworthy. Hence, in order to account for DM contributions as well, ϵ should be properly defined as $\epsilon = -\dot{H}/H$.

From the scalar field continuity equation $\dot{\rho}_\phi + 3H(\rho_\phi + p_\phi)$, substituting the values of $\rho_\phi = \frac{1}{2}\dot{\phi}^2 + V(\phi)$ and $p_\phi = \frac{1}{2}\dot{\phi}^2 - V(\phi)$ we find the equation of motion of ϕ

$$\ddot{\phi} + 3H\dot{\phi} + \frac{dV(\phi)}{d\phi} = 0 \tag{2.10}$$

which is the Klein Gordon equation, that can be equivalently derived by varying the action S_ϕ with respect to the scalar field ϕ.
The dynamics of Quintessence has been studied for a wide variety of potentials $V(\phi)$; depending on its analytical form, it is possible to classify Quintessence models between two main classes: the *thawing* and the *freezing* models. In the first case, as its name suggests, the scalar field starts from a nearly frozen condition in the earlier epochs, due to the Hubble friction, and it evolves once the field mass, i.e. $d^2V(\phi)/d\phi^2$, drops below the Hubble expansion rate. An example of thawing solution is [35] is

$$V(\phi) = V_0 + M^{4-n}\phi^n \tag{2.11}$$

By contrast, the second class is characterized by a scalar field that slows down at late times, as $V(\phi)$ tends to be shallower than in the early epochs [42]. An example of freezing model is the Ratra-Peebles potential [43]

$$V(\phi) = \frac{M^{4+n}}{\phi^n} \tag{2.12}$$

that is also the canonical example for the class of so-called tracking solutions [44], where the energy density of the field closely traces the background energy density $\rho_M + \rho_{rad}$ up to the recent cosmic acceleration, when it grows dominating the matter and radiation terms. Hence, it provides a possible solution to the coincidence problem.

It is desirable, for Quintessence models, to provide a solution to the fine-tuning problem: that is not so easy, since we have already a constraint on the field mass, given by the slow roll conditions [35]. Thus, if

$$|\eta| = \left| M_{Pl}^2 \frac{V_{,\phi\phi}}{V} \right| \lesssim 1 \tag{2.13}$$

then the mass of the scalar field $m_\phi = V_{,\phi\phi}$ at present must satisfy

$$m_\phi \lesssim \frac{V_0}{M_{Pl}^2} \simeq H_0^2 \rightarrow m_\phi \lesssim H_0^2 \simeq 10^{-33} eV \quad , \tag{2.14}$$

where V_0 is the value of the potential at present. The mass of the scalar field must be extremely small.

2.1.2 Modified gravity

General Relativity has been tested to very high precision at very small scales, i.e. in the Solar System, and astrophysically; however, on cosmological scales it has not yet been tested with similar accuracy. Consequently, exploring modifications to gravity on large scales and whether such modifications could be responsible for the late time acceleration is a natural step forward, taking care of recovering standard GR on small scales and at early times.
There are various ways in which the laws of gravity can be modified on the largest scales. Generally Modified Gravity (MG) models involve covariant modifications to the standard Einstein-Hilbert action, that can be for instance provided by adding higher order curvature invariants, as in the case of $f(R)$ gravity, or giving the graviton a mass, as in the case of massive gravity theories. The idea behind the latter example is that while in General Relativity the gravitational long-range force is mediated by a massless spin 2 particle, i.e. the graviton, giving a mass to this particle would mediate a force characterized by a Yukawa type profile $\sim \frac{1}{r}e^{-mr}$.
Modifications to the laws of gravity can originate from extra dimensional scenarios as well: in standard GR space and time constitute a curved 3+1 dimensional manifold, whereas these particular scenarios theorize that matter fields are confined to this 4-dimensional brane embedded in a higher dimensional bulk, into which gravity may leak. In the peculiar case of the Dvali-Gabadadze-Porrati (DGP) model, the higher dimensional bulk is a 5-dimensional Minkowksi bulk of infinite volume.
These models and many others are all reviewed in [45].
In what follows I will introduce the broad class of scalar tensor theories.

Scalar tensor theories

Many DE models rely on scalar fields, whereas the latters can also enable modifications to the Einstein-Hilbert action, this time being not minimally coupled to the gravitational tensor field.
Horndeski theory constitutes the most general scalar tensor theory, with second-order equations of motion, which is required to avoid Ostrogradsky's instability. Its action is [9]

$$S = \frac{1}{16\pi G}\int d^4x\sqrt{-g}\sum_{i=2}^{5}\mathcal{L}_i + \mathcal{L}_M(g_{\mu\nu}) \tag{2.15}$$

with

$$\begin{aligned}
&\mathcal{L}_2 = G_2(\phi, X) \qquad\qquad \mathcal{L}_3 = G_3(\phi, X)\Box\phi \\
&\mathcal{L}_4 = G_4(\phi, X)R + G_{4X}(\phi, X)[(\Box\phi)^2 - (\nabla_\mu\nabla_\nu\phi)(\nabla^\mu\nabla^\nu\phi)] \\
&\mathcal{L}_5 = G_5(\phi, X)G_{\mu\nu}\nabla^\mu\nabla^\nu\phi - \frac{1}{6}G_{5X}(\phi, X)[(\Box\phi)^3 - 3(\Box\phi)(\nabla_\mu\nabla_\nu\phi)(\nabla^\mu\nabla^\nu\phi) \\
&\qquad + 2(\nabla^\mu\nabla_\alpha\phi)(\nabla^\alpha\nabla_\beta\phi)(\nabla^\beta\nabla_\mu\phi)]
\end{aligned} \tag{2.16}$$

where $X = -\frac{1}{2}\partial^\mu\phi\partial_\mu\phi$ is the kinetic term, K and G_i are functions of ϕ and the subscript (X, ϕ) denotes partial derivative of G_i with respect to that variable.
The action of Eq.(2.15) includes a wide variety of theories, such as $f(R)$ and Brans-Dicke (BD) theories, that can be then obtained imposing conditions on the $\mathcal{L}_i$ terms, as we will see in a moment.

Brans-Dicke When referring to an additional scalar degree of freedom in the standard gravity sector, the Brans-Dicke theory is the more immediate example. Its action is obtained from Eq.(2.15) setting all the functions to zero, except for

$$G_2 = \frac{1}{2}\frac{\omega_{BD}}{\phi}\nabla^\mu\phi\nabla_\mu\phi - U(\phi) \qquad\qquad G_4 = \frac{1}{2}\phi \ , \tag{2.17}$$

where ω_{BD} is the Brans-Dicke parameter. The resulting action is

$$S = \frac{1}{16\pi G}\int d^4x\sqrt{-g}\left(\frac{1}{2}\phi R - \frac{1}{2}\frac{\omega_{BD}}{\phi}\nabla^\mu\phi\nabla_\mu\phi - U(\phi)\right) + S_M(g_{\mu\nu}, \psi) \tag{2.18}$$

f(R) theories $f(R)$ theories add to the gravitational sector a general function of R, named $f(R)$, such that the total action becomes

$$S = \frac{1}{16\pi G}\int d^4x\sqrt{-g}(R + f(R)) + S_M(g_{\mu\nu}, \psi) \quad . \tag{2.19}$$

Since we want to modify the Einstein-Hilbert sector $\sqrt{-g}R$, a natural choice would be to add terms to the action that are proportional to $\sqrt{-g}R^n$, where for $n > 1$ Starobinski (1979) showed that such terms lead to modifications of the standard cosmology at early times. For $n < 0$ such corrections become important in the late Universe and can lead to self-accelerating vacuum solutions [46].
The action of Eq.(2.19) can be inferred from Eq.(2.15) imposing [47]

$$G_2 = -\frac{1}{2}\left(R\frac{\partial f}{\partial R} - f(R)\right) \qquad\qquad G_4 = \frac{1}{2}\frac{\partial f}{\partial R} \quad , \tag{2.20}$$

where in [47] notation the standard R term is included in the function $f(R)$.

The extra term $f(R)$ will introduce terms to the l.h.s. of Einstein's equations, indeed varying the action with respect to $g^{\mu\nu}$

$$\begin{aligned}
\frac{\delta S}{\delta g^{\mu\nu}} &= \frac{1}{16\pi G}\int d^4x\left(\frac{\delta(\sqrt{-g}R)}{\delta g^{\mu\nu}} + \frac{\delta(\sqrt{-g}f(R))}{\delta g^{\mu\nu}} + 16\pi G\frac{\delta(\sqrt{-g}\mathcal{L}_M)}{\delta g^{\mu\nu}}\right)\delta g^{\mu\nu} \\
&= \frac{1}{16\pi G}\int d^4x\sqrt{-g}\left(-\frac{1}{2}g^{\mu\nu}R + R_{\mu\nu} + \frac{1}{\sqrt{-g}}\frac{\delta(\sqrt{-g})}{\delta g^{\mu\nu}}f(R) + \frac{\delta f(R)}{\delta g^{\mu\nu}} - 8\pi G T_{\mu\nu}\right)\delta g^{\mu\nu} \\
&= \frac{1}{16\pi G}\int d^4x\sqrt{-g}\left(-\frac{1}{2}g^{\mu\nu}R + R_{\mu\nu} + \frac{1}{\sqrt{-g}}\frac{\delta(\sqrt{-g})}{\delta g^{\mu\nu}}f(R) + \frac{\partial f(R)}{\partial R}\frac{\delta R}{\delta g^{\mu\nu}} - 8\pi G T_{\mu\nu}\right)\delta g^{\mu\nu} \\
&= \frac{1}{16\pi G}\int d^4x\sqrt{-g}\left(-\frac{1}{2}g^{\mu\nu}R + R_{\mu\nu} + \frac{1}{\sqrt{-g}}\frac{\delta(\sqrt{-g})}{\delta g^{\mu\nu}}f(R) + f_R\left(\frac{\delta R_{\mu\nu}}{\delta g^{\mu\nu}}g^{\mu\nu} + R_{\mu\nu}\right) - 8\pi G T_{\mu\nu}\right)\delta g^{\mu\nu} \\
&= 0
\end{aligned} \tag{2.21}$$

and using Eqs.(1.12)(1.13), together with the definition of the affine connection, yields

$$(1 + f_R)R_{\mu\nu} - \frac{1}{2}g_{\mu\nu}(R + f(R)) + (g_{\mu\nu}\Box - \nabla_\mu\nabla_\nu)f_R = 8\pi G T_{\mu\nu} \tag{2.22}$$

where $f_R = \partial f/\partial R$, ∇_μ is the covariant derivative and $\Box = g_{\mu\nu}\nabla_\mu\nabla_\nu$.
Then, having modified the l.h.s. of Einstein equations we expect that the Friedmann equations for a flat FLRW metric will present extra terms on the l.h.s. as well [32]

$$H^2 + \frac{f}{6} - \frac{\ddot{a}}{a}f_R + H\dot{f_R} = \frac{8\pi G}{3}\rho \tag{2.23a}$$

$$\frac{\ddot{a}}{a} - f_R H^2 + \frac{f}{6} + \frac{\ddot{f_R}}{2} = -\frac{4\pi G}{3}(\rho + 3p) \tag{2.23b}$$

where in the $f(R) = 0$ case we recover the standard Friedmann equations.

From another point of view, these extra terms can be interpreted as an additional effective fluid that contributes to the energy momentum tensor with an effective Equation of State [32]

$$w_{eff} = -\frac{1}{3} - \frac{2}{3}\frac{\left[H^2 f_R - \frac{1}{6} - H\dot{f}_R - \frac{1}{2}\ddot{f}_R\right]}{\left[-H^2 f_R - \frac{f}{6} - H\dot{f}_R - \frac{1}{2f_{RR}}\right]} \quad . \tag{2.24}$$

Hence, by determining the expansion history, we can specify how the fluid contribution to $H(z)$ evolves over time, i.e. the form of $f(R)$. Moreover, this effective fluid has an energy momentum tensor

$$8\pi G T^{eff}_{\mu\nu} = f_R R_{\mu\nu} - \frac{1}{2}g_{\mu\nu}f(R) + (g_{\mu\nu}\Box - \nabla_\mu\nabla_\nu)f_R \quad . \tag{2.25}$$

The additional scalar degree of freedom is represented by f_R, defined as the scalaron, whose equation of motion is defined by the trace of Eq.(2.22)[32]

$$\Box f_R = \frac{1}{3}(R + 2f - Rf_R) - \frac{8\pi G}{3}(\rho - 3p) \equiv \frac{\partial V_{eff}}{\partial f_R} \tag{2.26}$$

From the latter, restricting $|f \ll R|$ and $|f_R| \ll 1$ at high curvature [1], we can derive the mass of the scalaron as

$$m_\phi \equiv \frac{\partial^2 V_{eff}}{\partial f_R^2} = \frac{1}{3}\left[\frac{1 + f_R}{f_{RR}} - R\right] \sim \frac{1}{3f_{RR}} \tag{2.27}$$

where, in order to have stability against small perturbations we require $|f_{RR}R| \ll 1$ and $f_{RR} > 0$. As discussed in [32] [48], f_R needs to satisfy the following further conditions:

- f_R small at recent epochs, since we want to meet the solar and galactic scale constraints
- $f_R < 0$, in order to recover standard GR at early epochs
- $1 + f_R > 0$ for all finite R, to prevent the graviton from becoming ghost-like

2.1.3 Distinguishing between DE and MG models

Cosmological structure formation provides a powerful way of probing and constraining beyond ΛCDM models: the different coupling with gravity and/or matter will reflect in a different evolution of the density perturbations and, so, in a different large scale structure formation. In particular, MG models introduce an anisotropic stress term which can not be neglected and leads to a slightly different evolution.

Phenomenological approach

As already seen in Sect.1.3.3, large scale structure offers a broad variety of cosmological observables that enable us to study the evolution of cosmological perturbations. The growth of structures is affected by Ψ (Eq.(1.100)), while photons geodesics by a linear combination of Φ and Ψ, where Φ and Ψ are the scalar perturbations to the FLRW metric in Newtonian gauge (Eq.(1.87)).

During the epoch relevant for structure formation, in ΛCDM the two potentials are equal, due to a null anisotropic stress (as assumed when radiation content is negligible, Eq.(1.101)). That is also valid for minimally coupled DE models as well, since they simply add an homogeneous and isotropic fluid component, that does not affect the matter behaviour, due to the minimal couplings.
The viability of the evolutionary equations can be tested combining the cosmological observations described in Sect.1.3.3, as weak lensing and galaxy counts.
Since these equations have been derived in the standard GR framework, deviations from these equations would suggest that standard GR is not valid at large scales, i.e. that we need to modify the theory of gravity, or that we need a scalar field which is not minimally coupled to matter sector.
When one considers extended theories of gravity, these equations might change to possibly include time derivatives as well.
In a general manner, we can parameterize these deviations in terms of the following functions of time and scale: a rescaling of the Newton's constant $\mu(a, k)$ and a gravitational slip $\gamma(a, k)$,

[1] since we require consistency with the high redshift Universe

defined via

$$k^2\Psi(a,k) = -4\pi G a^2 \mu(a,k)\rho\Delta \tag{2.28}$$

$$\frac{\Phi(a,k)}{\Psi(a,k)} = \gamma(a,k) \tag{2.29}$$

While μ is closely linked to observables, since Ψ directly affects the growth of matter density perturbations via Eq.(1.100)

$$\ddot{\delta}_m + 2H\dot{\delta}_m + \frac{k^2}{a^2}\Psi = 0 \ , \tag{2.30}$$

an observational interpretation of γ is not that immediate. Hence, we can equivalently refer to another phenomenological function $\Sigma(a,k)$, defined via

$$k^2(\Psi + \Phi) = -8\pi G a^2 \Sigma(a,k)\rho\Delta \ \ , \tag{2.31}$$

which is related to $\mu(a,k)$ and $\gamma(a,k)$ via

$$\Sigma(a,k) = \frac{(\gamma(a,k)+1)\mu(a,k)}{2} \tag{2.32}$$

and it is directly linked to photon's geodesics.
Providing any two of these functions is sufficient to solve the equations of evolution of density perturbations [9].
In the ΛCDM model, based on GR, these phenomenological functions will reduce to $\mu(a,k) = \gamma(a,k) = \Sigma(a,k) = 1$.

This phenomenological approach encodes all our ignorance about the source of these deviations, i.e. the functional forms of these functions. However, in order to fit these functions to data, one might wonder what is the best form for these phenomenological functions. Since in the context of MG the linearly perturbed Einstein's equations can possibly yield time derivatives in Eqs.(1.101)(1.102), finding a closed form for $\mu(a,k)$, $\gamma(a,k)$ and $\Sigma(a,k)$ would require to solve these differential equations first, making them dependent on the initial conditions [49]. Though, as pointed out in [9] it would be possible to derive them in a specific gravity theory adopting the quasi-static approximation (QSA), namely restricting to scales well within the horizon and neglecting time derivatives of the metric perturbations with respect to their spatial ones. Hence, the differential equations become algebraic.
One of the goal of this Thesis is to provide a non-parametric reconstruction of μ and Σ over redshift, never restricting to any approximation or any assumption related to a particular functional form of these two phenomenological functions.

2.2 The H_0 tension

Since the discovery of the expansion of the Universe [22], there have been many attempts to measure the Hubble parameter H_0, as it would enable us to calculate the expansion rate at present, by definition, the observable size of the Universe and the age of the Universe itself. The Hubble constant can be estimated via both direct and indirect probes.
In the first case, the value of H_0 is measured through distance indicators in the nearby Universe, in particular, via *standard candles*, as Type Ia Supernovae, already treated in Sect.1.4.1, and Cepheids. The latter are variable stars, whose period of pulsation is related to their luminosity, i.e. to the absolute magnitude, the knowledge of which enables us to calculate the object distance via Eq.(1.106).
On the other hand, over the past 15 years, measurements of the Cosmic Microwave Background (CMB) temperature anisotropies have provided a powerful tool to indirectly estimate H_0 and to test the standard model. Indeed, CMB observations predominantly probe the physics of the early Universe, but given the proper cosmological model, it is possible to extrapolate from them standard cosmological parameters, defined at present time. Hence, this indirect measurement offers us the possibility to test self-consistency of the ΛCDM model.
In absence of significant systematic errors, we would expect, if the model is correct, direct and indirect (model-dependent) constraints on H_0 to be in accordance; however, if a significant inconsistency between the two is found, then this would imply that is necessary to investigate beyond the standard model.

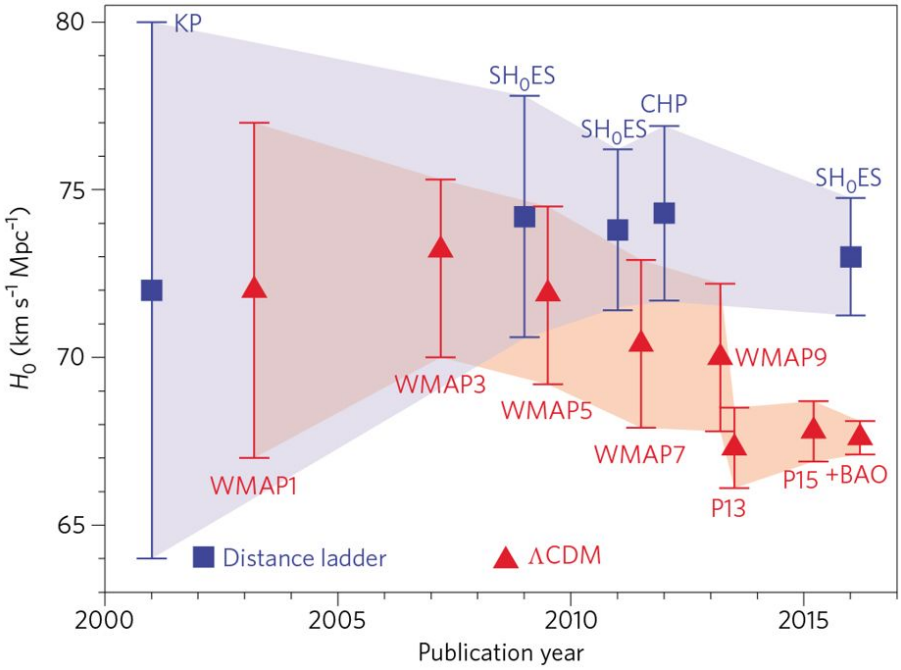

Figure 2.1: Recent values of H_0 as a function of publication date since the Hubble Key Project. The missions and collaborations taken into account are KP (*Key Project*) [50], *SH0ES* (*Supernovae H_0 for the Equation of State of Dark Energy*) [51], *CHP* (*Carnegie Hubble Program*) [52] for direct probes (blue squares in Figure) and *WMAP* (*Wilkinson Microwave Anisotropy Probe*) [53] and *Planck* [23] missions for CMB probes (red squares), assuming the ΛCDM model. Figure from [54].

Since the time of the Hubble Key Project, there has been incredible progress in decreasing known systematic errors, as it is shown in Fig.2.1 [54].

Referring to the estimates obtained from local measurements [4] and from high redshift observations [3]

$$H_0^{SH_0ES} = 73.48 \pm 1.66 \; kms^{-1}Mpc^{-1} \qquad H_0^{Planck} = 67.36 \pm 0.54 \; kms^{-1}Mpc^{-1}$$

a tension of 3.5σ is found, where the latter is defined as

$$T(H_0) = \frac{|H_0^{SH_0ES} - H_0^{Planck}|}{\sqrt{\sigma^2(H_0^{SH_0ES}) + \sigma^2(H_0^{Planck})}} \tag{2.33}$$

since the two measures are Gaussian distributed.

Is this tension due to systematic effects on the observations or is it a hint that we have to drop the assumption of a ΛCDM expansion?
In absence of evident systematic effects, we are prompted to investigate whether the tension could be alleviated with beyond ΛCDM models.

2.2.1 Parametric approach

In order to investigate possible departures from the standard cosmological model, one can either restrict to the choice of a particular model or work in the general parameterized frameworks, that could enable the detection of potential hints, that a fixed model would not detect. Hence, there had been many attempts into developing parameterized frameworks.

As we have just seen in the previous Section, by alternative models to the Cosmological Constant we mean DE and MG models, where both of them result in a freeing of additional degrees of freedom. In particular, at the background level the latter acts as an effective fluid component with Equation of State w_{DE}. Hence, in the past few years many parameterizations of the DE EoS have been adopted, or similarly of the expansion history.

Let us start from reviewing the most common parametric approach to the background dynamics. If the DE is not a Cosmological Constant with $w = -1$, then there is no reason why the DE Equation of State should remain constant; hence, in order to test a time-varying $w_{DE}(a)$, the most common example of a two-parameters description of the DE EoS is the Chevallier-Polarski-Linder (CPL) [5] [6] parameterization

$$w_{DE}(a) = w_0 + (1-a)w_a \quad , \tag{2.34}$$

where w_0 and w_a are constant. The first parameter is the value of the DE EoS at present ($w_0 = w(t_0)$), while w_a encodes the overall evolution of w_{DE} over time. CPL bounds the behaviour of the function up to infinite redshift. Even if its simplicity is an advantage, it has a limited capability, since it requires a linear relation between w and $w' = \frac{dw}{dlna}$ and it fails fitting EoS rapidly evolving. Extending the parameter space, on the basis of an expansion approach, another way to parameterize a time-varying EoS is via the Padé expansion [7] for instance

$$w_{DE}(a) = \frac{\sum_{n=0}^{N} \alpha_n a^n}{\sum_{m=0}^{M} \beta_m a^m} \quad . \tag{2.35}$$

These and many other parameterizations of the time-dependent DE EoS will then affect the expansion history, i.e. the background dynamics, since the Hubble parameter is defined as a function of the density parameters, whose evolution depends on the Equations of State of the different components, including DE.

However, at the level of cosmological perturbations, in order to distinguish between DE and MG models, we must also provide the phenomenological functions $\mu(a,k)$, $\gamma(a,k)$ and $\Sigma(a,k)$, in which deviations from the standard GR regime are encoded. Hence, while investigating alternative models to the Cosmological Constant via parametric approaches, we would like to provide appropriate time and scale dependencies of these functions.
But, as already pointed out in Sect.2.1.3, in the most general case we can not obtain a closed form for μ, γ and Σ, unless we restrict to the QSA approximation.
Let us then proceed to the overview of some of the proposed parameterizations of μ and γ, closely following [49] procedure first. Let us consider a broad class of MG theories that modifies the standard action with a Lagrangian density made up of geometric invariants, as R, $R_{\alpha\beta}R^{\alpha\beta}$,$\Delta R$ and so on, as well as N scalar degrees of freedom ϕ_i. Setting the Poisson and anisotropic stress equations and that obtained varying the action with respect to the field in Fourier space, as suggested by [49], we can adopt linear operators multiplying the potentials Φ, Ψ and the i-th scalar field perturbation $\delta\phi_i$, in which the background functions, (proper) time derivative and/or powers of k are encoded. In particular these operators are of the form

$$\hat{O} = \sum_{n,m}^{N,M} o_{n,m} k^n \partial_0^m \tag{2.36}$$

where N and M are maximum order of metric derivatives while the $o_{n,m}$ are functions of time, that, where needed, will have additional low/high indices as required by the operator.
As we restrict ourselves to the QSA, these operators become polynomials in k. Hence, the three equations above constitute now a system of algebraic equations, that provides μ and γ as ratios of polynomials in k. Without loss of generality, [49] provides a parametric form for the two phenomenological functions

$$\gamma(a,k) = \frac{p_1(a) + p_2(a)k^2}{1 + p_3(a)k^2} \qquad \mu(a,k) = \frac{1 + p_3(a)k^2}{p_4(a) + p_5(a)k^2} \tag{2.37}$$

where the $p_i(a)$ are background functions. Of particular interest is the fact that the denominator of γ is equal to the numerator of μ, which they find to be a general feature, since they did not adopted any particular model.

This choice is similar to the BZ parameterization [10]

$$\mu(a,k) = \frac{1 + \beta_1\lambda_1^2 k^2 a^s}{1 + \lambda_1^2 k^2 a^s} \qquad \gamma(a,k) = \frac{1 + \beta_2\lambda_2^2 k^2 a^s}{1 + \lambda_2^2 k^2 a^s} \tag{2.38}$$

where λ_i are dimensionally lengths and β_i are dimensionless couplings. However, there are some slight differences: the general feature involving the numerator/denominator of μ and γ is not set, the time dependence is restricted to a power law and finally the standard GR limit is recovered for $k \to 0$. Moreover, this last parameterization is used by [11] as starting point to derive parameterized forms of $\mu(a,k)$ and $\gamma(a,k)$ in the case of $f(r)$ theories.

As a final example, in [8], $\mu(a,k)$ and $\gamma(a,k)$ are parameterized as

$$\mu(a,k) = 1 + f_1(a)\frac{1 + c_1(\lambda H/k)^2}{1 + (\lambda H/k)^2} \qquad \gamma(a,k) = 1 + f_2(a)\frac{1 + c_2(\lambda H/k)^2}{1 + (\lambda H/k)^2} \tag{2.39}$$

where λ and c_i are constants and the $f_i(a)$ encode the deviations from standard GR as a function of a, via a time-varying DE density parameter, so that $f_i = E_{ii}\Omega_{DE}(a)$, or as an expansion $f_i = E_{i1} + E_{i2}(1-a)$. In particular, the two regimes of small scales and large scales will behave differently: for example, for small k, i.e. large scales, $\mu(a,k) \longrightarrow 1 + f_1(a)c_1$, while for large k, i.e. small scales, $\mu(a,k) \longrightarrow 1 + f_1(a)$.
While the previous parameterizations are obtained under the QSA, as stressed in [8] that is not the case for the parameterized forms of Eq.(2.39). The above Planck parameterization is set in the *(minimal) way to allow for (arbitrary) scale dependence, as data cover a sufficiently wide range of scales.*

2.2.2 Non-parametric approach

As I previously said, working in a general parameterized framework could enable the detection of peculiar aspects of the functions of interest, however this is not ensured; indeed the assumption on the analytical form of the parameterization could be still too much constraining.
There exists another way to compute the reconstruction, that consists of non-parametric methods that aim at determining the function given observational data, rather than the parameters associated to a particular assumed form of the function itself, such as w_0 and w_a for the CPL parameterization.

Hence, there had been the attempt to reconstruct in a non-parametric way the DE EoS and the expansion history $H(z)$ [55][56][57][58], where the main advantages of using the non-parametric approach are related to a higher freedom of the reconstructed function. First adopting this approach enables us to infer the unknown function with a minimum of assumptions, avoiding the restrictions of a model or a parametric form. Secondly, via the non-parametric approach we can potentially capture essential features of the function, hence all the information coming from data, that could be wiped out by model assumptions.
The hope is to avoid the possible biasing of results due to specific assumptions regarding the functional form of the function of interest, which may turn out to be incorrect [55].

However, a legitimate assumption is to require a sufficiently smooth function, which means that the function is expected to vary of small amounts while moving with infinitesimal steps on the curve. Hence, we can apply to the reconstructions a smoothness prior information in which is encoded the correlation between different redshifts [59].

One the basis of this last idea, the purpose of this Master project is to develop a model-independent reconstruction method in order to understand the behaviour over time of the DE EoS and of $\mu(a)$ and $\Sigma(a)$ in the MG case. The aim is to furnish a powerful tool to potentially highlight the nature of the mechanism driving the late cosmic acceleration. Of particular importance, will be the implementation of the method with the help of the correlation priors, where the latter naturally restrict us to the choice of a model.

3 | Non-parametric approach and Data Analysis

The lack of a theoretical understanding for the late cosmic acceleration, have prompted the exploration of many alternative models. In what follows, I will outline the non-parametric approach, used to reconstruct the behaviour over time of DE and MG functions, and the Bayesian analysis, addressing with a particular focus the use of a correlation prior within the Monte-Carlo parameter estimation.

3.1 Reconstruction method

Let us define the function to be reconstructed in a generic way, as $f(a)$. Since $f(a)$ must be reconstructed non-parametrically, the first step to take is to discretize it into binned $f_i(a) = f(a_i)$ with $i = 1, ..., N$, equally spaced in the interval $[a_{min}, 1]$. The function $f(a)$ can be reconstructed via smoothed step function and Gaussian Process (GP) (Fig. 3.1).

Smoothed step function

This reconstruction is computed as

$$f(a) = f(a_1) + \sum_{i=1}^{N-1} \frac{f(a_{i+1}) - f(a_i)}{2} \left\{ 1 + tanh \left[s \left(\frac{a - a_{i+1}}{a_{i+1} - a_i} \right) \right] \right\} \tag{3.1}$$

where s is the smoothing factor, at increasing s the function will be more smoothed at the transition points.
As it is going to be later discussed, for some of the functions of interests the computation of their derivative with respect to the scale factor is also needed. In the particular case in which the function is reconstructed via the smoothed step function method, the derivative is done in such a way that the incremental ratios calculated at the transition points $\bar{a}_j = (a_i + a_{i+1})/2$

$$f'(\bar{a}_j) = \frac{f(a_{i+1}) - f(a_i)}{a_{i+1} - a_i}$$

are interpolated via smoothed step function as well, as done in [60].

Gaussian Process

In a general manner, let us suppose that, given a function of the variable a without an analytical expression, we know only few $(a, f(a))$ training points and how they are correlated. Gaussian process is a solution to this regression problem: it is a distribution over functions fitting the training points.
A Gaussian Process is defined as a collection of random variables , any finite number of which have a joint Gaussian distribution[61].
Let us start considering the training points $\vec{a} = (a_1\ a_2\ a_3)$, we can always think of the function $f(a)$

evaluated at these points as a vector and, at each point a_i, $f(a_i)$ is a Gaussian random variable with mean $\mu(a_i)$ and variance $\sigma^2_{a,i}$. Considering then the whole vector, this will be modeled with a multivariate Gaussian distribution

$$\vec{f} = \begin{bmatrix} f_1 \\ f_2 \\ f_3 \end{bmatrix} \sim N(\vec{\mu}, C) = N\Bigg(\vec{\mu}, \begin{bmatrix} C_{11} & C_{12} & C_{13} \\ C_{21} & C_{22} & C_{23} \\ C_{31} & C_{33} & C_{33} \end{bmatrix}\Bigg) \tag{3.2}$$

where N stands for Normal distribution and C is the covariance matrix, as $C_{ij} = C(\vec{f}(a_i), \vec{f}(a_j))$ denotes the correlation between two points a_i and a_j, i.e. how strongly they influence each other. We expect that the closer a_i and a_j are, the more they will be correlated and the more they will influence each others f_i and f_j values.
The Gaussian Process regression is available in the python package sklearn and the covariance function we choose is the Radial Basis Function (RBF):

$$C(a, a') = e^{-\frac{|a-a'|^2}{2l^2}} \tag{3.3}$$

where l is the correlation length, such that

$$C(a, a') = \begin{cases} 0 & |a - a'| \gg l \\ 1 & a = a' \end{cases} \tag{3.4}$$

This kernel is both stationary, because is a function of $a - a'$, and isotropic, since it is a function of its module $|a - a'|$.

So now, given the noise-free training points, we are interested to know what will be the value of the function at a point a_*, defined as $f(a_*)$. Since we expect the function to be smooth, for a small variation of the a variable we do not expect the function at that point to be far different from those adjacent.
Hence, assuming that $f(a_*)$ will be Gaussian distributed as well, i.e. $f(a_*) \sim N(\mu_*, C(a_*, a_*))$, where $C(a_*, a_*)$ is the self-covariance, the joint distribution will assume the form of

$$\begin{bmatrix} \vec{f} \\ f_* \end{bmatrix} \sim N\Bigg(\begin{bmatrix} \vec{\mu} \\ \mu_* \end{bmatrix}, \begin{bmatrix} C(\vec{a}, \vec{a}') & C(\vec{a}, a_*) \\ C(a_*, \vec{a}) & C(a_*, a_*) \end{bmatrix}\Bigg) \tag{3.5}$$

Thus once specified the mean and correlation functions, considering now all the fitting points, the Gaussian Process will be defined as

$$f(\vec{a}) \sim GP(\mu(\vec{a}), C(\vec{a}, \vec{a}')) \tag{3.6}$$

Therefore, for this reconstruction method, a_i and $f_i(a)$ alone are not sufficient, the correlation length is also needed; but then, the problem is to find the criterion to obtain it without having data a priori. This is one of the reasons why imposing a correlation prior is helpful. In Sect.3.2.2 the analytical expression of the correlation priors used within this work automatically gives the correlation length; even if they refer to kernels (Tabs.3.1 and 3.2) which are different from that of Eq.(3.3), we can assume that the extrapolated correlation length will be a good approximation for the GP reconstruction.
Moreover, since the correlation length is provided by the correlation prior in terms of scale factor, this justifies the choice of bins equally spaced in a.

In [61] the aim is to reconstruct a function through Gaussian Process given the training points, that are observed with their errorbars, so that GP is effectively set as the believed distribution of the function itself. In this work, the training points are parameters sampled and obtained through the data analysis and once the GP properties are fixed, there exists only one Gaussian Process fitting them and, during the data analysis, the training points themselves are modified, not the GP reconstruction.

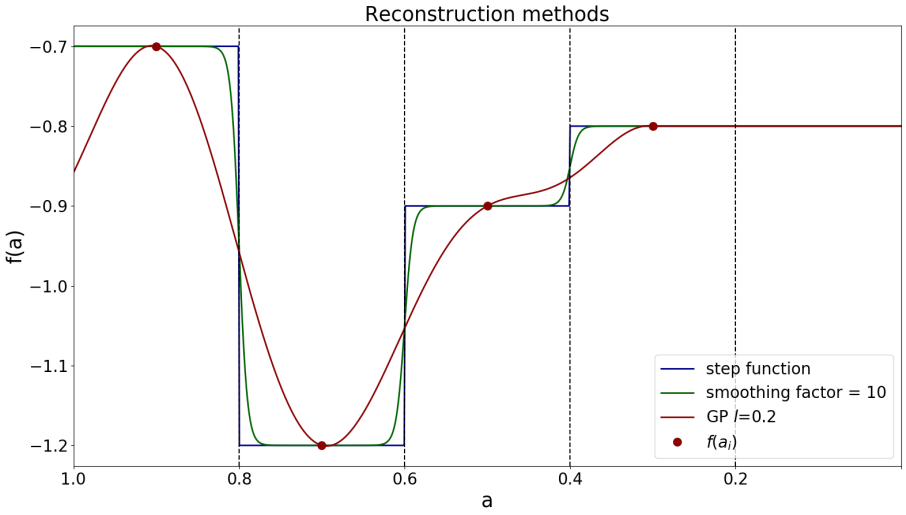

Figure 3.1: The reconstruction methods implemented are three: step function, smoothed step function and Gaussian Process; the red dots are the chosen $f(a_i)$. Moreover, we decided to constrain the values of $f(a < a_{min}) = f(a_{min})$.

Since we are dealing with two methods for the non-parametric approach, an interesting point would be to compare them, as in Fig.3.1. Let us suppose we fix the scale factor interval over which we want to reconstruct the function, we intuitively expect that increasing the number of bins within that interval will enable the reconstructed function to become insensitive to both the binning properties and to the reconstruction method. Indeed, on one hand, a higher number of bins will enable the emergence of additional peculiar features, while on the other hand, we expect that a denser binning will make the smoothed step reconstruction approximate that obtained via Gaussian Process.

Within this work, the outlined method is applied to the reconstruction of the DE EoS and of the two phenomenological functions $\mu(a)$ and $\Sigma(a)$, where the latters are reconstructed if we are dealing with MG models. While working with DE models the reconstruction of the DE EoS is computed in CAMB [1], otherwise it must be computed in MGCAMB [2] [62][63], along with $\mu(a)$ and $\Sigma(a)$, for MG models. Hence, since CAMB and MGCAMB work with parameterizations of the functions we are interested in, I modified them implementing the approach above. Moreover, their reconstruction alone is not sufficient for the CAMB/MGCAMB computation: some functions of them must be computed, as explained in what follows.

Those that I defined as the binned values of the function $f(a)$ are new parameters for these codes; in particular they will be sampled (Sect.3.2.1) within a given range $f_{low} \leq f_i \leq f_{up}$ and obtained with their errors through the data analysis.
Thus, one of the main differences between the two methods is that the smoothed step reconstruction will be all enclosed within that range, by its definition, but, that is not true for Gaussian Process, that fits the training points without being necessary all included in the range $[f_{low}, f_{up}]$. So, passing to the redshift notation, the reconstruction before z_1 and after z_N could behave in any way. On one hand, I added the $f(z = 0)$ parameter, which will be free to vary in the same range of all the other $f(z_i)$, or equivalently we could set the condition $f(z < z_1) = f(z_1)$ in the case in which z_1 is sufficiently smaller than z_N, since we do not expect the function to vary significantly within $[0, z_1]$, compared to variations happening within a bigger redshift interval. On the other hand, I fixed $f(z > z_N) = f(z_N)$, as it can be seen from Fig. 3.1, as for the other methods.

[1] https://camb.info/
[2] http://aliojjati.github.io/MGCAMB/home.html

In order to reconstruct a generic w_{DE}, we will also consider time-varying EoS crossing the so called "Phantom divide" at $w_{DE} = -1$. As explained in [64][65], unless we add new degrees of freedom, a single scalar field can not cross the Phantom divide maintaining gravitational stability [66], which is the reason why for Quintessence we are later going to impose -1 as a lower limit for $w_{DE,i}$. But as [65] puts in evidence, Type Ia Supernovae data do not exclude the DE EoS to go below the Phantom divide; since we want to obtain a non-parametric reconstruction of a generally time-dependent w_{DE} based on data, the crossing would be unavoidable. For this reason we must adopt the PPF description.

The problem arises when considering the momentum conservation equation [64]; in the particular case in which $w = -1$, assumed that the sound speed is fixed and denoting with $\dot{}$ derivatives with respect to $ln\ a$, [66]

$$\frac{\dot{p}}{\dot{\rho}} = \left(w - \frac{1}{3} \frac{d\ ln(1+w)}{dlna} \right) \tag{3.7}$$

will diverge leading to gravitational instability of the Dark Energy perturbations.

Thus, the PPF description of the effective DE stress tensor consists on the use of a new variable Γ [67]. Together with the momentum and energy conservation laws, Γ needs to fulfill a boundary condition that replaces the relationship between pressure and density fluctuations: the condition imposed is on the relationship between DE and matter momentum densities at large scales and a transition scale, under which DE becomes relatively smooth.
The variable is defined in [64] under these conditions as

$$\Gamma = \frac{4\pi G a^2}{k^2 c_K} \rho_{DE} \delta_{DE}^{(rest)} \tag{3.8}$$

with $c_K = 1 - 3K/k^2$ (K background curvature) and the rest frame defined with respect to the Dark Energy component.

The DE EoS affects the expansion history via ρ_{DE}, which is given in Eq.(1.25), depending on the value of the Equation of State. In terms of the binning in redshift, Eq.(1.25) translates into

$$\rho_{DE}(z) \propto \begin{cases} exp\left[3 \int_0^z \frac{1+w(z)}{1+z} dz \right] & z \leq z_N \\ \left(\frac{1+z}{1+z_N} \right)^{3(1+w_N)} \rho_{DE}(z_N) & z > z_N \ [w = const!] \end{cases} \tag{3.9}$$

where the integral is computed via trapezoidal method and where we assumed that after a given z_N, w_{DE} takes the value of the last bin and stays constant in the past.
Fig.3.2 shows examples of Ω_{DE} [3] and the w_{DE} used to obtain them, with both binned and GP reconstructions.

So, the Equation of State is reconstructed and enters the background evolution, while $\mu(z)$ and $\Sigma(z)$ (and $\gamma(z)$) enter the evolution of perturbations via their time derivatives, done with respect to the scale factor.

The computation of the time derivatives is dependent on the reconstruction method and it is based on the calculation of the incremental ratio.
In the case of the Gaussian Process the derivative is computed taking the incremental ratio for a certain number of sub-bins and interpolating those to obtain a continuous curve; while for the smoothed step function alternative, the computation of the derivative has been explained above.
Fig.3.3 shows examples of $\dot{\mu}(z)$ and the $\mu(z)$ used to obtain them, with both binned and GP reconstructions.

[3] I here recall that the density parameter of the i-th Universe component is defined as $\Omega_i(t) = \frac{\rho_i(t)}{\rho_c(t)}$

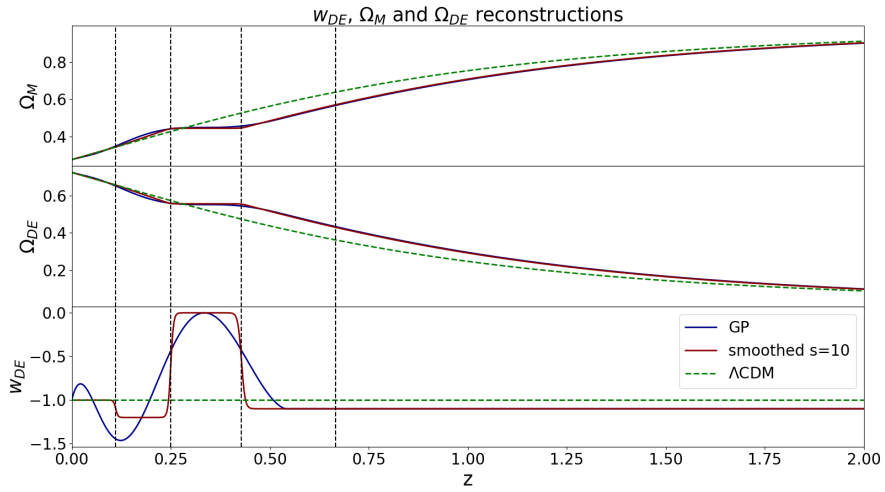

Figure 3.2: The upper plot shows the evolution of the Matter and Dark Energy densities, obtained for the reconstructions showed in the lower plot. In particular here I compare the Λ EoS and predicted density parameters, with those for the w_{DE} reconstructed via Gaussian Process and smoothed step function, for the same input parameters.

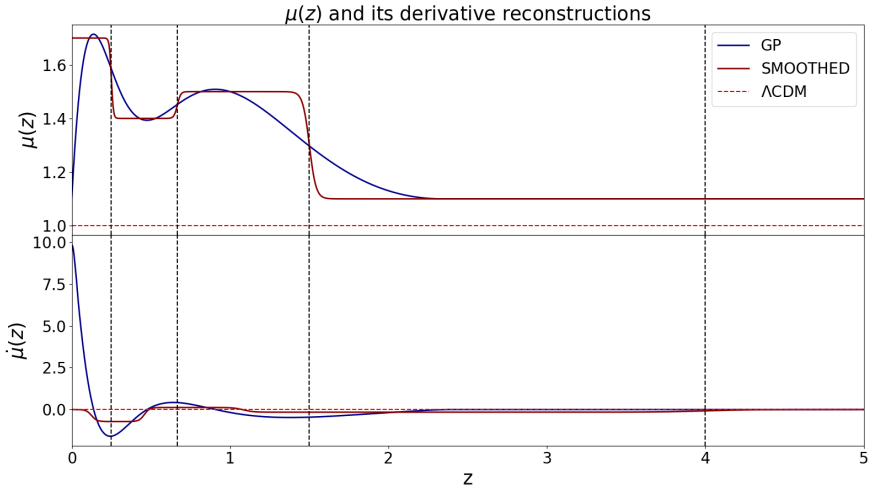

Figure 3.3: The upper plot shows the two method of reconstruction for $\mu(z)$ (as for $\Sigma(z)$), while the lower plots its derivative. The difference between the smoothed step function and the Gaussian Process is clear, however, given a certain redshift interval for the reconstruction, increasing the number of bins the derivatives will be more similar.

3.2 Bayesian analysis: parameter estimation

Together with the standard cosmological parameters, the discretized values of the reconstructed functions will be used to compute cosmological observables fitted to the data. The process of obtaining from data the values of the N parameters X_i $(i = 1, .., N)$ describing the model is called parameter estimation. Bayes theorem

$$p(X|\Theta) \propto p(\Theta|X)p(X) \tag{3.10}$$

provides a relation between the posterior distribution $p(X|\Theta)$, the prior distribution $p(X)$ and the likelihood $p(\Theta|X)$, where Θ denotes the data vector [68].
The posterior distribution represents the knowledge about X given the observed data Θ, i.e. the probability distribution associated to the estimated parameters we are looking for; the prior distribution is the believed distribution of the parameters X and the likelihood, $L(\Theta; X) = p(\Theta|X)$, is the probability distribution of data given the parameters.
Let us suppose for example that a set of given data points have Gaussian errors and we want to fit them with the model, the χ^2 is defined as

$$\chi^2 = \sum_i \frac{(\Theta_i - \tilde{\Theta}_i)^2}{\sigma_i^2} \tag{3.11}$$

where Θ_i are the observed data and $\tilde{\Theta}_i$ are the predictions of the model at each point; hence, the χ^2 will test the goodness of fit.
If data are correlated, then

$$\chi^2 = \sum_{ij} (\Theta_i - \tilde{\Theta}_i) D_{ij}^{-1} (\Theta_j - \tilde{\Theta}_j) \tag{3.12}$$

where D is data covariance matrix.
The likelihood, defined in the Gaussian case as

$$L(\Theta; X) = \prod_i \frac{1}{\sqrt{2\pi}\sigma} exp\left[\frac{(\Theta_i - \tilde{\Theta}_i)^2}{\sigma_i^2}\right] \propto e^{-\chi^2} \tag{3.13}$$

tells us how likely the observed data distribution is, once we define the model.

If, a priori, there is no knowledge about the tendency of X to assume a particular value instead of the others, then the $p(X) = const$ is called uniform prior and Eq.(3.10) becomes $p(X|\Theta) \propto L(\Theta; X)$.

We are now anyway left with the problem of computing $L(\Theta; X)$ and $p(X|\Theta)$ at different values of the parameters X_i $(i = 1, .., N)$. This is in general a complicated task, as we should compute these functions at each point of the multi-dimensional parameter space. In order to make this feasible, a commonly used approach is to sample the parameter space using Monte Carlo Markov Chains approaches.

3.2.1 Monte Carlo Markov Chain

A Monte Carlo Markov chain is a memory-less stochastic process that moves in a given parameter space. Being memory-less means that this stochastic process fulfills the Markov property that $p(X_i \mid X_0...X_{i-1}) = p(X_i \mid X_{i-1})$, which means that the probability to transit from a point X_{i-1} to X_i will depend only on X_{i-1} and not on the previous ones.
Hence, the chain moves from a point X_i to X_{i+1}, randomly generated (Monte Carlo) from a proposal distribution, according to a transition probability $T(X_i, X_{i+1})$, which is set by the Metropolis-Hastings algorithm to be [69]

$$\begin{aligned} T(X_i, X_{i+1}) &= \alpha(X_i, X_{i+1}) q(X_i, X_{i+1}) \\ &= min\left[1, \frac{P(X_{i+1}|\Theta) q(X_{i+1}, X_i)}{P(X_i|\Theta) q(X_i, X_{i+1})}\right] q(X_i, X_{i+1}) \end{aligned} \tag{3.14}$$

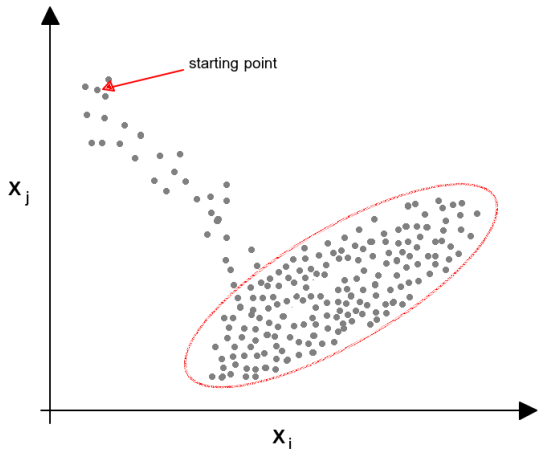

Figure 3.4: *Burn-in* phase

where $q(X_i, X_{i+1})$ is the proposal distribution, i.e. the steps distribution.
In the case in which the proposal distribution is symmetric [68], the previous transition probability simplifies in

$$T(X_i, X_{i+1}) = min\left[1, \frac{P(X_{i+1}|\Theta)}{P(X_i|\Theta)}\right] q(X_i, X_{i+1}) \quad . \tag{3.15}$$

This can be also understood intuitively, the transition probability will be proportional to both the probability of generating X_{i+1} starting from X_i (given the proposal distribution $q(X_i, X_{i+1})$) and the value of α, where, fixed $q(X_i, X_{i+1})$, if $\alpha > 1$ the consecutive code iteration will be done choosing the set of parameters X_{i+1}, otherwise this choice will be done only $\alpha\%$ of the times.

Since the sampling starts from a random point, it will take some time for the chain to get close to the peak of the final distribution; this time is the so called *burn-in* phase (Fig.3.4).

This kind of sampling is implemented in the MCMC software CosmoMC [4] ([69]; [70]), which is connected to CAMB or MGCAMB and is therefore able to sample the parameter space and to obtain at each point the corresponding theoretical predictions needed to compute $p(X|\Theta)$. In particular, it explores the parameter space, varying the model parameters within a given range $X_{low} \leq X \leq X_{up}$.

In order to understand when the MCMC chains are converged, CosmoMC uses the Gelman-Rubin criterion [68]. This method is based on the fact that, if there are M chains, each one made by N point after the *burn-in* phase, ideally, the mean value $\bar{X}^J$ calculated in one chain J is equal to its mean $\bar{X}$ calculated considering the whole sample, i.e. all the M chains

$$\bar{X}^J = \frac{1}{N}\sum_{i=1}^{N} X_i^J \tag{3.16}$$

$$\bar{X} = \frac{1}{NM}\sum_{J=1}^{M}\sum_{i=1}^{N} X_i^J \tag{3.17}$$

The test gives the value of R defined as

$$R = \frac{\frac{N-1}{N}W + \frac{B}{N}(1+\frac{1}{M})}{W} \tag{3.18}$$

[4] https://cosmologist.info/cosmomc/

where

$$W = \frac{1}{M(N-1)} \sum_{J=1}^{M} \sum_{i=1}^{N} (X_i^J - \bar{X}^J)^2 \tag{3.19}$$

$$\frac{B}{N} = \frac{1}{(M-1)} \sum_{J=1}^{M} (\bar{X}^J - \bar{X})^2 \tag{3.20}$$

so that $R \geq 1$. Ideally, the chains will be converged when $R = 1$; practically, a $R - 1 \sim 0.01$ is still a good convergence.

Once the chains finish and we have the posterior distribution $p(X|\Theta)$, where both X and Θ are vectors, we want to extrapolate as many information as possible on the parameters.
Assuming that the prior is not flat, as it is in general, the peak of the posterior distribution will be different from the peak of the likelihood; thus, we can not use the peak of the likelihood, defined as the maximum likelihood estimate, as a good estimate of X.
But still we can derive many properties, first the mean value, defined as

$$\hat{X} = \int dX \; X \; p(X|\Theta) \quad , \tag{3.21}$$

then, the errors.

But, we want to estimate the errors for a parameter X_i; to do this it is necessary to marginalize, i.e. to project the multidimensional distribution $p(X|\Theta)$ in the X_i one dimension. Marginalizing over all the other parameters means to derive

$$p(X_i|\Theta) = \int dX_1..dX_{i-1}dX_{i+1}..dX_N \; p(X|\Theta) \tag{3.22}$$

Furthermore, as a consequence, the confidence levels ($1\sigma = 68.27\%, \; 2\sigma = 95.45\%, \; 3\sigma = 99.73\%$) are defined such that, for example in the 1σ case

$$\int_R dX_i \; p(X_i|\Theta) = 0.6827 \tag{3.23}$$

where if $R = [x, x']$ then $X_i = \hat{X}_{i\,-(\hat{X}_i - x)}^{\,+(x' - \hat{X}_i)}$ at 1σ.
Notice that if the parameter X_i obtained after the marginalization is Gaussian distributed, the 1σ estimate will reduce to $X_i = \hat{X}_i \pm \|x - \hat{X}_i\|$, since $x' = x$.

3.2.2 The correlation prior

We said above that $p(X|\Theta)$ is computed through the likelihood $L(\Theta; X)$ and the prior $p(X)$. For our reconstructions, since we assume that we are working with smooth functions, we can use as prior information the fact that f_i $(i = 1, .., N)$ is correlated with the values of the adjacent bins. For this reason, as shown by [59], a correlation prior can be imposed; in this way if a bin is unconstrained there is no risk it can behave far differently from those close by.
Referring to (3.10), the net effect of the prior is that

$$\begin{cases} p(X) \propto e^{-\chi^2_{PRIOR}/2} \\ \chi^2_{PRIOR} = (\vec{f} - \vec{f}_{FID})^T C^{-1} (\vec{f} - \vec{f}_{FID}) \end{cases} \tag{3.24}$$

where C is the covariance matrix, $\vec{f}$ is the vector of $(f_1 \; .... \; f_N)$ and $\vec{f}_{FID}$ is the vector of the fiducial binned f values. To avoid any dependence on the fiducial value, I computed $f_{FID,i}$ as the mean of f_i with those adjacent:

$$f_{FID,i} = \begin{cases} (f_i + f_{i+1})/2 & i = 1 \\ (f_{i-1} + f_i + f_{i+1})/3 & i = 2, .., N-1 \\ (f_{i-1} + 2f_i)/3 & i = N \end{cases} \tag{3.25}$$

Assuming this prior distribution means that we are assuming that our f_i parameters are Gaussian distributed and in particular the covariance matrix describes its fluctuation around the fiducial model.

Using Bayes theorem, we can encode this prior directly in an overall χ^2. Indeed, since the posterior is the product of the two exponentials of Eqs.(3.13) and (3.24), the resulting $p(X|\Theta)$ will be proportional to the exponential of the sum of the two χ^2 related to data and prior, so that

$$\begin{cases} p(X|\Theta) \propto e^{-\chi^2} \\ \chi^2 = \chi^2_{DATA} + \chi^2_{CORR\ PRIOR} \end{cases} \tag{3.26}$$

Following [71] we write the covariance matrix as

$$C(a, a') = \sqrt{C(a)C(a')}\tilde{C}(a, a')$$

with $C(a)$ autocorrelation matrix and $\tilde{C}(a, a')$ correlation matrix, functions only of the scale factors. For the Dark Energy EoS we used as analytical fittings to $C(a)$ and $\tilde{C}(a, a')$ those obtained by [71], via minimization of the residuals, for two classes of models: Quintessence and Horndeski.
The two correlations fitting formula are the exponential and the CPZ parameterizations (Tab.3.1), such that if δa (or $\delta ln(a)$) is much higher than the correlation length ξ then the correlation tends to zero. The prior that minimizes the best the residuals in all the cases is the exponential one.

Autocorrelation matrix		α	β	γ	x
$C(x) = \alpha + \beta exp(\gamma(x - x_0))$	Quintessence	0.03	0.3	6.5	a
	Horndeski	0.05	0.8	2	$ln(a)$
Correlation matrix		ξ	n	x	y
$\tilde{C}(x, y) = exp\left[\left(-\frac{\lvert x-y\rvert}{\xi}\right)^n\right]$	Quintessence	0.7	1.8	a	a'
	Horndeski	0.3	1.2	$ln(a)$	$ln(a')$
$\tilde{C}(x, y) = \frac{1}{1+\left(\frac{\lvert x-y\rvert}{\xi}\right)^n}$	Quintessence	0.6	2	a	a'
	Horndeski	0.2	2	$ln(a)$	$ln(a')$

Table 3.1: Summary of the autocorrelation and correlation analytical fits obtained by [71]. The first parameterization of the correlation matrix is the exponential, while the second is the CPZ [59]. In particular ξ is the correlation length used for the Gaussian Process method.

For $\mu(z)$ and $\Sigma(z)$ I used the CPZ analytical fit to the correlation matrix found by [72] (Tab.3.2), while for the autocorrelation matrix there was no fitting. For this reason, once known the binning, I directly took the numerical values for $C(a)$.

Correlation matrix		ξ	n	x	y
$\tilde{C}(x, y) = \frac{1}{1+\left(\frac{\lvert x-y\rvert}{\xi}\right)^n}$	μ	0.31	1.74	a	a'
	Σ	0.38	1.7	a	a'

Table 3.2: CPZ fitting parameters for the correlation matrix in the Horndeski case; taken from [72]

The choice of the binning properties is very important.

First, given a certain redshift interval for the reconstruction, a high number of bins implies a lower dependence of the reconstruction on the binning properties, such as the size. As outlined by [59], the correlation length sets the so called "number of effective degrees of freedom" $N_{eff} = (a_{max} - a_{min})/\xi$; as long as $N > N_{eff}$ the dependence of the reconstruction on the number of bins is negligible.
Furthermore, as already said, for increasing number of bins also the dependence on the

reconstruction method itself is suppressed, indeed for higher N the step function is going to approach the reconstruction obtained with the Gaussian Process.

However, overbinning is possible as well. Indeed, let us focus on the following input parameters: the correlation length ξ, the bin width Δa and the proposal density of $f_i(a)$ $(i = 1, .., N)$. The correlation length sets the strength of the influence of one bin on another; if the distance between two points a_i and a_j is much smaller than this length they will be highly correlated. The risk is that if a sufficiently high proposal density (i.e. long step) is given, CosmoMC will vary $f(a_i)$ with respect to $f(a_j)$ more than what the correlation can predict. This can lead to huge values of the χ^2. But on the other hand, we can not give a too low proposal density, because otherwise the code would not be as efficient as we want. Thus, there is a practical upper limit to N.
In Fig.3.5 I plotted[5] the results obtained for the EoS running CosmoMC without any dataset, but only with the CPZ correlation prior, in both the Horndeski and Quintessence case (different prior parameters), for the same input binning parameters. The constraints given by the Quintessence CPZ prior seems to be slightly more binding.

[5]https://getdist.readthedocs.io/

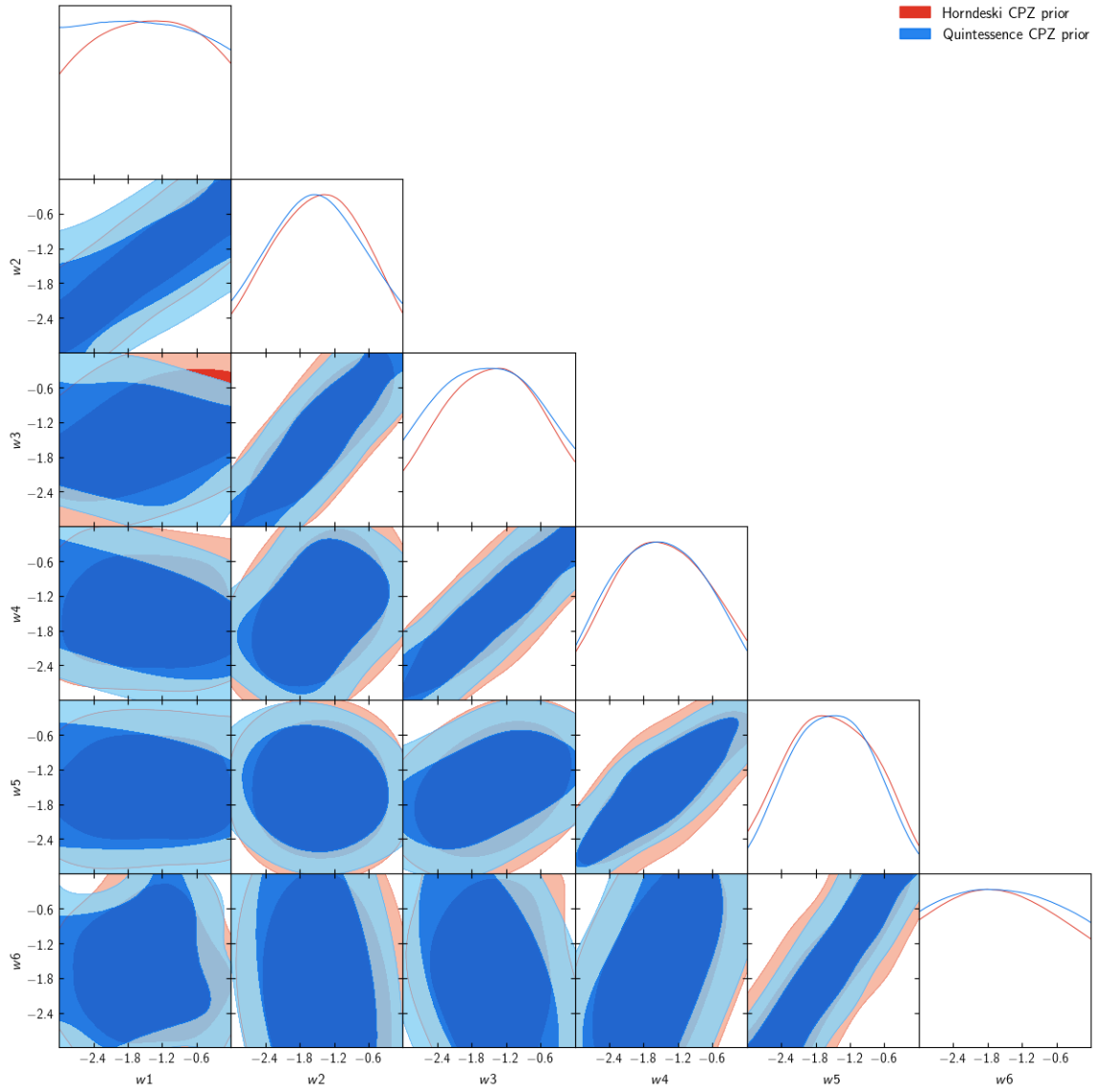

Figure 3.5: This is the triangle plot referred to the only CPZ prior runs in the case of Quintessence and Horndeski, given the same input parameters for the reconstruction of the EoS. It shows the effect of a different correlation length.

4 | Results

The non-parametric approach enables us to reconstruct the DE Equation of State $w_{DE}(z)$ and the two phenomenological functions $\mu(z)$ and $\Sigma(z)$ in a model-independent way. The only way in which we will restrict the analysis to a particular class of models, as Quintessence and Horndeski, is imposing the correlation priors (Sect.3.2.2), since the latter have been obtained imposing specific theoretical conditions [71]. I here want to remind that the use of the correlation prior restricts us in the choice of the binning properties as well. Thus, Crittenden et al.[59] defined the "number of effective degrees of freedom" as $N_{eff} = (a_{max} - a_{min})/\xi$, where the correlation length ξ is given by the correlation prior; as long as $N > N_{eff}$ the dependence of the reconstruction on the binning properties is negligible. We will require this condition to be satisfied in every reconstruction.

The reconstruction parameters $f_i(a)$ $(i = 1, .., N)$ are sampled within an appropriate range during the data analysis:

- **Quintessence** EoS lays in the region above the Phantom divide (Eq.(2.7)) in the $(z, w_Q(z))$ space, so that $w_{Q,i}$ is sampled in the range $[-1, 0]$. The reconstruction of $w_Q(z)$ is done using both the CPZ and exponential correlation priors (Tab.3.1), to highlight how they differently affect the inferred $w_{Q,i}$ parameters. Since it is a simple scalar field minimally coupled to gravity, there is no need to compute $\mu(z)$ and $\Sigma(z)$, as this model does not provide any modification to perturbation theory with respect to ΛCDM ($\mu(z) = \Sigma(z) = 1$).

- **Horndeski** EoS has no particular restriction in the values that it can assume, hence $w_{H,i}$ is sampled within the reasonable range $[-3, 0]$, that still includes ΛCDM. The reconstruction of $w_H(z)$ is obtained applying the exponential prior (Tab.3.1) to the data analysis. Moreover, since it is a MG model, there is the need to compute $\mu(z)$ and $\Sigma(z)$; in particular the sampling range is fixed on the basis of the results obtained by [8] in the DE-related and time-related parametrizations of f_i in Eq.(2.39). So, μ_i and Σ_i vary within the range $[0.2, 2]$ and they are reconstructed using their CPZ correlation priors (Tab.3.2), provided by [72].

4.1 Data

The datasets I used for the analysis are the JLA ('Joint Light-curve Analysis') dataset [73], that unifies Type Ia SNe observations of SDSS-II (Sloan Digital Sky Survey) and SNLS (Supernova Legacy Survey) collaborations, for a total of 740 Type Ia SNe up to redshift $z \sim 1$, the 6dFGS (6dF Galaxy Survey) [74] and SDSS Data Release 7 [75] for BAO and Planck 2015 data [23] for CMB.
However, the choice of the datasets is a bit tricky in the Horndeski case, since it is a MG model and in principle it requires a proper computation of the density perturbations evolution, via the two phenomenological functions μ and Σ. Since we first compute the reconstruction of the EoS, without getting into account μ and Σ, only background observables (SNe and BAO) can be used; when including also perturbations observables (CMB), μ and Σ need to be included in order to account for the modified growth of structures.

4.2 Code validation

As stated in the previous Chapter, the non-parametric reconstruction of $w_{DE}(z)$, $\mu(z)$ and $\Sigma(z)$ was included in CAMB and MGCAMB and then linked to CosmoMC. It was therefore necessary to check that the standard case was still working properly. For this reason I made tests with $w = const$ cases, which are those computed by the standard CAMB, reconstructing the constant DE EoS via the smoothed step function method. In particular, I here consider the ΛCDM case ($w_\Lambda = -1$), using all the datasets listed above. The resulting standard cosmological parameters are compared in Fig.4.1, they are in accordance.

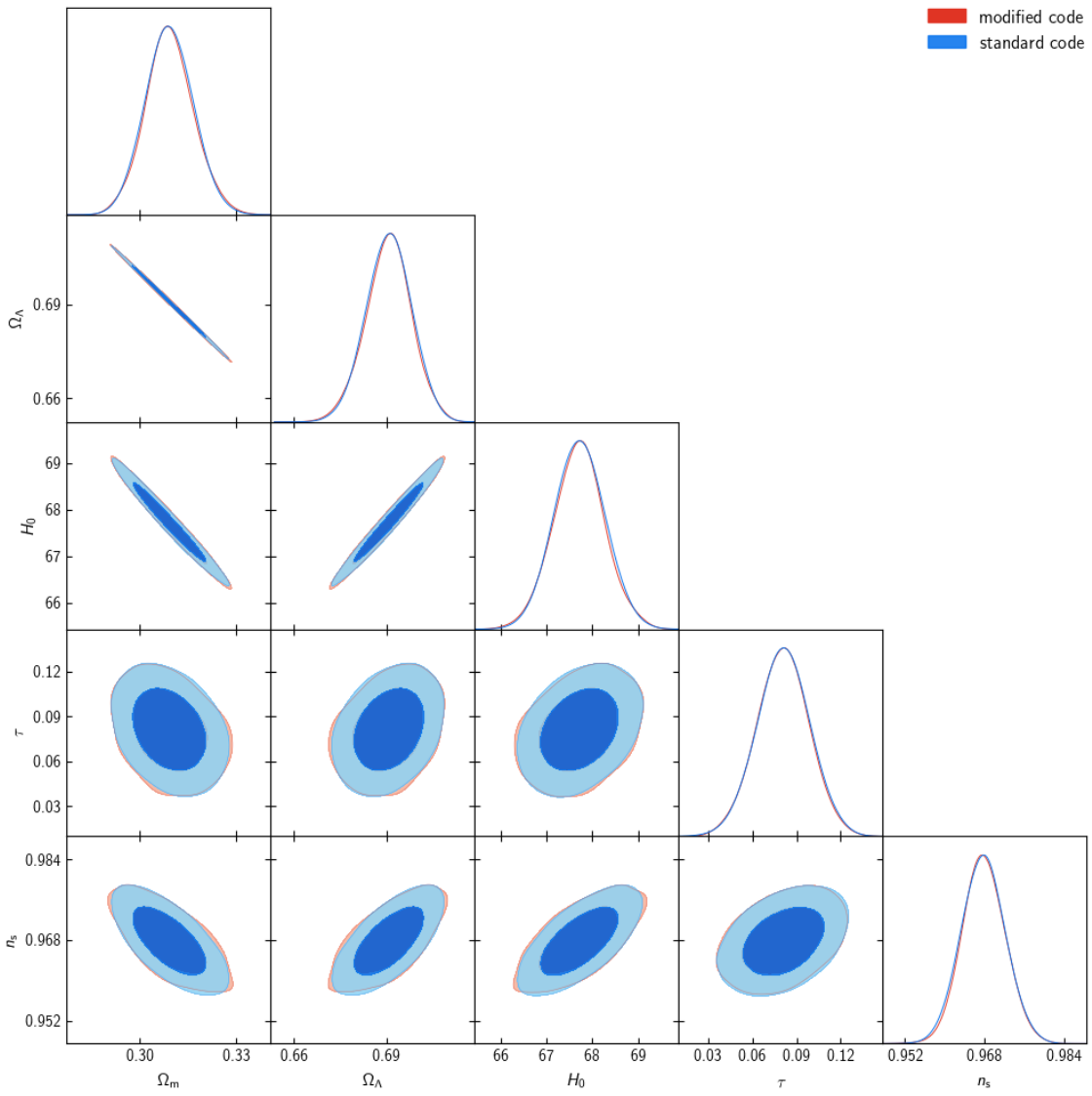

Figure 4.1: The cosmological parameters obtained with the standard and the modified CosmoMC in ΛCDM case are the same. H_0, Ω_m and Ω_Λ parameters has been already encountered throughout the text, while τ is the reionization optical depth and n_s is the scalar spectral index ($n_s = 1$ is typical of Harrison-Zel'dovich power spectrum)

4.3 Quintessence

The first set of results reported is for a DE with $w_{DE} \neq -1$ obtained for canonical Quintessence models.
I discretized the scale factor reconstruction interval $[a_{min}, 1]$, such that in one correlation length ($\xi_{exp} = 0.6 \sim \xi_{CPZ} = 0.7$) there were approximately four bins: $\vec{a} = (0.85\ 0.7\ 0.55\ 0.4\ 0.25\ 0.1)$.

Fig.4.2 shows the results obtained reconstructing the DE EoS via the smoothed step function reconstruction.
An interesting point to highlight is the effect of different correlation priors on the inferred parameters. For this purpose, in the smoothed step reconstruction case, I first ran the code with only the datasets and, then, added the exponential and CPZ priors.
Even from a first look at Fig.4.2, it is possible to understand the effect of the prior on $w_{DE,i}$ parameters. The use of the prior, independently of which one, reduces the 2D contours of the inferred $w_{DE,i}$ with respect to those obtained with only the datasets. Indeed, we do not expect the additional prior to make the contours larger since it provides information, but, at least equal or smaller. Hence, the two priors affect the inferred probability distributions of $w_{DE,i}$ differently, where the most evident distinction is on the parameter $w_{DE,5}$, for which the peaks in Fig.4.2 are slightly different.

SMOOTHED STEP FUNCTION RECONSTRUCTION			
Parameter	JLA+BAO+Planck	JLA+BAO+Planck (exp prior)	JLA+BAO+Planck (CPZ prior)
$\Omega_b h^2$.....	0.02242 ± 0.00021	0.02242 ± 0.00021	0.02242 ± 0.00021
$\Omega_c h^2$.....	0.1164 ± 0.0015	0.1165 ± 0.0015	0.1166 ± 0.0015
H_0	$65.1^{+1.6}_{-0.94}$	$65.1^{+1.6}_{-0.95}$	$65.1^{+1.5}_{-0.94}$
Ω_Λ.....	$0.670^{+0.017}_{-0.0099}$	$0.670^{+0.016}_{-0.010}$	$0.670^{+0.016}_{-0.0099}$
Ω_m.....	$0.330^{+0.0099}_{-0.017}$	$0.330^{+0.010}_{-0.016}$	$0.3296^{+0.0099}_{-0.016}$
$w_{DE,1}$.....	$-0.803,\ < -0.757$	$-0.805,\ < -0.759$	$-0.803,\ < -0.761$
$w_{DE,2}$.....	$-0.937,\ < -0.926$	$-0.935,\ < -0.924$	$-0.936,\ < -0.923$
$w_{DE,3}$.....	$-0.930,\ < -0.916$	$-0.930,\ < -0.914$	$-0.929,\ < -0.914$
$w_{DE,4}$.....	$-0.908,\ < -0.891$	$-0.920,\ < -0.895$	$-0.912,\ < -0.902$
$w_{DE,5}$.....	$-0.848,\ < -0.820$	$-0.876,\ < -0.831$	$-0.865,\ < -0.844$
$w_{DE,6}$.....	$-0.768,\ < -0.708$	$-0.801,\ < -0.732$	$-0.787,\ < -0.750$

Table 4.1: Mean values and 1σ confidence levels of the Quintessence case inferred parameters, using the datasets without and with the priors, reconstructing the Equation of State via smoothed step function. The input scale factors associated to the $\vec{w}_{DE}$ are $\vec{a} = (0.85\ 0.7\ 0.55\ 0.4\ 0.25\ 0.1)$.

The comparison of the three cases, bin by bin, can be quantified as a percentage difference of the mean values inferred adding the exponential(exp) and CPZ priors with respect to the mean values obtained using only the datasets. Hence, we notice that the main differences associated to the choice of a particular prior are related to the behaviour of $w_{DE,4}$ (exp: -1.32%, CPZ: -0.44%), $w_{DE,5}$ (exp: -3.3%, CPZ :-2.01%) and $w_{DE,6}$ (exp: -4.3%, CPZ: -2.47%) mean values and 1σ confidence levels, given in Tab.4.1, while $w_{DE,1}$ (exp: -0.249%, CPZ: 0%), $w_{DE,2}$ (exp: $+0.214\%$, CPZ: $+0.107\%$) and $w_{DE,3}$ (exp: 0%, CPZ: $+0.108\%$) do not differ significantly case by case.
The larger impact of the correlation priors in the last three bins can be explained with the fact that these redshifts contain much less data; therefore the constraining power of the prior is comparable to that of the data.

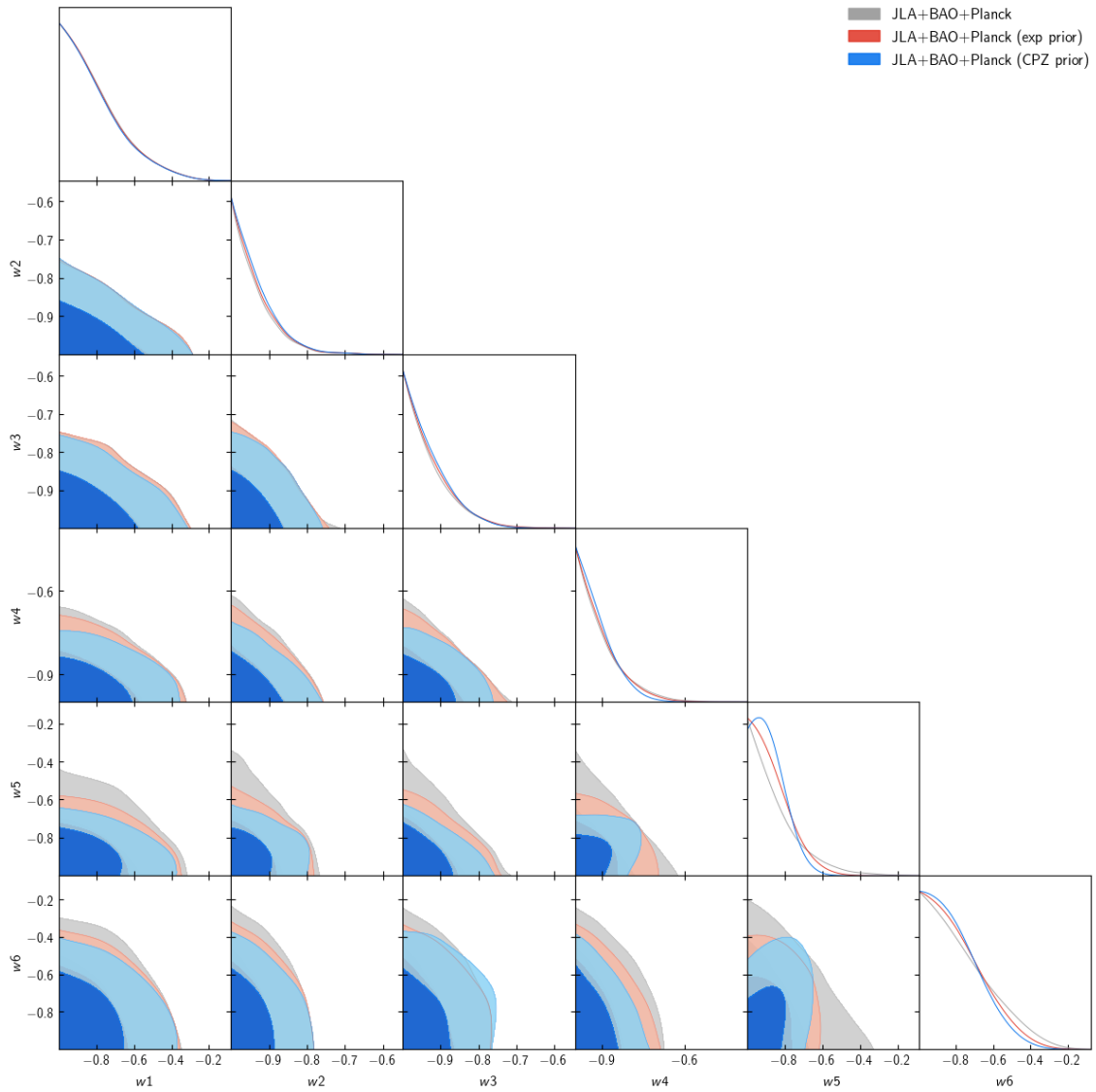

Figure 4.2: This plot shows the 2D contours between each of the $w_{DE,i}$ at 1σ and 2σ, for smoothed step reconstruction of the Quintessence Equation of State w_{DE}. All the cases (datasets alone or with a prior, exponential or CPZ) are included. The input scale factors are $\vec{a} = (0.85\ 0.7\ 0.55\ 0.4\ 0.25\ 0.1)$

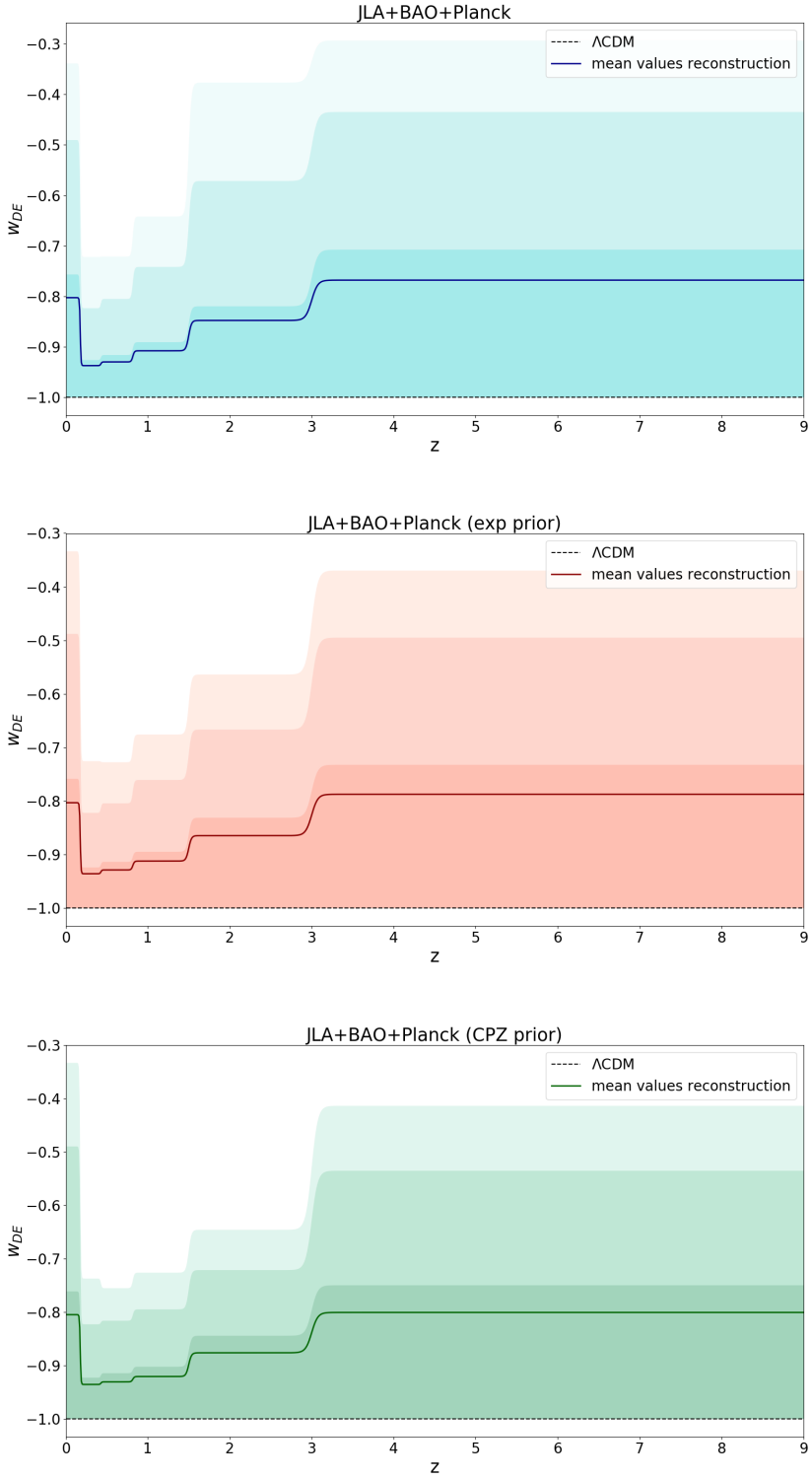

Figure 4.3: These plots show the Quintessence EoS smoothed step reconstructions obtained including, respectively from the top to the bottom, the datasets alone, data with the exponential correlation prior and then data with the CPZ prior. For each case, the shaded areas are those filling the reconstructions within the 68%, 95% and 99% confidence levels of all the $w_{DE,i}$, while the continuous lines are the reconstructions obtained using the mean values (Tab.4.1). The dashed line is the $w_\Lambda = -1$ case.

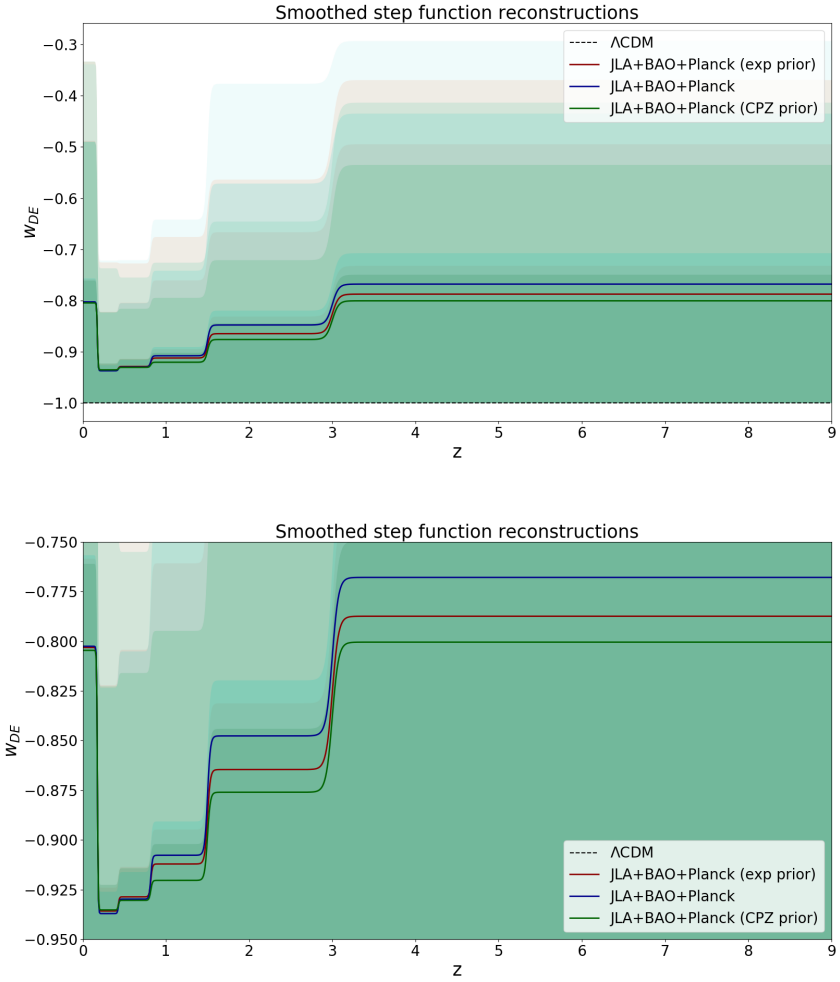

Figure 4.4: These plots show the superposition of the Quintessence EoS reconstructions of Fig.4.3, obtained via smoothed step function. The lower one is a zoom of the upper plot. The input scale factors are $\vec{a} = (0.85\ 0.7\ 0.55\ 0.4\ 0.25\ 0.1)$.

The final reconstructions obtained via the smoothed step function are shown in Figs.4.3 and 4.4. The visible difference between the effects of the two priors is linked to the already discussed behaviour of $w_{DE,4}$, $w_{DE,5}$ and $w_{DE,6}$, for which the priors are severely constraining.
Apart from the first bin, the mean tendency of the function is to increase over redshift, independently of the correlation priors. The behaviour of the first bin could be both due to a lack of data or to the particular reconstruction method. The following Gaussian Process reconstruction will make this clear.
The Cosmological Constant EoS $w_\Lambda = -1$ is still included within the 1σ confidence level reconstructions and therefore the ΛCDM limit is compatible with data also when using this non-parametric approach.

Let us proceed to the comparison between the previous reconstructions and those obtained via Gaussian Process method, using the datasets alone or with the CPZ prior as well. The correlation length ξ of the Gaussian Process is set equal to that of the prior, even if the latter is not used in the first case, but its ξ can still be though to be the fiducial one.

Since there are no data to constrain $w_{DE,0}$ I do not include it in the free parameters of the analysis. Then, there are two possible ways to proceed: letting the Gaussian Process extrapolate

GAUSSIAN PROCESS RECONSTRUCTION		
Parameter	JLA+BAO+Planck	JLA+BAO+Planck (CPZ prior)
$\Omega_b h^2$.....	$0.02242^{+0.00022}_{-0.00020}$	0.02241 ± 0.00021
$\Omega_c h^2$.....	0.1166 ± 0.0015	0.1167 ± 0.0014
H_0	$62.8^{+1.6}_{-2.0}$	$63.4^{+2.2}_{-1.6}$
Ω_Λ.....	0.645 ± 0.020	$0.651^{+0.025}_{-0.017}$
Ω_m.....	0.355 ± 0.020	$0.349^{+0.017}_{-0.025}$
$w_{DE,1}$.....	$-0.809, < -0.764$	$-0.775, < -0.723$
$w_{DE,2}$.....	$-0.931, < -0.916$	$-0.945, < -0.933$
$w_{DE,3}$.....	$-0.928, < -0.914$	$-0.920, < -0.901$
$w_{DE,4}$.....	$-0.907, < -0.889$	$-0.929, < -0.911$
$w_{DE,5}$.....	$-0.848, < -0.816$	$-0.868, < -0.833$
$w_{DE,6}$.....	$-0.761, < -0.691$	$-0.786, < -0.726$

Table 4.2: Mean values and 1σ confidence levels of the Quintessence case inferred parameters, using the datasets without and with the CPZ prior, reconstructing the Equation of State via Gaussian Process method. The input scale factors associated to the $\vec{w}_{DE}$ are $\vec{a} = (0.85\ 0.7\ 0.55\ 0.4\ 0.25\ 0.1)$.

the $w_{DE,0}$ value once given the $w_{DE,i}$ $(i = 1, .., N)$ inferred parameters as training points or setting the condition $w_{DE}(z < z_1) = w_{DE,1}$.

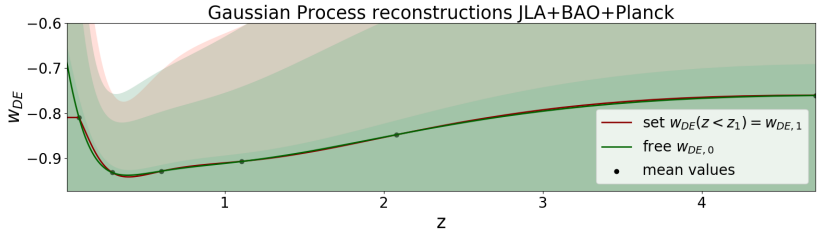

Figure 4.5: This plot is the superposition of the Quintessence EoS reconstructions obtained via Gaussian Process including the datasets alone, respectively setting $w_{DE,0}$ to be freely extrapolated by the GP itself or $w_{DE}(z < z_1) = w_{DE,1}$. The continuous lines are the reconstructions obtained using the mean values (Tab.4.2).

To keep the reconstruction as general as possible, the best choice would be the first approach; however, if we think that from present to $z_1 = 0.18$ the Equation of State is not going to vary significantly, compared to variations happening within a bigger redshift interval, the second approach is valid. Since such a strict condition on the value of $w_{DE}(z < z_1)$ does not change significantly the behaviour of the reconstruction on higher redshifts (Fig.4.5), we are going to bind the GP reconstruction with this condition.
The inferred reconstructions are shown and compared in Fig.4.6.
We here observe that, as in the smoothed step case, the addition of the prior largely affects the earliest time reconstruction (referring to $w_{DE,4}$, $w_{DE,5}$ and $w_{DE,6}$); however, differently from above, now the prior affects more evidently the first bins: the mean values of the reconstruction obtained adding the prior respectively differ from the $w_{DE,1}$, $w_{DE,2}$ and $w_{DE,3}$ means obtained with only the datasets by +4.2%, −1.5% and +0.86%. This could be linked to the unconstrained parameter $w_{DE,0}$, to which $w_{DE,1}$ is highly correlated.

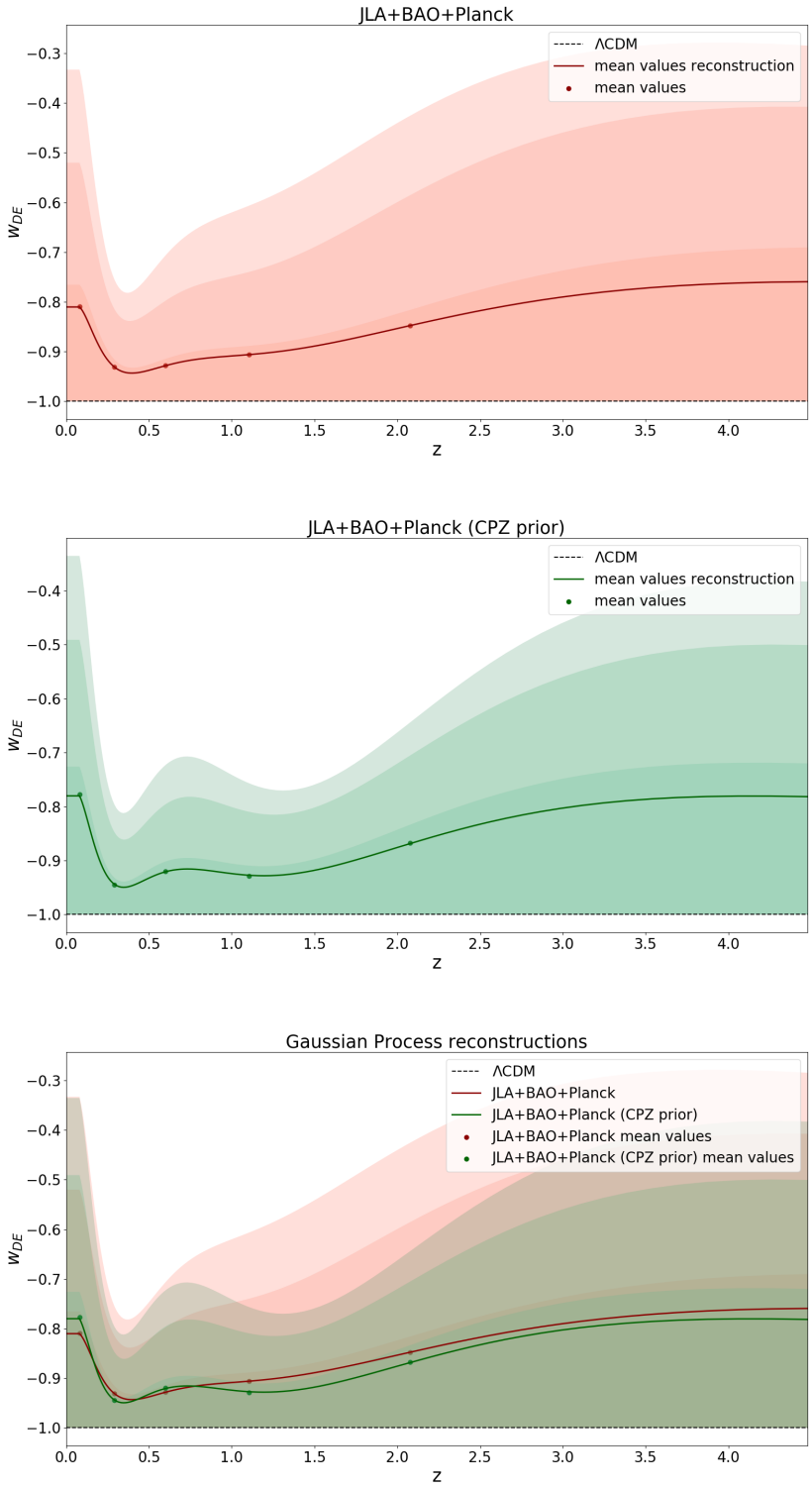

Figure 4.6: These are the Quintessence EoS reconstructions obtained via Gaussian Process including, respectively from the top to the bottom, the datasets alone and with the CPZ prior and the comparison of the two. For each case, the shaded areas are those filling the reconstructions within the 68%, 95% and 99% confidence levels of all the $w_{DE,i}$, while the continuous lines are the reconstructions obtained using the mean values (Tab.4.2). The input scale factors are $\vec{a} = (0.85\ 0.7\ 0.55\ 0.4\ 0.25\ 0.1)$.

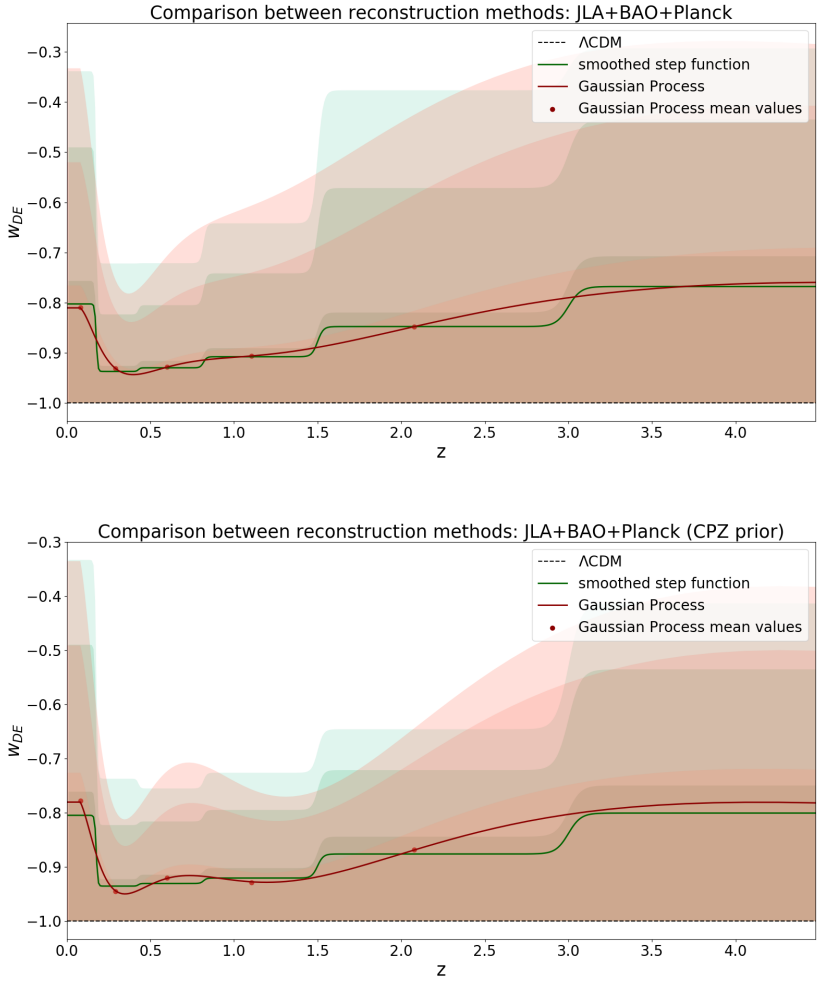

Figure 4.7: The upper plot is the superposition of the smoothed step function and Gaussian Process reconstructions for Quintessence EoS obtained including the datasets without the prior. The lower plot refers to the reconstructions obtained including the CPZ prior. For each case, the shaded areas are those filling the reconstructions within the 68%, 95% and 99% confidence levels of all the $w_{DE,i}$, while the continuous lines are the reconstructions obtained using the mean values. The input scale factors are $\vec{a} = (0.85\ 0.7\ 0.55\ 0.4\ 0.25\ 0.1)$.

The comparison between the smoothed step reconstructions and those obtained via Gaussian Process, in both the cases without and with the CPZ prior, is shown in Fig.4.7.
As expected the smoothed step function tends to mimic the Gaussian Process and the results of the two methods are consistent with each other; in the Figure I also plotted the inferred training points of the Gaussian Process to put them in evidence with respect to those obtained from the smoothed step function method.
The addition of the correlation prior in the Gaussian Process reconstruction affects the first three bins behaviour more significantly than it does in the smoothed step case, with respect to the reconstructions obtained using the datasets alone. Hence, if the smoothed step and GP $w_{DE,i}$ mean values inferred without the prior are very close to each, they are slightly different using the CPZ prior.
Again, apart from the first bin and independently of the prior, the mean tendency of the function is to increase over redshift; hence, the behaviour of $w_{DE,1}$ do not seem to be linked to the particular reconstruction method.

4.4 Horndeski class of MG models

As already seen, introducing a scalar field not minimally coupled to gravity induces modifications at the level of both background evolution and cosmological perturbations. In this Section I focus first on the effects of Horndeski models on the background expansion, and only in a second time I will include the effects at the perturbation level.
In Sec.4.4.1 I will present the results obtained for the reconstruction of the DE Equation of State alone, hence Planck data could not be used. Due to the limited data I will only show the results obtained using both the datasets and the prior, since with only background data the convergence of the chain was computationally demanding. The assumed correlation prior for the EoS is the exponential one. While providing the results I will refer to this case as HDE.
In Sec.4.4.2, on the other hand, I will reconstruct the effective EoS, including its exponential prior, along with the two phenomenological functions $\mu(z)$ and $\Sigma(z)$ via our modified version of MGCosmoMC, including their CPZ priors. Thus, including modifications to linear order scalar perturbations, Planck data can finally be used, allowing us to reconstruct $w_{DE}(z)$ up to higher redshifts, with respect to the previous case. Furthermore I will compare the EoS reconstruction made with MGCosmoMC with that of Sec.4.4.1, including wrongly Planck data, to show the importance of self-consistency. While providing the results I will refer to this case as HMG.

4.4.1 HDE: Reconstruction of the EoS alone

I discretized the scale factor reconstruction interval $[a_{min}, 1]$, such that in one correlation length ($\xi_{exp} = 0.3$) there were three bins: $\vec{a} = (0.9\ 0.8\ 0.7\ 0.6\ 0.5\ 0.4)$. In this case, since we are not using Planck data, the reconstruction can only be made up to $z_6 = 1.5$.

The behaviour of the obtained $w_{DE,i}$ is shown in Tab.4.3; for both the smoothed step function and Gaussian Process reconstructions, the last bins are the less constrained. The $w_{DE,6}$ is highly unconstrained with respect to the others, since the 68% confidence level cover the whole allowed range of values for $w_{DE,i}$ ($\in [-3, 0]$); moreover, the bins highly correlated to this unconstrained bin will suffer of larger confidence levels.
This high uncertainty on $w_{DE,6}$ is caused by the lack of data, on one hand we are not using high redshift observations (CMB), on the other, JLA datasets is not fully constraining in the redshift interval $z \sim [1, 1.5]$, since the number of SNe in this range of redshift is much smaller than at smaller z.

HDE RECONSTRUCTIONS: JLA+BAO (exp prior)		
Parameter	Smoothed step function	Gaussian Process
$\Omega_b h^2$.....	$0.041^{+0.012}_{-0.031}$	$0.049^{+0.017}_{-0.031}$
$\Omega_c h^2$.....	$0.181^{+0.084}_{-0.12}$	$0.157^{+0.067}_{-0.10}$
H_0	$82.06,\ > 76.6$	$83.44,\ > 79.7$
Ω_Λ.....	0.684 ± 0.086	0.713 ± 0.072
Ω_m.....	0.316 ± 0.086	0.287 ± 0.072
$w_{DE,1}$.....	$-1.10^{+0.30}_{-0.22}$	$-1.10^{+0.28}_{-0.23}$
$w_{DE,2}$.....	$-0.97^{+0.36}_{-0.22}$	$-0.86^{+0.26}_{-0.18}$
$w_{DE,3}$.....	$-1.09^{+0.60}_{-0.30}$	$-0.98^{+0.44}_{-0.25}$
$w_{DE,4}$.....	$-1.21^{+0.73}_{-0.39}$	$-1.05^{+0.58}_{-0.34}$
$w_{DE,5}$.....	$-1.44^{+0.75}_{-0.63}$	$-1.36^{+0.74}_{-0.62}$
$w_{DE,6}$.....	$-1.52\ \in [-3, 0]$	$-1.43\ \in [-3, 0]$

Table 4.3: Mean values and 1σ confidence levels of the Horndeski case, reconstructing the Equation of State via smoothed step function and via Gaussian Process. The input scale factors associated to the $\vec{w}_{DE}$ are $\vec{a} = (0.9\ 0.8\ 0.7\ 0.6\ 0.5\ 0.4)$. Here the bound shown with the $\in [-3, 0]$ notation indicates a lack of constraining power, with the 1σ region extending over the full prior range.

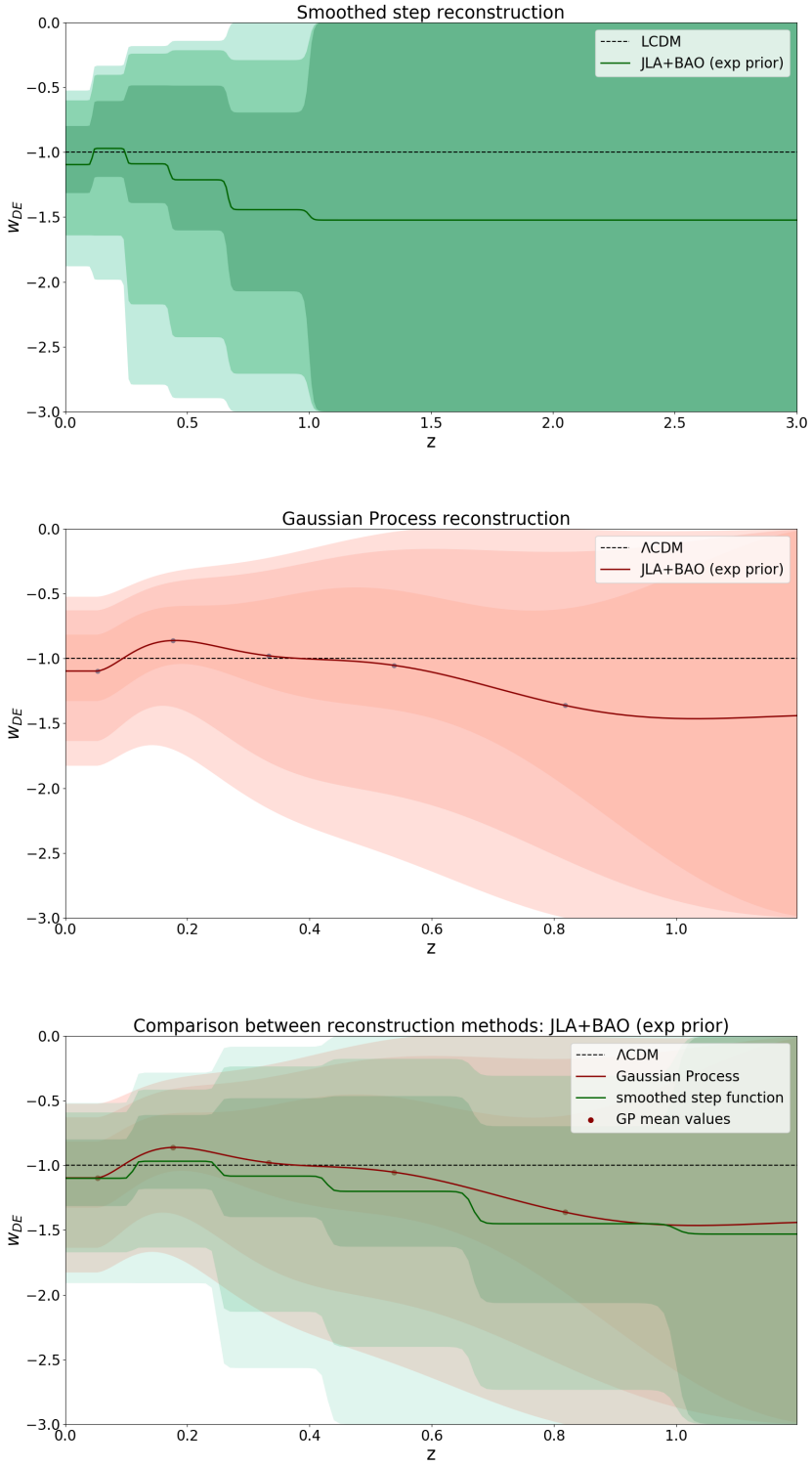

Figure 4.8: These are the Horndeski EoS reconstructions obtained via smoothed step function (upper plot) and via Gaussian Process (central plot), compared in the lower plot; these are inferred using JLA, BAO and the exponential prior. For each case, the shaded areas are those filling the reconstructions within the 68%, 95% and 99% confidence levels of all the $w_{DE,i}$, while the continuous lines are the reconstructions obtained using the mean values (Tab.4.3). The input scale factors are $\vec{a} = (0.9\ 0.8\ 0.7\ 0.6\ 0.5\ 0.4)$.

The plots in Fig.4.8 are obtained reconstructing the EoS using the inferred $w_{DE,i}$ mean values and their confidence levels limits, via smoothed step function in the upper plot, and via Gaussian Process in the one below. The lower plot is the superposition of these two reconstructions.
The function tends to decrease over redshift, independently of the reconstruction method; however, while in Quintessence case the first bin was the one that differed from the mean tendency, this time could be the first or the second one.
Even though the mean values reconstructed with the two methods differ more than in the Quintessence case (Fig.4.7), also in this case the results are compatible with each other within 1σ, and again the ΛCDM limit is also included within 1σ, thus in agreement with the data.

4.4.2 HMG: Reconstruction of all the functions

Let us now analyze the resulting reconstructions of the Equation of State $w_{DE}(z)$ and the two functions $\mu(z)$ and Σ(z), for which only the smoothed step reconstruction was applied.

Comparison with the previous results

The first main point to tackle is the comparison between the EoS reconstructions obtained in the HDE and HMG cases, hence the consistency choice of not using high redshift Planck data for the reconstruction of the $w_{DE}(z)$ of a MG model if its modifications to perturbations are not taken into account in $\mu(z)$ and $\Sigma(z)$.
In order to make the two cases comparable, the binning properties of the EoS must be the same for both, I discretized the scale factor reconstruction interval $[a_{min}, 1]$, such that $\vec{a} = (0.9\ 0.8\ 0.7\ 0.6\ 0.5\ 0.4)$.

So first, we need to wrongly add Planck data to the smoothed step reconstruction treated in Sec.4.4.1, in order to later highlight the differences with the HMG case, stressing the importance of a proper choice of datasets.
Hence, let us compare the previous results with the one obtained including high redshift observations. The resulting inferred EoS parameters are shown in Tab.4.4, while the two reconstructions are compared by superposition in Fig.4.10. Using high redshift data, highly reduces the 1σ c.l. reconstruction, i.e. that obtained using the 68% c.l. lower and upper limits.
This is due both to the increased constraining power on $w_{DE,i}$ and to the breaking of degeneracies between these and the cosmological parameters, which are now better constrained.

HDE SMOOTHED STEP RECONSTRUCTIONS		
Parameter	JLA+BAO (exp prior)	JLA+BAO+Planck (exp prior)
$\Omega_b h^2$.....	$0.041^{+0.012}_{-0.031}$	0.02218 ± 0.00022
$\Omega_c h^2$.....	$0.181^{+0.084}_{-0.12}$	0.1207 ± 0.0021
H_0	> 76.6	68.1 ± 1.2
Ω_Λ.....	0.684 ± 0.086	0.690 ± 0.011
Ω_m.....	0.316 ± 0.086	0.310 ± 0.011
$w_{DE,1}$.....	$-1.10^{+0.30}_{-0.21}$	-1.07 ± 0.21
$w_{DE,2}$.....	$-0.97^{+0.36}_{-0.22}$	-0.91 ± 0.20
$w_{DE,3}$.....	$-1.09^{+0.60}_{-0.30}$	-0.95 ± 0.25
$w_{DE,4}$.....	$-1.21^{+0.73}_{-0.39}$	-0.96 ± 0.32
$w_{DE,5}$.....	$-1.44^{+0.75}_{-0.63}$	-1.22 ± 0.32
$w_{DE,6}$.....	$-1.52, \in [-3, 0]$	$-1.46^{+0.59}_{-0.35}$

Table 4.4: Mean values and 1σ confidence levels of the Horndeski case, reconstructing the Equation of State via smoothed step function, including JLA,BAO and the exponential prior first and, then, adding Planck data. The input scale factors associated to the $\vec{w}_{DE}$ are $\vec{a} = (0.9\ 0.8\ 0.7\ 0.6\ 0.5\ 0.4)$.Here the bound shown with the $\in [-3, 0]$ notation indicates a lack of constraining power, with the 1σ region extending over the full prior range.

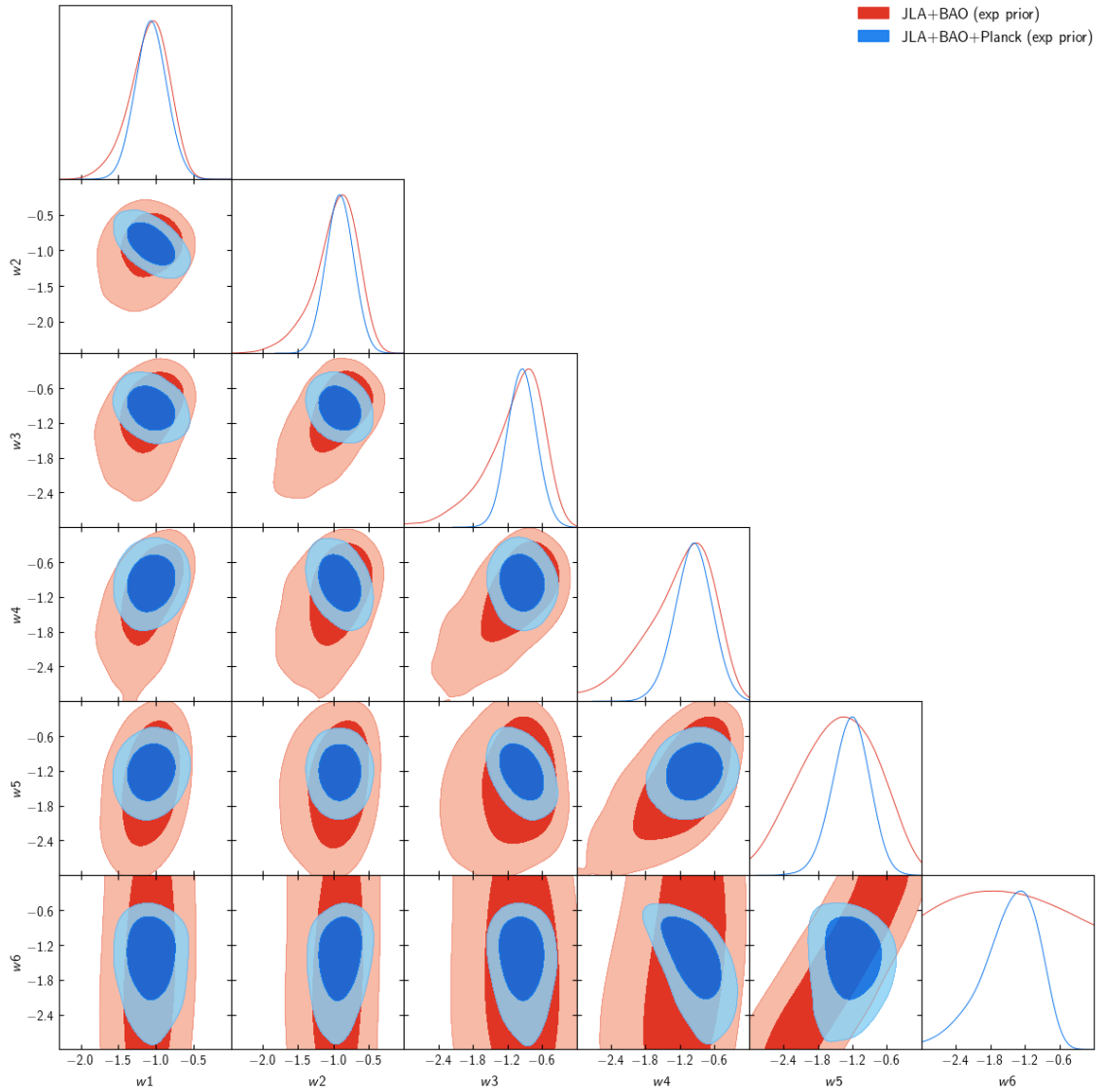

Figure 4.9: This triangle plot shows the 2D contours between each of the $w_{DE,i}$ at 1σ and 2σ, for smoothed step reconstruction of the Horndeski Equation of State w_{DE}, obtained including JLA,BAO and the exponential prior first and, then, adding Planck data.

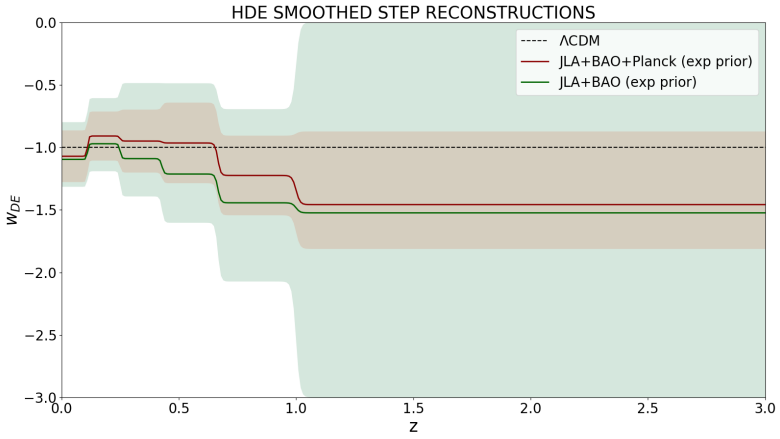

Figure 4.10: This plot shows the superposition of the Horndeski EoS smoothed step function reconstructions, obtained without and with Planck data in HDE case. For each case, the shaded areas are those filling the reconstructions within the 68% confidence levels of all the $w_{DE,i}$, while the continuous lines are the reconstructions obtained using the mean values (Tab.4.4). The input scale factors are $\vec{a} = (0.9\ 0.8\ 0.7\ 0.6\ 0.5\ 0.4)$.

Let us then move on to the comparison with HDE (including Planck data) and HMG reconstructions. While the binning properties of the EoS are the same as before, $\mu(z)$ and $\Sigma(z)$ a priori have different binning properties. The vector of the binned scale factor for their reconstruction is $\vec{a} = (0.85\ 0.7\ 0.55\ 0.4)$, still satisfying the condition $N > (a_{max} - a_{min})/\xi$ ($\xi_\mu = 0.31$, $\xi_\Sigma = 0.38$), where the binned values of $\mu(z)$ and $\Sigma(z)$ will vary during the Bayesian analysis in the range $[0.2, 2]$ [8]. The transition scale factor a_{trans}, i.e. the scale factor below which standard GR regime is recovered, is set to $a_{trans} = 0.1$.
Since both the EoS and the two phenomenological functions affect the evolution over time of density perturbations, we expect that a reconstruction of $\mu(z)$ and $\Sigma(z)$ will affect the behaviour of the reconstructed EoS, as it can be seen in Fig.4.11.

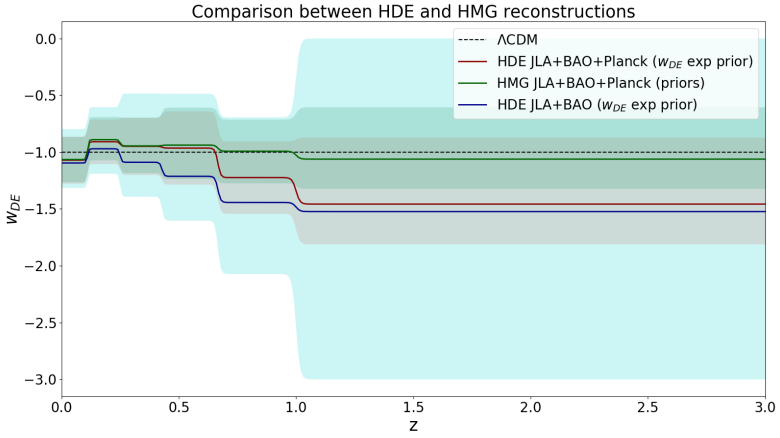

Figure 4.11: These are the Horndeski EoS reconstructions obtained including JLA,BAO and exponential prior for w_{DE} in HDE case and JLA, BAO, Planck and the EoS prior in HDE and HMG cases, where the latter needed also the μ and Σ correlation priors. For each case, the shaded areas are those filling the reconstructions within the 68% confidence levels of all the $w_{DE,i}$, while the continuous lines are the reconstructions obtained using the mean values (Tabs.4.4,4.5). The input scale factors are $\vec{a} = (0.9\ 0.8\ 0.7\ 0.6\ 0.5\ 0.4)$ for the EoS, while $\vec{a} = (0.85\ 0.7\ 0.55\ 0.4)$ for $\mu(z)$ and $\Sigma(z)$.

The inferred parameters for the reconstructions are resumed in Tab.4.5.

SMOOTHED STEP RECONSTRUCTIONS JLA+BAO+Planck			
Parameter	HDE (exp prior)	HMG	HMG (priors)
$\Omega_b h^2$.....	0.02218 ± 0.00022	0.02260 ± 0.00029	0.02261 ± 0.00029
$\Omega_c h^2$.....	0.1207 ± 0.0021	0.1168 ± 0.0025	0.1167 ± 0.0025
H_0	68.1 ± 1.2	68.1 ± 1.3	$67.8^{+1.2}_{-1.3}$
Ω_Λ.....	0.690 ± 0.011	0.697 ± 0.012	0.695 ± 0.011
Ω_m.....	0.310 ± 0.011	0.303 ± 0.012	0.305 ± 0.011
$w_{DE,1}$.....	-1.07 ± 0.21	-1.13 ± 0.24	-1.07 ± 0.20
$w_{DE,2}$.....	-0.91 ± 0.20	-0.77 ± 0.30	-0.89 ± 0.19
$w_{DE,3}$.....	-0.95 ± 0.25	-1.09 ± 0.43	-0.94 ± 0.24
$w_{DE,4}$.....	-0.96 ± 0.32	$-0.88^{+0.70}_{-0.38}$	-0.93 ± 0.31
$w_{DE,5}$.....	-1.22 ± 0.32	$-0.99^{+0.65}_{-0.43}$	-0.996 ± 0.28
$w_{DE,6}$.....	$-1.46^{+0.59}_{-0.35}$	$-1.12^{+0.67}_{-0.31}$	$-1.05^{+0.44}_{-0.25}$
μ_1.....	–	1.41 ± 0.30	1.34 ± 0.32
μ_2.....	–	$1.32^{+0.22}_{-0.29}$	1.27 ± 0.23
μ_3.....	–	$1.18^{+0.14}_{-0.19}$	1.18 ± 0.13
μ_4.....	–	1.103 ± 0.055	1.105 ± 0.056
Σ_1.....	–	$1.31^{+0.27}_{-0.34}$	$1.25^{+0.20}_{-0.28}$
Σ_2.....	–	$1.16^{+0.21}_{-0.26}$	$1.17^{+0.13}_{-0.18}$
Σ_3.....	–	$1.07^{+0.16}_{-0.14}$	1.08 ± 0.10
Σ_4.....	–	1.087 ± 0.049	1.089 ± 0.052

Table 4.5: Mean values and 1σ confidence levels of the Horndeski case. The first column of results refers to the reconstruction of the Equation of State via smoothed step function in HDE case including JLA,BAO, Planck as datasets and the w_{DE} exponential prior. The other columns refer to the reconstruction of the Equation of State, μ and Σ via smoothed step function in HMG case, including all the datasets without and with all the correlation priors (for w_{DE}, μ and Σ). The input scale factors are $\vec{a} = (0.9\ 0.8\ 0.7\ 0.6\ 0.5\ 0.4)$ for the EoS, while $\vec{a} = (0.85\ 0.7\ 0.55\ 0.4)$ for $\mu(z)$ and $\Sigma(z)$.

From Fig.4.11 it can be seen that Planck data highly constrain the DE EoS $w_{DE}(z)$ at higher redshifts, even in the HMG case, despite the higher number of parameters, since we included also the μ_i and Σ_i $(i = 1, .., 4)$ parameters. Furthermore the two phenomenological functions reconstructions seem to make the DE EoS get closer to ΛCDM limit, independently of the use of the correlation priors, as it can be seen from Tab.4.5.

For both the HDE and HMG cases, the reconstruction of the DE EoS is compatible within 1σ with the Cosmological Constant ($w_\Lambda = -1$); in the HMG case, for which also the two phenomenological functions have been included, the reconstructions of $\mu(z)$ and $\Sigma(z)$ are compatible with the standard GR regime, i.e. $\mu(z) = \Sigma(z) = 1$, within 2σ. Hence, again the ΛCDM limit is in agreement with the data.

Upper redshift limit for Equation of State

Since now Planck data can be consistently used, the reconstruction of the Horndeski Equation of State can be made up to a higher redshift.
So, I discretized the scale factor $\vec{a}$ = (0.9 0.8 0.7 0.6 0.5 0.4 0.3 0.2 0.1) for the EoS, while the binning properties of $\mu(z)$ and $\Sigma(z)$ are the same as in the previous paragraph.

The inferred reconstruction parameters are resumed in Tab.4.6.

HMG SMOOTHED STEP FUNCTION RECONSTRUCTIONS		
Parameter	JLA+BAO+Planck	JLA+BAO+Planck (priors)
$\Omega_b h^2$.....	0.02258 ± 0.00028	0.02258 ± 0.00029
$\Omega_c h^2$.....	0.1170 ± 0.0024	0.1168 ± 0.0023
H_0	$67.1^{+2.3}_{-4.7}$	66.4 ± 2.6
Ω_Λ.....	$0.686^{+0.027}_{-0.040}$	0.681 ± 0.024
Ω_m.....	$0.314^{+0.040}_{-0.027}$	0.319 ± 0.024
$w_{DE,1}$.....	$-0.874,\ > -1.12$	-0.82 ± 0.39
$w_{DE,2}$.....	$-0.94^{+0.59}_{-0.50}$	-0.95 ± 0.23
$w_{DE,3}$.....	-1.04 ± 0.42	-1.01 ± 0.26
$w_{DE,4}$.....	$-0.83^{+0.57}_{-0.38}$	-0.90 ± 0.28
$w_{DE,5}$.....	$-0.90^{+0.55}_{-0.41}$	-0.91 ± 0.32
$w_{DE,6}$.....	$-1.19^{+1.0}_{-0.45}$	$-1.05^{+0.47}_{-0.39}$
$w_{DE,7}$.....	$-1.28^{+1.2}_{-0.42}$	$-1.22^{+0.65}_{-0.48}$
$w_{DE,8}$.....	$-1.45,\ \in [-3,0]$	$-1.40^{+0.82}_{-0.68}$
$w_{DE,9}$.....	$-1.49,\ \in [-3,0]$	$-1.49,\ \in [-3,0]$
μ_1.....	$1.41^{+0.35}_{-0.30}$	1.36 ± 0.31
μ_2.....	$1.32^{+0.24}_{-0.28}$	1.27 ± 0.24
μ_3.....	$1.19^{+0.15}_{-0.19}$	$1.17^{+0.13}_{-0.16}$
μ_4.....	$1.102^{+0.053}_{-0.058}$	1.107 ± 0.053
Σ_1.....	$1.31^{+0.27}_{-0.34}$	$1.24^{+0.20}_{-0.26}$
Σ_2.....	$1.14^{+0.19}_{-0.25}$	$1.15^{+0.14}_{-0.18}$
Σ_3.....	$1.07^{+0.17}_{-0.15}$	1.09 ± 0.11
Σ_4.....	1.085 ± 0.049	$1.088^{+0.053}_{-0.047}$

Table 4.6: Mean values and 1σ confidence levels of the Horndeski case, reconstructing the Equation of State, μ and Σ via smoothed step functions including all the datasets without and with all the correlation priors. The input scale factors are $\vec{a}$ = (0.9 0.8 0.7 0.6 0.5 0.4 0.3 0.2 0.1) for the EoS, while $\vec{a}$ = (0.85 0.7 0.55 0.4) for $\mu(z)$ and $\Sigma(z)$. Here the bound shown with the $\in [-3,0]$ notation for the EoS parameters indicates a lack of constraining power, with the 1σ region extending over the full prior range.

Let us first show in Fig.4.12 the effect of the correlation priors on the reconstruction of the Equation of State $w_{DE}(z)$, while in Fig.4.14 for $\mu(z)$ and Σ. Once again, the correlation prior reduces the 1σ confidence level region, still including the Cosmological Constant. The mean values slightly vary from one case to the other, it could be both for the effect of the EoS prior in absence of data or to how the μ and Σ priors affect the two phenomenological functions and hence affects the EoS, since they are correlated.

A higher number of bins for the Equation of State, with respect to the previous results obtained binning the scale factor in $\vec{a}$ = (0.9 0.8 0.7 0.6 0.5 0.4), will reflect in a slight different behaviour of $w_{DE}(z)$; the comparison between the two reconstructions obtained using the priors is plotted in Fig.4.13. In particular, we expect the same overall trend of the function in the two cases, but slightly different behaviors bin by bin, since, for the first case, a lot of information is lost, cutting the reconstruction at $a = 0.4$. Indeed, if $w_{DE}(z > z_{final}) = w_{DE}(z_{final})$ and the bins are correlated, since it is probable that the final w_{DE} is different in the two cases, this will lead to differences in the preceding bins.

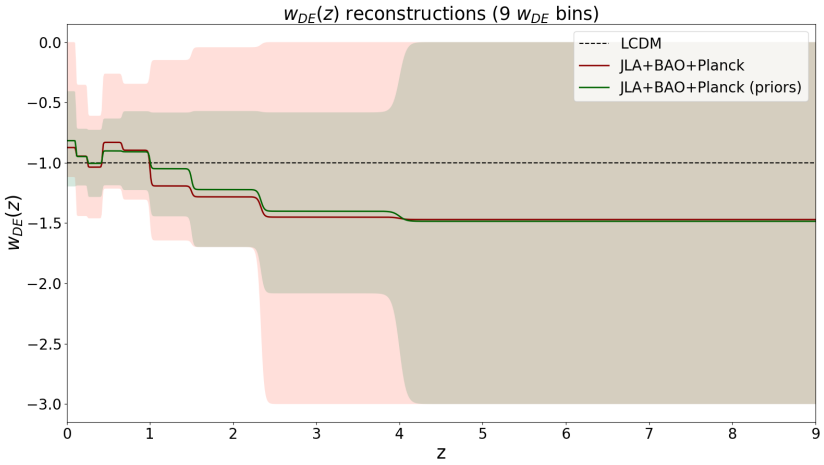

Figure 4.12: These are the Horndeski $w_{DE}(z)$ reconstructions obtained including all the datasets without and with the priors, obtained binning the scale factor in $\vec{a} = (0.9\ 0.8\ 0.7\ 0.6\ 0.5\ 0.4\ 0.3\ 0.2\ 0.1)$ for the EoS and in $\vec{a}_\mu = (0.85\ 0.7\ 0.55\ 0.4)$ for $\mu(z)$ and $\Sigma(z)$. For each case, the shaded areas are those filling the reconstructions within the 68% confidence levels, while the continuous lines are the reconstructions obtained using the mean values.

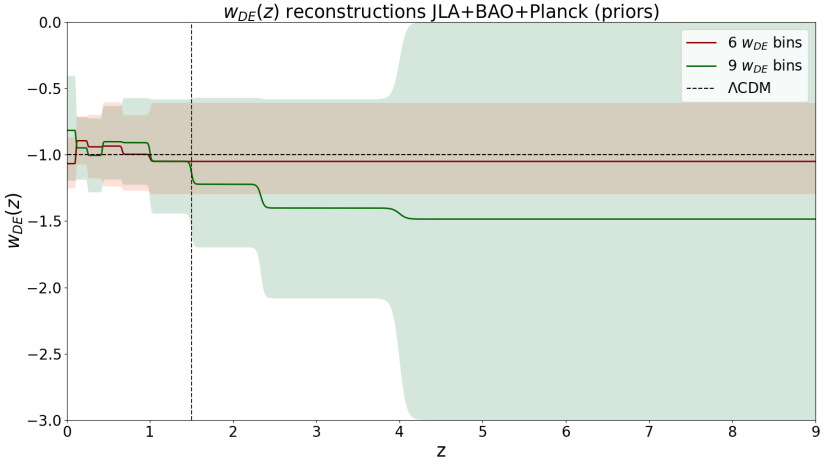

Figure 4.13: These are the Horndeski EoS reconstructions obtained including JLA, BAO, Planck datasets along with the priors in HMG case, obtained binning the scale factor in $\vec{a} = (0.9\ 0.8\ 0.7\ 0.6\ 0.5\ 0.4)$ (6 bins case) and $\vec{a} = (0.9\ 0.8\ 0.7\ 0.6\ 0.5\ 0.4\ 0.3\ 0.2\ 0.1)$ (9 bins case), given the same binning properties for $\mu(z)$ and $\Sigma(z)$ ($\vec{a}_\mu = (0.85\ 0.7\ 0.55\ 0.4)$). For each case, the shaded areas are those filling the reconstructions within the 68% confidence levels of all the $w_{DE,i}$, while the continuous lines are the reconstructions obtained using the mean values.

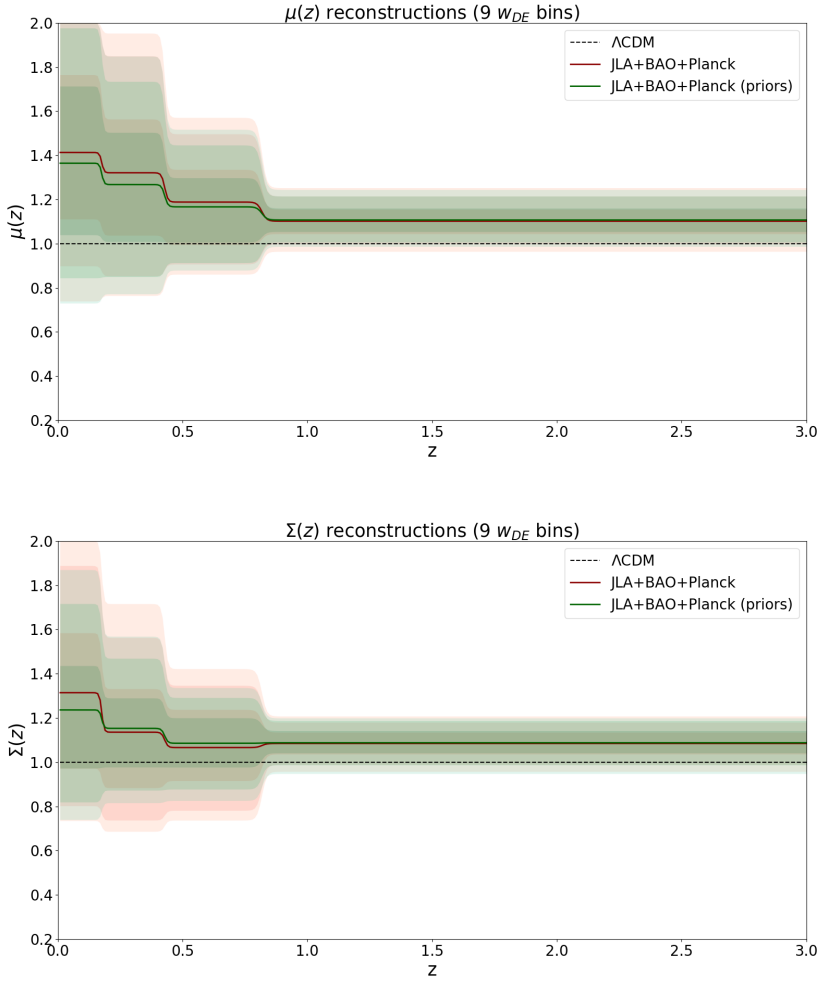

Figure 4.14: These are the Horndeski $\mu(z)$ (upper plot) and $\Sigma(z)$ (lower plot) reconstructions obtained including all the datasets without and with the priors, obtained binning the scale factor in $\vec{a}$ = (0.9 0.8 0.7 0.6 0.5 0.4 0.3 0.2 0.1) for the EoS and in $\vec{a}_\mu$ = (0.85 0.7 0.55 0.4) for $\mu(z)$ and $\Sigma(z)$. For each case, the shaded areas are those filling the reconstructions within the 68%, 95% and 99% confidence levels, while the continuous lines are the reconstructions obtained using the mean values.

Reconstruction of $\mu(z)$ and $\Sigma(z)$ up to a_{trans}

I here present the final results obtained in the case in which the Horndeski Equation of State scale factor binning is $\vec{a}$ = (0.9 0.8 0.7 0.6 0.5 0.4 0.3 0.2 0.1), while that of $\mu(z)$ and $\Sigma(z)$ is $\vec{a}$ = (0.85 0.7 0.55 0.4 0.25 0.1), then up to the transition scale factor $a_{trans} = 0.1$.

HMG SMOOTHED STEP FUNCTION RECONSTRUCTIONS		
Parameter	JLA+BAO+Planck	JLA+BAO+Planck (exp prior)
$\Omega_b h^2$.....	0.02264 ± 0.00028	0.02266 ± 0.00028
$\Omega_c h^2$.....	0.1161 ± 0.0024	0.1158 ± 0.0024
H_0	$67.0^{+2.3}_{-4.5}$	66.4 ± 2.5
Ω_Λ.....	$0.687^{+0.028}_{-0.039}$	0.683 ± 0.24
Ω_m.....	$0.313^{+0.039}_{-0.028}$	0.317 ± 0.24
$w_{DE,1}$.....	$-0.87^{+0.87}_{-0.24}$	-0.83 ± 0.38
$w_{DE,2}$.....	$-0.93^{+0.59}_{-0.49}$	-0.96 ± 0.23
$w_{DE,3}$.....	$-1.06^{+0.37}_{-0.42}$	-0.998 ± 0.25
$w_{DE,4}$.....	$-0.78^{+0.55}_{-0.35}$	-0.89 ± 0.26
$w_{DE,5}$.....	$-0.92^{+0.70}_{-0.40}$	$-0.83^{+0.35}_{-0.32}$
$w_{DE,6}$.....	$-1.01, > -1.29$	$-0.89^{+0.42}_{-0.34}$
$w_{DE,7}$.....	$-1.27, > -1.68$	$-1.16^{+0.64}_{-0.49}$
$w_{DE,8}$.....	$-1.47, \in [-3, 0]$	$-1.48^{+0.76}_{-0.67}$
$w_{DE,9}$.....	$-1.52, \in [-3, 0]$	-1.58 ± 0.78
μ_1.....	$1.53^{+0.42}_{-0.18}$	$1.46^{+0.43}_{-0.23}$
μ_2.....	1.43 ± 0.25	1.38 ± 0.25
μ_3.....	$1.34^{+0.20}_{-0.23}$	$1.31^{+0.19}_{-0.22}$
μ_4.....	1.23 ± 0.15	$1.23^{+0.16}_{-0.14}$
μ_5.....	1.12 ± 0.10	1.14 ± 0.10
μ_6.....	$1.021^{+0.089}_{-0.14}$	$1.05^{+0.12}_{-0.15}$
Σ_1.....	1.42 ± 0.32	1.35 ± 0.30
Σ_2.....	1.34 ± 0.29	1.29 ± 0.26
Σ_3.....	1.28 ± 0.26	1.22 ± 0.24
Σ_4.....	$1.20^{+0.24}_{-0.20}$	1.18 ± 0.20
Σ_5.....	$1.18^{+0.17}_{-0.11}$	1.16 ± 0.14
Σ_6.....	$1.118^{+0.071}_{-0.063}$	1.123 ± 0.061

Table 4.7: Results of the Horndeski case, without and with the priors, reconstructing the Equation of State, $\mu(z)$ and $\Sigma(z)$ via smoothed step function. The input scale factors associated to the $\vec{w}_{DE}$ are $\vec{a}$ = (0.9 0.8 0.7 0.6 0.5 0.4 0.3 0.2 0.1), while for $\vec{\mu}$ and $\vec{\Sigma}$ are $\vec{a}$ = (0.85 0.7 0.55 0.4 0.25 0.1). Here the bound shown with the $\in [-3, 0]$ notation for the EoS parameters indicates a lack of constraining power, with the 1σ region extending over the full prior range.

In Fig.4.15 I plotted the reconstructions for $w_{DE}(z)$ (upper plot), $\mu(z)$ (central plot) and $\Sigma(z)$ (lower plot) obtained including JLA, BAO, Planck and the correlation priors for all these functions.
The effective Equation of State mean behaviour is oscillating, crossing the Phantom divide once, and then decreases below -1. Such a particular pattern, at least referring to the reconstruction obtained using the $w_{DE,i}$ mean values, would have never been caught by a CPL-like parametrization (Eq.(2.34)) for instance. The Cosmological Constant limit $w_\Lambda = -1$ is still in agreement with the reconstruction within 1σ.
On the other hand, the two phenomenological functions tends to decrease over time up to a_{trans}, reaching very closely 1 in the case of $\mu(z)$. This behaviour meets the 'late times' Planck parametrization (Eq.(2.39)), where the time dependence of $\mu(z)$ and $\Sigma(z)$ is assumed to be the same of the DE density parameter $\Omega_{DE}(z)$. While the ΛCDM ($\mu(z) = \Sigma(z) = 1$) is in agreement with the $\mu(z)$ results within 1σ, ΛCDM is within 2σ for $\Sigma(z)$, which is again consistent with the results of Planck.

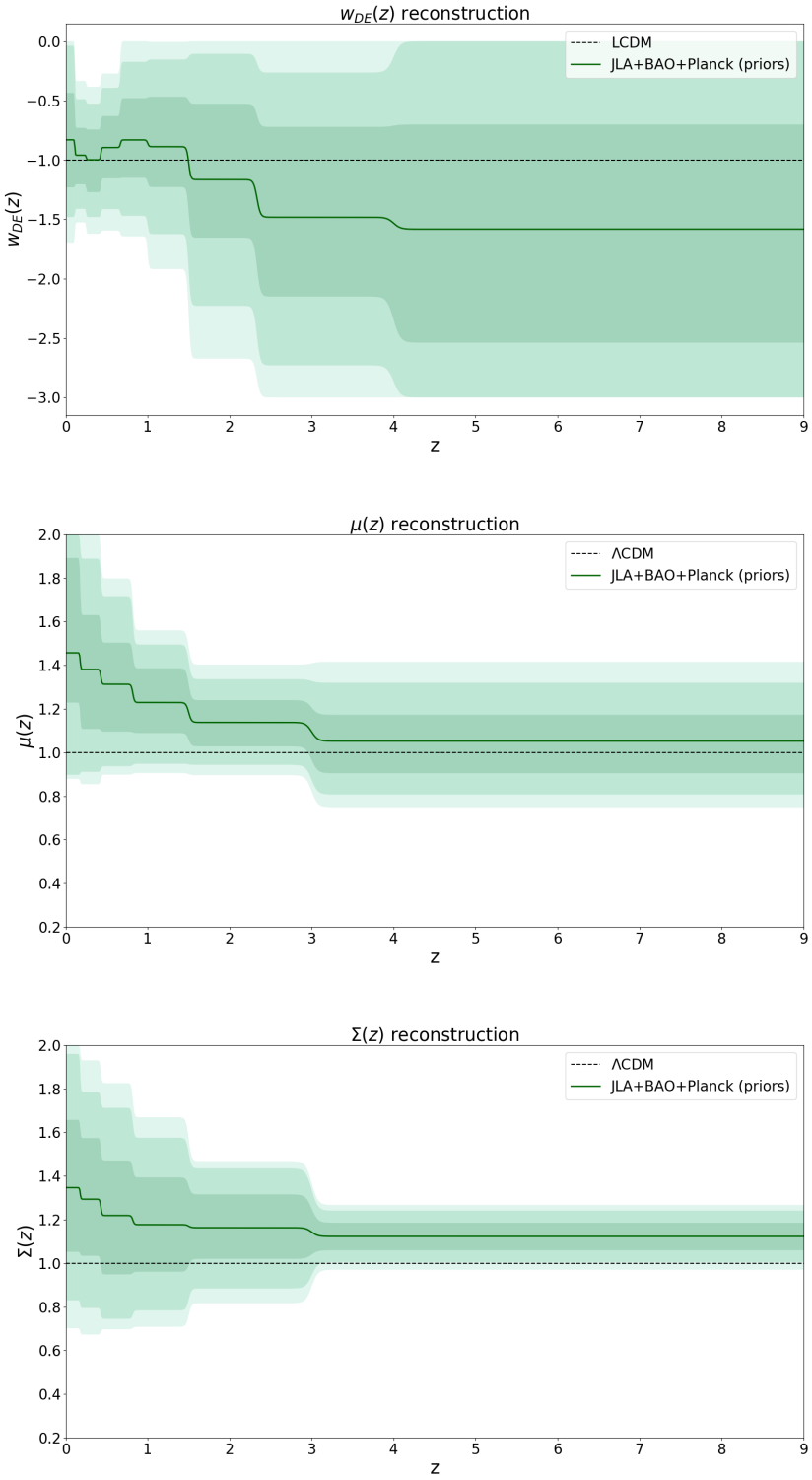

Figure 4.15: These are the Horndeski $w_{DE}(z)$ (upper plot), $\mu(z)$ (central plot) and $\Sigma(z)$ (lower plot) reconstructions obtained including all the datasets without and with the priors, obtained binning the scale factor in $\vec{a} = (0.9\ 0.8\ 0.7\ 0.6\ 0.5\ 0.4\ 0.3\ 0.2\ 0.1)$ for the EoS and in $\vec{a}_\mu = (0.85\ 0.7\ 0.55\ 0.4\ 0.25\ 0.1)$ for $\mu(z)$ and $\Sigma(z)$. For each case, the shaded areas are those filling the reconstructions within the 68%, 95% and 99% confidence levels, while the continuous lines are the reconstructions obtained using the mean values.

5 | Discussion and conclusions

5.1 Model-independent results

Without assuming any prior, the reconstructions are model-independent, hence the $w(z)$, $\mu(z)$ and $\Sigma(z)$ obtained in Horndeski case without imposing the prior could be actually treated as the most general reconstructions of this work, since no model dependent condition is imposed on the reconstruction.
In the three figures below I show the results of the last paragraph of the previous Chapter, without having assumed any prior: the Cosmological Constant case is within 1σ in the EoS reconstruction, while within 2σ in the $\mu(z)$ and $\Sigma(z)$ reconstructions.

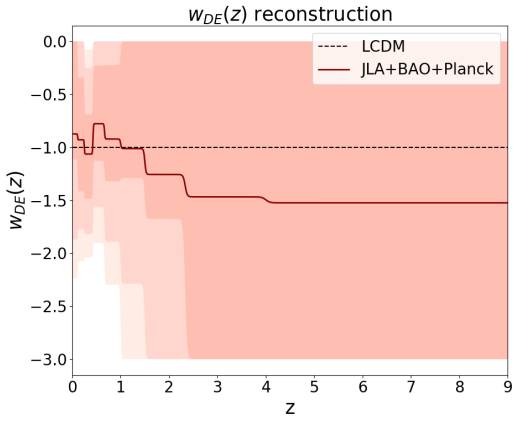

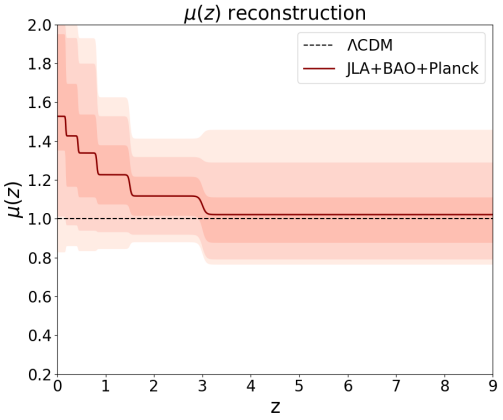

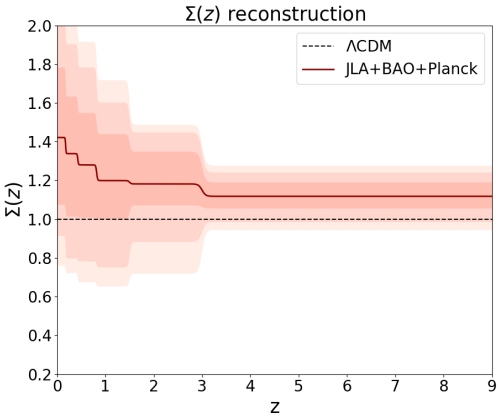

The obtained model-independent reconstructions reveal the strength of the non-parametric approach.

At the background level, the mechanism driving the late cosmic acceleration affects the expansion history via an effective DE Equation of State (upper plot panel) that seems to have an oscillating pattern, at least reconstructing the function using the mean inferred $w_{DE,i}$ (red solid line). Of course, additional data could be able to further constrain the function.
The power of the non-parametric approach lies in catching this oscillating pattern, or any other particular, that for instance a CPL-like parametrization (Eq.(2.34)) would have never caught.

This same mechanism could potentially turn out to be a modification to the laws of gravity on large scale. Thus, since we want to keep the reconstruction as general as possible without restricting ourselves to DE models, we need to examine the two phenomenological functions as well.
The behaviour of $\mu(z)$ and $\Sigma(z)$ seems to be in agreement with the 'late times' Planck parametrizations [8]. Indeed, referring to the parametrizations of Eq.(2.39) and neglecting the scale dependence of the phenomenological functions, $\mu(a)$ and $\Sigma(a)$ take the form

$$\begin{aligned} \mu(a) &= 1 + f_1(a) \\ \Sigma(a) &= 1 + f_2(a) \end{aligned} \tag{5.1}$$

where assuming $f_i = E_{ii}\Omega_{DE}(a)$ would represent well the behaviour of $\mu(z)$ and $\Sigma(z)$ (low panels), that tend to standard GR limit for higher redshifts.

5.2 Quintessence and Horndeski

The non-parametric approach has been implemented as a model-independent reconstruction for $w(z)$, $\mu(z)$ and $\Sigma(z)$, as long as we do not include any theoretical condition coming from the correlation priors. Throughout the data analysis we have also restricted ourselves to the choice of particular models, for which the priors were given, i.e. Quintessence DE model and the broad class of Horndeski scalar tensor theories (MG).

For Quintessence case, in order to fulfill the theoretical conditions of the model, the correlation prior was not sufficient, indeed it was also necessary to impose the lower limit of the EoS to $w_{DE} = -1$, cutting-off a severe range of solutions. The w_{DE}(z) reconstructed with the smoothed step and Gaussian Process methods are shown and compared in Fig.4.7, from which we concluded that the two methods are in agreement with each other.
Furthermore, while working assuming Quintessence model, we also had the chance to test the effects of both the exponential and CPZ (Tab.3.1) priors on the reconstruction, where we have later deduced that the constraining power of the correlation prior largely increases where there are less data.

Secondly, we analyzed the broad class of Horndeski scalar tensor theories, accounting also for the two phenomenological functions $\mu(z)$ and $\Sigma(z)$ while working with observables related to the evolution of the density perturbations, as the CMB. Indeed, there is a degeneracy between the effective EoS, $\mu(z)$ and $\Sigma(z)$, since on one hand the evolution of matter density perturbations is both linked to the expansion history and the scalar perturbation Ψ, while on the other hand photon's geodesics are linked to a linear combination of Ψ and Φ, to which $\mu(z)$ and $\Sigma(z)$ are related by definition.
The non-parametric approach makes the effective Equation of State reveal an oscillating pattern, that evolves to values below -1 at higher redshifts.
As already pointed out in Sect.5.1, the behaviour of $\mu(z)$ and $\Sigma(z)$ obtained through the non-parametric approach could be further compared with the 'late times' Planck parametrization, neglecting the scale dependence, since $\mu(z)$ and $\Sigma(z)$ at higher redshifts tends to 1, with $\Sigma(z)$ being slightly more departing from 1 with respect to $\mu(z)$.

5.3 H_0 tension

We have seen within this work that the tension between local and high redshift estimates of the H_0 parameter is one of the facts that have prompted the exploration of alternative models to the Cosmological Constant.
Referring to the estimates obtained from local measurements [4] and from high redshift observations [3]

$$H_0^{SH_0ES} = 73.48 \pm 1.66\ kms^{-1}Mpc^{-1} \qquad H_0^{Planck} = 67.36 \pm 0.54\ kms^{-1}Mpc^{-1}\ ,$$

I here want to show the comparison between these two and the inferred values of H_0 for all the HMG cases computed, namely for all the Horndeski cases in which all $w(z)$, $\mu(z)$ and $\Sigma(z)$ are reconstructed using all the datasets.

HMG RECONSTRUCTIONS						
	w_{DE} bins	μ and Σ bins	priors	H_0	Ω_M	Ω_{DE}
CASE 1	6	4	×	68.1 ± 1.3	0.303 ± 0.012	0.697 ± 0.012
			✓	$67.8^{+1.2}_{-1.3}$	0.305 ± 0.011	0.695 ± 0.011
CASE 2	9	4	×	$67.1^{+2.3}_{-4.7}$	$0.314^{+0.040}_{-0.027}$	$0.686^{+0.027}_{-0.040}$
			✓	66.4 ± 2.6	0.319 ± 0.024	0.681 ± 0.024
CASE 3	9	6	×	$67.0^{+2.3}_{-4.5}$	$0.313^{+0.039}_{-0.028}$	$0.687^{+0.028}_{-0.039}$
			✓	66.4 ± 2.5	0.317 ± 0.24	0.683 ± 0.24

Table 5.1: Inferred mean values and 1σ c.l. of the cosmological parameters, in all the Horndeski HMG cases, without and with the priors, reconstructing the EoS and the phenomenological functions via smoothed step function.

We can see that in all these cases the tension between high and low redshift measurements of H_0 is reduced to $\sim 2\sigma$, whereas in ΛCDM the tension is larger than 3σ.
We notice from Fig.5.1 that this is mainly due to the bigger errors on H_0, because of its degeneracies with DE/MG parameters, rather than to a shift in the mean value of the parameter.

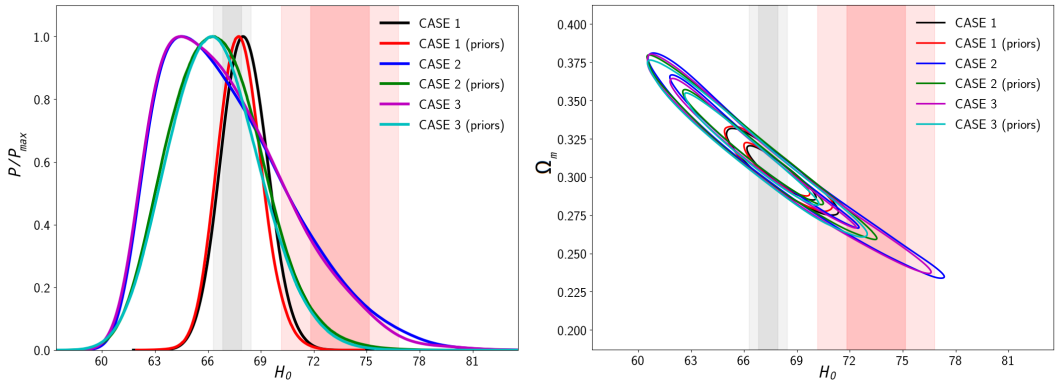

Figure 5.1: The gray vertical region refers to the Planck inferred value of H_0, while the red vertical region to the local measurements estimate.

To this end, it is pointless trying to ease the tension considering Quintessence results, since, as justified in the Appendix, the inferred H_0 parameter is smaller than the one that would be obtained under the Cosmological Constant assumption.

5.4 Future prospects

A tremendous boost to this investigation will be given by the upcoming surveys, here briefly described, that are specifically designed to understand and constrain the physics of the late cosmic acceleration phase, providing, for instance, a map of the matter distribution, that, as we have seen, is one of the most promising ways to distinguish between DE and MG models.

5.4.1 The Dark Energy Spectroscopic Instrument (DESI)

The Dark Energy Spectroscopic Instrument (DESI) is a Stage IV ground-based Dark Energy experiment [76]. The five year Survey will be conducted on the Mayall 4-meter telescope at Kitt Peak National Observatory starting in 2019 [77], where the instrument will be installed at prime focus on the telescope, along with a new optical corrector, which will provide a three-degree diameter field of view.

DESI will study BAO (primary measurements) and the growth of structure through RSD with a wide-area galaxy and quasar redshift survey, with in total more than 30 million galaxy and quasar redshifts, covering 14000 deg^2 and constructing a 3D map spanning the nearby Universe to 11 billion light years.
Specifically, the spectrograph will be capable of taking up to 5,000 simultaneous spectra over a wavelength range from 360 nm to 980 nm, probing redshifts up to 1.0 for luminous red galaxies, 1.7 for emission line galaxies ([O II]) and 3.5 for the Lyman-α forest [1] from quasars, that will be then used also to trace the distribution of neutral hydrogen along with the matter distribution. Moreover, DESI will perform a Bright Galaxy Survey of the $z < 0.4$ Universe, allowing the study of cosmic structure in the DE-dominated epoch with much denser sampling.
Finally, comparing the expansion history and the growth of large scale structure from redshift space distortions will allow DESI to test General Relativity.

5.4.2 EUCLID

In 2021 there is going to be the launch of the long-awaited EUCLID [78] satellite, with the main goal of understanding the physics related to the late cosmic acceleration, mapping the geometry and evolution of the Universe with unprecedented precision.

EUCLID is a space-based mission, equipped with a 1.2m telescope, along with three imaging and spectroscopic instruments working in the visible and near-infrared wavelength bands, that will provide images of a billion galaxies and measure nearly 100 million galaxy redshifts, covering at least 15000 deg^2 of sky. These instruments are:

- VIS[2], that will work on visual imaging of all the galaxies of the survey, with a 0.1arcsec resolution. It will be used to measure the shapes of galaxies and derive the gravitational lensing effects induced by LSS on distant background galaxies.
- NISP[3], that is designed for near-infrared (between 900 and 2000 nm) imaging photometry and spectroscopy, both characterized by 0.3arcsec resolution. This instrument aims at providing near infrared photometry of all galaxies observed also with VIS, to derive photometric redshifts and rough estimates of distances of galaxies seen by VIS, and near infrared low resolution spectra and redshifts of millions galaxies, mapping their distribution and clustering and describing how they changed over the last 10 billion.

[1] The forest is a collection of absorption features in the spectra of distant quasars blue-ward of the Ly-α emission line, where the absorption is caused by neutral gas in the intergalactic medium.
[2] https://www.euclid-ec.org/?page$_id = 2485$
[3] https://www.euclid-ec.org/?page$_id = 2490$

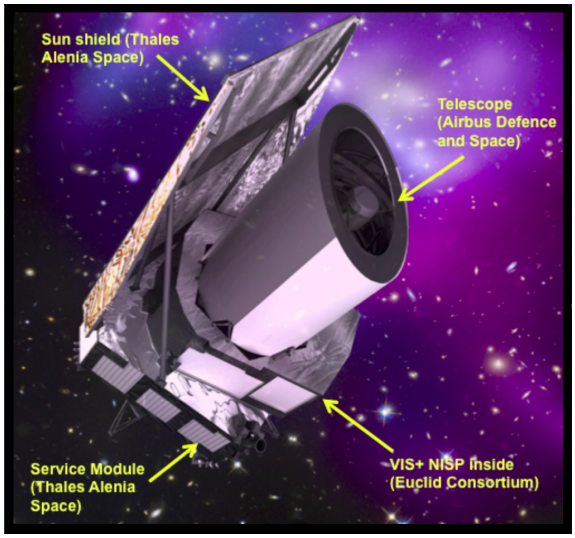

Figure 5.2: Figure adapted from [https://www.euclid-ec.org/?page$_id = 2686$]

This high-precision survey mission is firstly designed to place high accuracy constraints on Dark Energy and Gravity, where we have seen that the main alternatives to the Cosmological Constant are not only dynamical DE scalar fields, but also modifications to the standard GR theory.
Weak Lensing and Galaxy Clustering are the most sensitive probes of Dark Energy and of the theory of Gravity on cosmological scales; moreover, since they are also affected by the properties of Dark Matter, EUCLID is going to investigate the Dark Matter sector as well.
Concerning Weak Lensing, EUCLID will measure the shape and spectra of galaxies in the visible (VIS) and near-infrared (NISP) out to redshift 2, thus covering the period over which the Universe expansion had been accelerated, and the pattern of light distortions out to redshift 3. By measuring the correlations in the shapes of the 1.5 billion galaxies that EUCLID will image, the expansion and growth history of the Universe can be determined with high precision, along with a map of the distribution of (dark and luminous) matter.
Other important observables are peculiar velocities, that, as already seen, leave a characteristic pattern in redshift space, in form of distortions. Redshift space distortions provide us an independent measurement of the growth rate, which, together with that from lensing tomography, will be EUCLID's key measurement to detect the gravitational slip and break the DE versus MG degeneracy [79].
In addition to these main probes, EUCLID will provide abundance and properties of galaxy clusters and strong lensing and possible luminosity distance through Type Ia Supernovae, for few thousand of which EUCLID will provide NIR lightcurves and spectroscopic redshifts for many of the host galaxies.

Finally, EUCLID's capabilities can test the Cosmological Principle assumption to new levels and, combined with CMB experiments, this mission will also place constraint on cosmic initial conditions [80].

5.5 Summary

Throughout this Thesis we have outlined the key points of the non-parametric approach, aimed at reconstructing Dark Energy and Modified Gravity functions, given the knowledge on their correlation priors. The main purpose is to infer via Bayesian analysis, i.e. from data, the behaviour of the Dark Energy Equation of State $w_{DE}(z)$ and the two phenomenological functions $\mu(z)$ and $\Sigma(z)$.
I developed the analysis for Quintessence (DE) and Horndeski (MG) models, for which the correlation priors of the Equations of State were provided by [71], while those for $\mu(z)$ and $\Sigma(z)$ by [72]. An important observation is that the efficiency of the correlation prior, in constraining the binned functions, highly increases at redshifts for which there are less data.
In order to obtain reconstructions independent on the binning properties, we have set the number of bins to fulfill the condition of [59], where the correlation length is that set by the correlation prior. Moreover, since we also require the reconstructions to be independent on the method, we both tested smoothed step and Gaussian Process methods, finding that they provide reconstructions in agreement to each other. We expect that a denser binning would not only show off peculiar aspects of these functions but would make the reconstructions highly independent on the method as well.

The mean behaviour of these functions shows peculiar features compared to the standard ΛCDM case, which is still compatible with the most general reconstructed functions, as $w_\Lambda = -1$ is included within 1σ for all the w_{DE} reconstructions, while $\mu_\Lambda = \Sigma_\Lambda = 1$ within at least 2σ for every reconstruction of the two phenomenological functions, also when theoretical priors are included. Thus no evidence for modifications of the ΛCDM paradigm is found.

I have also shown that allowing for free redshift evolution for $w_{DE}(z)$, $\mu(z)$ and $\Sigma(z)$ results in looser constraints on H_0 with respect to ΛCDM. This allows to mitigate the tension between high and low redshift measurements from $\sim 3.5\sigma$ to $\sim 2\sigma$.

In the near future, several surveys will place high precision constraints from many observables linked to the nature of the late cosmic acceleration, boosting the benefit of the non-parametric approach here designed and, possibly, enabling us to detect or rule out classes of DE/MG models.

Appendices

APPENDIX A. Effect of the Quintessence prior

Since we already know that Quintessence equation of state can not lay below $w_{DE} = -1$, the mean $\overline{w}_{DE} = \left(\sum_{i=1}^{N} w_{DE,i}\right)/N$ is going to be higher than $w_\Lambda = -1$, so that it is worth comparing the behaviour of the obtained parameters with those of ΛCDM, where we expect that the inferred one will behave similarly to those for $w_{DE} = -0.9$ with respect to ΛCDM case.

SMOOTHED STEP FUNCTION RECONSTRUCTION			
Parameter	JLA+BAO+Planck	JLA+BAO+Planck (exp prior)	JLA+BAO+Planck (CPZ prior)
H_0	$65.1^{+1.6}_{-0.94}$	$65.1^{+1.6}_{-0.95}$	$65.1^{+1.5}_{-0.94}$
Ω_Λ.....	$0.670^{+0.017}_{-0.0099}$	$0.670^{+0.016}_{-0.010}$	$0.670^{+0.016}_{-0.0099}$
Ω_m.....	$0.3301^{+0.0099}_{-0.017}$	$0.330^{+0.010}_{-0.016}$	$0.3296^{+0.0099}_{-0.016}$

Table 2: Inferred mean values and 1σ c.l. of the cosmological parameters, in Quintessence cases, without and with the priors, reconstructing the EoS via smoothed step function.

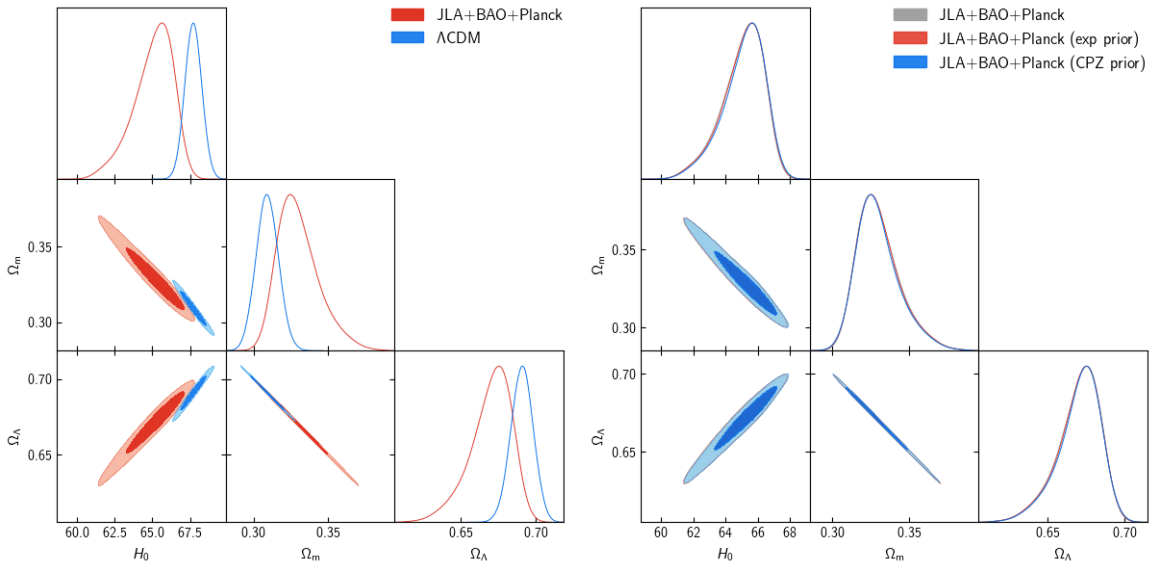

Figure 3: These are two triangle plots for the cosmological parameters H_0, Ω_Λ and Ω_m inferred in the Quintessence case, reconstructing the equation of state via smoothed step function. The left plot includes the results of Quintessence run with datasets alone and ΛCDM, the right one is the comparison between the runs without and with the priors.

Constant DE Equation of state

Let us focus on the $w = -0.9$ case, which is the one of interest. The behaviour of its inferred cosmological parameters of Fig.4 with respect to the ΛCDM case can be explained as follows.
Starting from the density parameters, let us suppose that the redshift z_* at which the Matter and Dark Energy components are equal is known. For $w_{DE} = const$ the Dark Energy density evolves as $\rho_{DE,0}(1+z_*)^{3(1+w_{DE})}$. At z_*, $\rho_m(z_*) = \rho_{DE}(z_*) \longleftrightarrow \rho_{m,0}(1+z_*)^3 = \rho_{DE,0}(1+z_*)^{3(1+w_{DE})}$:

$$\frac{\rho_{m,0}}{\rho_{DE,0}} = (1+z_*)^{3w_{DE}} \longleftrightarrow \frac{\Omega_{m,0}}{\Omega_{DE,0}} = (1+z_*)^{3w_{DE}}$$

$$\begin{cases} \Lambda\text{CDM} & \frac{\Omega_{m,0}}{\Omega_{DE,0}} = (1+z_*)^{-3} \\ w_{DE} = -0.9 & \frac{\Omega_{m,0}}{\Omega_{DE,0}} = (1+z_*)^{-2.7} \end{cases} \tag{2}$$

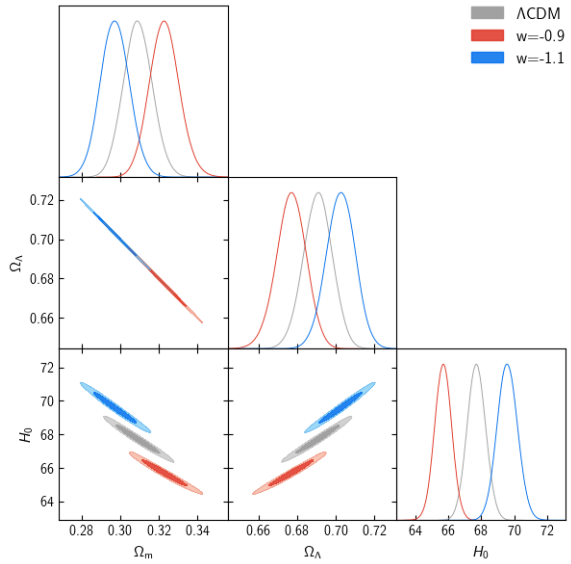

Figure 4: These are the cosmological parameters H_0, Ω_Λ and Ω_m obtained in the ΛCDM, $w = -1.1$ and $w = -0.9$ cases.

but then, since $(1+z_*)^{-3} < (1+z_*)^{-2.7}$ and under the assumption of a flat Universe $\Omega_{m,0}+\Omega_{DE,0} \sim 1$, the matter density parameter for ΛCDM must be lower than that of the $w_{DE} = -0.9$ case, as it happens in Fig.4.
On the other hand the resulting behaviour of H_0 can be understood starting from the following relation between the luminosity distance and H_0:

$$d_L = \frac{z}{H_0}\left(1 + \frac{1}{2}(1 - q_0)z\right)$$

where in the hypothesis of a flat Universe the deceleration parameter is equal to $q_0 = \frac{1+3w_{DE}\Omega_{DE}}{2}$. Let us suppose that the luminosity distance $d_L(z)$ of a Type Ia Supernova of given redshift is known, then:

$$\frac{z}{H_{0(\Lambda\text{CDM})}}\left(1 + \frac{1}{2}(1 - q_{0(\Lambda\text{CDM})})z\right) = \frac{z}{H_0}\left(1 + \frac{1}{2}(1 - q_0)z\right)$$

(if not specified I am referring to the $w_{DE} = -0.9$ case). From the previous result we know that $\Omega_{DE} < \Omega_\Lambda$ and w_{DE} are known. From a trivial calculation, the result is that $H_{0(\Lambda\text{CDM})} = cH_0 > H_0$, that is the result in Fig.4.

As expected, the cosmological parameters inferred in the Quintessence model behave more similarly to those for $w_{DE} = -0.9$ than to ΛCDM case.
As we have no restrictions in the Horndeski EoS, that crosses the Phantom divide, this same reasoning can not be done for this case.

Bibliography

[1] A. G. Riess, A. V. Filippenko, P. Challis, A. Clocchiatti, A. Diercks, P. M. Garnavich, R. L. Gilliland, C. J. Hogan, S. Jha, R. P. Kirshner, B. Leibundgut, M. M. Phillips, D. Reiss, B. P. Schmidt, R. A. Schommer, R. C. Smith, J. Spyromilio, C. Stubbs, N. B. Suntzeff, and J. Tonry. Observational Evidence from Supernovae for an Accelerating Universe and a Cosmological Constant. , 116:1009–1038, September 1998.

[2] S. Perlmutter et al. Measurements of and from 42 high-redshift supernovae. *The Astrophysical Journal*, 517(2):565, 1999.

[3] N. Aghanim et al. Planck 2018 results. VI. Cosmological parameters. 2018.

[4] A. G. Riess, S. Casertano, W. Yuan, L. Macri, J. Anderson, J. W. MacKenty, J. B. Bowers, K. I. Clubb, A. V. Filippenko, D. O. Jones, and B. E. Tucker. New Parallaxes of Galactic Cepheids from Spatially Scanning the Hubble Space Telescope: Implications for the Hubble Constant. , 855:136, March 2018.

[5] Michel Chevallier and David Polarski. Accelerating universes with scaling dark matter. *Int. J. Mod. Phys.*, D10:213–224, 2001.

[6] Eric V. Linder. Exploring the expansion history of the universe. *Phys. Rev. Lett.*, 90:091301, 2003.

[7] Mehdi Rezaei, Mohammad Malekjani, Spyros Basilakos, Ahmad Mehrabi, and David F. Mota. Constraints to Dark Energy Using PADE Parameterizations. *Astrophys. J.*, 843(1):65, 2017.

[8] P. A. R. Ade et al. Planck 2015 results. XIV. Dark energy and modified gravity. *Astron. Astrophys.*, 594:A14, 2016.

[9] Levon Pogosian and Alessandra Silvestri. What can cosmology tell us about gravity? constraining horndeski gravity with Σ and μ. *Phys. Rev. D*, 94:104014, Nov 2016.

[10] Edmund Bertschinger and Phillip Zukin. Distinguishing Modified Gravity from Dark Energy. *Phys. Rev.*, D78:024015, 2008.

[11] T. Giannantonio, M. Martinelli, A. Silvestri, and A. Melchiorri. New constraints on parametrised modified gravity from correlations of the CMB with large scale structure. , 4:030, April 2010.

[12] Sean Carroll. An introduction to General Relativity, Spacetime and Geometry. 2004.

[13] S. Dodelson. *Modern Cosmology*. 2003.

[14] Edward W. Kolb and Michael S. Turner. The Early Universe. *Front. Phys.*, 69:1–547, 1990.

[15] J. Yoo and Y. Watanabe. Theoretical Models of Dark Energy. *International Journal of Modern Physics D*, 21:1230002, December 2012.

[16] Austin Joyce, Lucas Lombriser, and Fabian Schmidt. Dark Energy Versus Modified Gravity. *Ann. Rev. Nucl. Part. Sci.*, 66:95–122, 2016.

[17] Robert R. Caldwell and Marc Kamionkowski. The Physics of Cosmic Acceleration. *Ann. Rev. Nucl. Part. Sci.*, 59:397–429, 2009.

[18] Joshua A. Frieman, Michael S. Turner, and Dragan Huterer. Dark energy and the accelerating universe. *Annual Review of Astronomy and Astrophysics*, 46(1):385–432, 2008.

[19] Eric V. Linder. Mapping the Cosmological Expansion. *Rept. Prog. Phys.*, 71:056901, 2008.

[20] David H. Weinberg, Michael J. Mortonson, Daniel J. Eisenstein, Christopher Hirata, Adam G. Riess, and Eduardo Rozo. Observational probes of cosmic acceleration. *Physics Reports*, 530(2):87 – 255, 2013. Observational Probes of Cosmic Acceleration.

[21] James B. Hartle. *Gravity, An introduction to Einstein's General Relativity.* 2003.

[22] Edwin Hubble. A relation between distance and radial velocity among extra-galactic nebulae. 1929.

[23] Planck Collaboration, P. A. R. Ade, et al. Planck 2015 results. XIII. Cosmological parameters. , 594:A13, September 2016.

[24] A. B. Balantekin and W. C. Haxton. Neutrino Oscillations. *Prog. Part. Nucl. Phys.*, 71:150–161, 2013.

[25] Daniel Baumann. Cosmology, Part III, lectures.

[26] F. Lucchin P. Coles. *Cosmology, The Origin and Evolution of Cosmic Structure.* 2002.

[27] P. A. R. Ade et al. Planck 2013 results. XVI. Cosmological parameters. *Astron. Astrophys.*, 571:A16, 2014.

[28] Daniel Baumann. Inflation. In *Physics of the large and the small, TASI 09, proceedings of the Theoretical Advanced Study Institute in Elementary Particle Physics, Boulder, Colorado, USA, 1-26 June 2009*, pages 523–686, 2011.

[29] Sabino Matarrese and Nicola Bartolo. *Early Universe Cosmology Lecture notes.* 2006.

[30] Sabino Matarrese, Silvia Mollerach, and Marco Bruni. Second order perturbations of the Einstein-de Sitter universe. *Phys. Rev.*, D58:043504, 1998.

[31] James M. Bardeen. Gauge Invariant Cosmological Perturbations. *Phys. Rev.*, D22:1882–1905, 1980.

[32] Alessandra Silvestri and Mark Trodden. Approaches to understanding cosmic acceleration. *Reports on Progress in Physics*, 72(9):096901, 2009.

[33] Bhuvnesh Jain and Pengjie Zhang. Observational Tests of Modified Gravity. *Phys. Rev.*, D78:063503, 2008.

[34] J. E. Carlstrom, G. P. Holder, and E. D. Reese. Cosmology with the Sunyaev-Zel'dovich Effect. , 40:643–680, 2002.

[35] S.Tsujikawa L. Amendola. *Dark Energy, Theory and Observations.* 2010.

[36] Daniel J. Eisenstein et al. Detection of the Baryon Acoustic Peak in the Large-Scale Correlation Function of SDSS Luminous Red Galaxies. *Astrophys. J.*, 633:560–574, 2005.

[37] N. Suzuki, , others, and T. Supernova Cosmology Project. The Hubble Space Telescope Cluster Supernova Survey. V. Improving the Dark-energy Constraints above z 1 and Building an Early-type-hosted Supernova Sample. , 746:85, February 2012.

[38] David H. Lyth and Andrew R. Liddle.

[39] Michaël Malquarti, Edmund J. Copeland, Andrew R. Liddle, and Mark Trodden. A new view of k-essence. *Phys. Rev. D*, 67:123503, Jun 2003.

[40] A. Pourtsidou, C. Skordis, and E. J. Copeland. Models of dark matter coupled to dark energy. *Phys. Rev.*, D88(8):083505, 2013.

[41] Edmund J. Copeland, M. Sami, and Shinji Tsujikawa. Dynamics of dark energy. *Int. J. Mod. Phys.*, D15:1753–1936, 2006.

[42] Shinji Tsujikawa. Quintessence: a review. *Classical and Quantum Gravity*, 30(21):214003, 2013.

[43] Bharat Ratra and P. J. E. Peebles. Cosmological consequences of a rolling homogeneous scalar field. *Phys. Rev. D*, 37:3406–3427, Jun 1988.

[44] Paul J. Steinhardt, Li-Min Wang, and Ivaylo Zlatev. Cosmological tracking solutions. *Phys. Rev.*, D59:123504, 1999.

[45] Timothy Clifton, Pedro G. Ferreira, Antonio Padilla, and Constantinos Skordis. Modified Gravity and Cosmology. *Phys. Rept.*, 513:1–189, 2012.

[46] Sean M. Carroll, Vikram Duvvuri, Mark Trodden, and Michael S. Turner. Is cosmic speed - up due to new gravitational physics? *Phys. Rev.*, D70:043528, 2004.

[47] Eleftherios Papantonopoulos. *Modifications of Einstein's Theory of Gravity at Large Distances.* 2014.

[48] Levon Pogosian and Alessandra Silvestri. The pattern of growth in viable f(R) cosmologies. *Phys. Rev.*, D77:023503, 2008. [Erratum: Phys. Rev.D81,049901(2010)].

[49] Alessandra Silvestri, Levon Pogosian, and Roman V. Buniy. Practical approach to cosmological perturbations in modified gravity. *Phys. Rev.*, D87(10):104015, 2013.

[50] W. L. Freedman et al. Final results from the Hubble Space Telescope key project to measure the Hubble constant. *Astrophys. J.*, 553:47–72, 2001.

[51] A. G. Riess, L. M. Macri, S. L. Hoffmann, D. Scolnic, S. Casertano, A. V. Filippenko, B. E. Tucker, M. J. Reid, D. O. Jones, J. M. Silverman, R. Chornock, P. Challis, W. Yuan, P. J. Brown, and R. J. Foley. A 2.4% Determination of the Local Value of the Hubble Constant. , 826:56, July 2016.

[52] W. L. Freedman, B. F. Madore, V. Scowcroft, C. Burns, A. Monson, S. E. Persson, M. Seibert, and J. Rigby. Carnegie Hubble Program: A Mid-infrared Calibration of the Hubble Constant. , 758:24, October 2012.

[53] G. Hinshaw, D. Larson, E. Komatsu, D. N. Spergel, C. L. Bennett, J. Dunkley, M. R. Nolta, M. Halpern, R. S. Hill, N. Odegard, L. Page, K. M. Smith, J. L. Weiland, B. Gold, N. Jarosik, A. Kogut, M. Limon, S. S. Meyer, G. S. Tucker, E. Wollack, and E. L. Wright. Nine-year Wilkinson Microwave Anisotropy Probe (WMAP) Observations: Cosmological Parameter Results. , 208:19, October 2013.

[54] Wendy L. Freedman. Cosmology at a Crossroads. *Nat. Astron.*, 1:0121, 2017.

[55] T. Holsclaw, U. Alam, B. Sansó, H. Lee, K. Heitmann, S. Habib, and D. Higdon. Nonparametric Dark Energy Reconstruction from Supernova Data. *Physical Review Letters*, 105(24):241302, December 2010.

[56] T. Holsclaw, U. Alam, B. Sansó, H. Lee, K. Heitmann, S. Habib, and D. Higdon. Nonparametric reconstruction of the dark energy equation of state. , 82(10):103502, November 2010.

[57] M. Seikel, C. Clarkson, and M. Smith. Reconstruction of dark energy and expansion dynamics using Gaussian processes. , 6:036, June 2012.

[58] Y. Wang, L. Pogosian, G.-B. Zhao, and A. Zucca. Evolution of dark energy reconstructed from the latest observations. *ArXiv e-prints*, July 2018.

[59] Robert G. Crittenden, Levon Pogosian, and Gong-Bo Zhao. Investigating dark energy experiments with principal components. *Journal of Cosmology and Astroparticle Physics*, 2009(12):025, 2009.

[60] S. Casas, M. Kunz, M. Martinelli, and V. Pettorino. Linear and non-linear Modified Gravity forecasts with future surveys. *Physics of the Dark Universe*, 18:73–104, December 2017.

[61] Carl Edward Rasmussen and Chris Williams. *Gaussian Processes for Machine Learning*. 2006.

[62] Alireza Hojjati, Levon Pogosian, and Gong-Bo Zhao. Testing gravity with camb and cosmomc. *Journal of Cosmology and Astroparticle Physics*, 2011(08):005, 2011.

[63] Gong-Bo Zhao, Levon Pogosian, Alessandra Silvestri, and Joel Zylberberg. Searching for modified growth patterns with tomographic surveys. *Phys. Rev. D*, 79:083513, Apr 2009.

[64] Wenjuan Fang, Wayne Hu, and Antony Lewis. Crossing the phantom divide with parametrized post-friedmann dark energy. *Phys. Rev. D*, 78:087303, Oct 2008.

[65] R.R Caldwell. A phantom menace? cosmological consequences of a dark energy component with super-negative equation of state. *Physics Letters B*, 545(1):23 – 29, 2002.

[66] Wayne Hu. Crossing the phantom divide: Dark energy internal degrees of freedom. *Phys. Rev. D*, 71:047301, Feb 2005.

[67] Wayne Hu. Parametrized Post-Friedmann Signatures of Acceleration in the CMB. *Phys. Rev.*, D77:103524, 2008.

[68] A. Heavens. Statistical techniques in cosmology. *ArXiv e-prints*, June 2009.

[69] Antony Lewis and Sarah Bridle. Cosmological parameters from CMB and other data: A Monte Carlo approach. *Phys. Rev.*, D66:103511, 2002.

[70] Antony Lewis. Efficient sampling of fast and slow cosmological parameters. *Phys. Rev.*, D87(10):103529, 2013.

[71] Marco Raveri, Philip Bull, Alessandra Silvestri, and Levon Pogosian. Priors on the effective dark energy equation of state in scalar-tensor theories. *Phys. Rev. D*, 96:083509, Oct 2017.

[72] Juan Espejo, Simone Peirone, Marco Raveri, Kazuya Koyama, Levon Pogosian, and Alessandra Silvestri. Phenomenology of Large Scale Structure in scalar-tensor theories: joint prior covariance of $w_{\rm DE}$, Σ and μ in Horndeski. 2018.

[73] M. Betoule et al. Improved cosmological constraints from a joint analysis of the SDSS-II and SNLS supernova samples. *Astron. Astrophys.*, 568:A22, 2014.

[74] Florian Beutler, Chris Blake, Matthew Colless, D. Heath Jones, Lister Staveley-Smith, Lachlan Campbell, Quentin Parker, Will Saunders, and Fred Watson. The 6df galaxy survey: baryon acoustic oscillations and the local hubble constant. *Monthly Notices of the Royal Astronomical Society*, 416(4):3017–3032, 2011.

[75] Ashley J. Ross, Lado Samushia, Cullan Howlett, Will J. Percival, Angela Burden, and Marc Manera. The clustering of the sdss dr7 main galaxy sample i. a 4 per cent distance measure at z = 0.15. *Monthly Notices of the Royal Astronomical Society*, 449(1):835–847, 2015.

[76] Andreas Albrecht et al. Report of the Dark Energy Task Force. 2006.

[77] Amir Aghamousa et al. The DESI Experiment Part I: Science,Targeting, and Survey Design. 2016.

[78] A. Refregier, A. Amara, T. D. Kitching, A. Rassat, R. Scaramella, J. Weller, and f. t. Euclid Imaging Consortium. Euclid Imaging Consortium Science Book. *ArXiv e-prints*, January 2010.

[79] R. Laureijs, J. Amiaux, S. Arduini, J. . Augueres, J. Brinchmann, R. Cole, M. Cropper, C. Dabin, L. Duvet, A. Ealet, and et al. Euclid Definition Study Report. *ArXiv e-prints*, October 2011.

[80] Luca Amendola et al. Cosmology and fundamental physics with the Euclid satellite. *Living Rev. Rel.*, 21(1):2, 2018.

Acknowledgements

Vorrei rigraziare tutti coloro che hanno fatto parte del mio percorso fino ad oggi.
Un sentito ringraziamento va al Professor Nicola Bartolo e ad Alessandra, che mi hanno permesso di fare questa bellissima esperienza a Leiden, dimostrandosi sempre assai disponibili nei miei confronti, e a Matteo, che, nonostante sia una delle persone più impegnate che io conosca, si è dimostrato molto paziente con me, fornendomi un grandissimo aiuto durante lo svolgimento del progetto.
Ringrazio gli storici amici di Mestre, che mi sono sempre stati vicino e con cui ho condiviso moltissime avventure, la pazza compagnia di Astronomia, che ha allietato il mio studio con bizzarre esperienze, e Mario, per avermi regalato mille risate e avermi spronata ad uscire dai miei schemi.
Ringrazio la mia famiglia, che da ogni angolo del pianeta ha sempre fatto il tifo per me, e mio fratello Giovanni, la cui perseveranza e ambizione sono per me fonte di ammirazione.
Infine, il ringraziamento più importante va ai miei genitori, che mi hanno sempre sostenuta, anche nelle scelte più discutibili e nei momenti peggiori, e a cui devo ciò che sono e ciò che ho.